Characteristics on HDS of gas oil over alumina-silica supports

Joo Il Park, Masashi Yasudome, Jin Miyawaki, Seong Ho Yoon and Isao Mochida*

Institute of Materials Chemistry and Engineering, Kyushu University, Fukuoka 816-8580, Japan

Introduction

The issue on high activity of catalysts and process development for the deep HDS gas oil is to deeply desulfurize the refractory sulfur species such as 4,6-dialkyl-dibenzothiophenes (4,6-DMDBT) which are present at a large amount in the gas oil, and rapid HDS reactive sulfur species.

The latter issue objectives can be attained as rapid as possible HDS of the reactive species within shorter time to leave longer time for the deep HDS of refractory sulfur species which tends to be slow. The most effective catalyst to these issues is not always same. Hence, two catalyst layers bed has been proposed very practically for the rapid HDS of the reactive sulfur species and even deep HDS of the refractory sulfur species at lower temperature[1].

The former issue has been overcome through the hydrogenation of the neighboring phenyl groups to the thiophene ring which moderate the steric hindrance of S atom to approach the active site of NiMoS surface[2,3]. High H_2S content under reaction condition, due to high S contents in the gas oil, inhibits the elimination of S in the thiophene ring by occupation of H_2S over the active sites, even though its steric hindrance is moderated. Acidic support has been proved to enhance the ring hydrogenation and liberation of H_2S on the active site of NiMoS species. However, it is necessary to control carefully their acidity due to the excess cracking of gas oil and strong inhibition of basic poisons[4].

The aims of this research are to examine the HDS activities of NiMoS supported on three types of alumina-silica supports with the different synthetic methods in dual catalytic bed to demonstrate the performance under the commercial test conditions, and investigate their characteristics.

Experimental

The active metal of Mo (Mo oxide 5%) and Ni (Ni oxide 20%) impregnated by pore filling method (NMASA-1, -2, -3) were supported on amorphous alumina-silica carriers (ASA-1, -2, -3) synthesized differently from co-precipitation of alumina and silica sources in water, which was received by catalyst company in Japan. The content of silicon oxide in the catalyst carrier was 28% for ASA-1, 27% for ASA-2, 24% for ASA-3. The HDS activity of each catalyst was investigated by pilot plant unit which was consisted of two fixed bed reactor in series. The sulfur and carbon species in the feed and product oils were analysed GC-AED. The characterization of catalysts was accomplished by BET, XRD, SEM, HR-TEM, ^{27}Al and ^{31}Si solid NMR as well as NH_3-TPD.

Results

The HDS activities over NMASA-1, -2 and -3 with dual catalystic bed which the first and second layer catalysts were LX6 in all cases and three variable catalysts, respectively. The combination of LX6 and NMASA-2 was much more active than other 2 combinations, providing 6.6ppm sulfur (less than 10 ppm S) at 345^{o}C which LX6 and NMASA-2 appear to share their respective roles for rapid HDS of reactive and/or refractory sulfur species evidenced by sulfur GC-AED chromatograms. The difference in their activity was found in the remaining refractory sulfur species. LX6/NMASA-2 combination removed almost refractory sulfur species under the present conditions.

From the reactivity, ASA-2(27) was found the best support for the second layer catalyst which may be attributed to the crystal size of alumina, in order of ASA-1(3.39nm) > ASA-2 (2.92nm) > ASA-3 (2.62nm) evidenced by XRD, SEM and HR-TEM. The largest size of alumina crystal is certainly worst, and the medium size appears better than the smallest size. Better activity over ASA-2 (27) support could be also provided since octahedral coordination of Al species, suggesting extra-framework Al species, confirmed by ^{27}Al MAS NMR.

The sulfur contents of product oils over NMASA-2 with various silica amounts in the dual catalytic system were also investigated. HDS activity was found much affected by silica contents in NMASA-2, being optimized at 27% silica. Both of increasing and decreasing contents of silica from 27% reduced its HDS activity. From the sulfur GC-AED chromatograms of product oils over LX6/NMASA-2 series catalysts, the refractory sulfur compounds such 4,6-DMDBT were still remained in the product oils except NMASA-2(12) and NMASA-2(27) which presented higher removal activity of refractory sulfur compounds.

Conclusion

NMASA-2 catalyst showed much enhanced activity of HDS for gas oil (SRGO) with a role of rapid HDS of reactive and/or refractory sulfur species. HDS activity was also much affected by silica contents in NMASA-2. Improved HDS reactivity could be speculated by the adequate crystal size of alumina and octahedral coordination of Al species indicating extra-framework Al.

Acknowledgement

This research was supported by the Global-Center of Excellence (G-COE) in Novel Carbon Resource Sciences, Kyushu University

References

(1) N. Kunisada, K.H. Choi, Y. Korai, I. Mochida, K. Nakano, Appl. Catal. A: Gen. 279 (2005) 235

(2) R. Shafi, G.J. Hutchings, Catal. Today 59 (2000) 423

(3) X. Li, A. Wang, M. Egorova, R. Prins, J. Catal. 250 (2007) 283

(4) S.D. Murti Sumbogo, H. Yang, K.H. Choi, Y.Korai, I. Mochida, Appl. Catal. A: Gen. 252 (2003) 331

Investigations on 1-methyl naphthalene to (alkyl)benzene over surface modified USY zeolite

Joo Il Park, Jin Miyawaki, Seong Ho Yoon and Isao Mochida*

Institute of Materials Chemistry and Engineering, Kyushu University, Fukuoka 816-8580, Japan

Introduction

With the increasing demand for diesel fuel, the hydro-treatment of LCO produced from fluid catalytic cracking (FCC) is a possible way to improve its quality by performing HDS, HDN, HYD and even partial hydrocracking so that it can be incorporated into the diesel pool with the increased cetane number which reflects the ignition properties of diesel fuels [1-3]. Generally, considerable ignition delays (low cetane number) can lead to rough engine operation, misfiring, incompletion combustion and poor stability. It could be overcome by conversion of the poly-aromatics into benzene or (alkyl) benzenes like a toluene and xylene, i.e. resulting from partial HC and HYD followed by opening of the saturated rings. Taking into account the backgrounds, ring opening of the polycyclic aromatics in LCO into (alkyl) benzene over improved supports or/and even active phases should be promising. In this sense, alumina coated zeolite as a catalyst, together with model compound (1-MN) were investigated for ring opening reactivity.

Experimental

NiMo catalysts were supported on γ-alumina (NMA), on physical mixtures of alumina and USY-zeolite (USY-zeolite contents: 50%, NMAZ), and on USY-zeolites surface modified with different coating amounts of alumina (USY-zeolite content: 50%, NMACZ-1 and NMACZ-2 (0), (10), (20), (40)) obtained from a catalyst company in Japan. Loading amounts of nickel oxide and molybdenium oxide were fixed at 5 and 20 wt%, for each catalyst. Reaction was performed by using autoclave (150cc), in which reactant, presulfided catalysts and H_2 gas (5MPa) were charged. Product distributions could be checked by GC-AED for quantitative analysis and GC-MS for qualitative analysis as well. The physical properties of catalysts were investigated by BET analysis of N_2 adsorption isotherm and XRD and other characteristics were studied by XPS, HR-TEM, pyridine FT-IR.

Results

Under the reaction conditions used in this work, 1-MN was partially isomerized to 2 methyl naphthalene (2-MN) on the γ-alumina, alumina coated USY zeolite and physical mixture of USY zeolite and Al supported bimetal (Ni, Mo) catalysts, which might be assumed by product distribution of 6-methyl tetralin (6-MT) and 5-methyl tetralin (5-MT). It also might be speculated by isomerization between 5-MT and 6-MT followed by hydrogenation of 1-MN to 5-MT.

The presence of coated alumina on the surface of USY zeolite readily changed the product distribution pattern which was related to ring opening products from (alkyl) tetralin and decalin. Especially, total (alkyl) benzene yields over NMACZ-2 was improved by the lowest coating amounted alumina, even if the yields of total (alkyl) cycloalkane decreased or was similar with much higher alumina coating amounted kind. Improvement of the activity is suggested to be due to the enhancement of surface acidity which is evidenced by pyridine FT-IR and even NH_3-TPD.

After sulfidation of catalysts, the binding energies of Mo^{4+}, Ni $2p_3$ and S 2p of NMACZ-1, NMACZ-2, and NMAZ were lower than those of NMA, suggesting that the weaker interactions between Mo or Ni and supports or between Mo and Ni species occurred. Especially, the weaker interaction between Mo and support has been reported to lead a higher reducibility which could be thought to improve hydrocracking reactivity on the catalyst, contrary to NMA. From the HR-TEM, it was found that the characteristics of the surface with alumina coatings may affect to the distributions and layer numbers of MoS, together with expecting to reactivity on HYD and HC. Brönsted and Lewis acid sites of NMACZ-2 was much more (about 30%) than those of NMACZ-1 catalysts which might be attributed to naked zeolite surface by lower alumina coating amounts evidenced by Si/Al from XPS data. The similar behavior in NH_3-TPD has been observed in previous work [4]. Increase of pyridine desorption temperature could be led to reduce the each acid sites. In the case of NMACZ-1, the degradation was accompanied by reduction in Brönsted and Lewis acid sites of 57% and 72%, respectively, comparing from initial to final desorption temperature, while those of NMACZ-2 were maintained in smaller portion of reduction rate (31% and 53%, respectively). Much higher strength of acid in NMACZ-2 compared with NMACZ-1 seems to suggest the presence of mainly strongly chemisorbed pyridinium species over zeolite surface, contributing to improvement of hydro-cracking reactivity.

Conclusion

NMACZ-2 carrying USY-zeolite coated with a lower amount of alumina, showed much enhanced activity of ring opening of tetralin species, which could be explained by acid characteristics on the presence of mainly strongly chemisrbed pyridinium over zeolite surface. The surface Mo species as a active phase were closely associated with the surface alumina species distributions. The larger MoS_2 crystalline are preferably formed on Al-rich surface. During sulfidation, Mo and Ni species tend to migrate into bulk, and more Mo species than Ni species were likely to be migrated.

Acknowledgement

This research was supported by the Global-Center of Excellence (G-COE) in Novel Carbon Resource Sciences, Kyushu University

References

(1) M. Bouchy, S.P. Denys, P. Dufresne, S. Kasztelan, Ind. Eng. Chem. Res. 32 (1993) 1592

(2) A. Stanislaus, B. Cooper, Catal. Rev.-Sci. Eng. 36(1) (1994) 75.

(3) W. Li, Z. Wang, M. Zhang, K. Tao, Catal. Comm. 6 (2005) 656

(4) N. Kunisada, K.H. Choi, Y. Korai, I. Mochida, K. Nakano, Appl. Catal. A: Gen. 276 (2004) 51

Origin of the versatile Brønsted acidity of amorphous silica-alumina used as catalytic support in hydrocracking

P. Raybaud, C. Chizallet

IFP
Direction Catalyse et Séparation
Rond-point de l'échangeur de Solaize
BP 3 - 69360 Solaize - France
email: pascal.raybaud@ifp.fr

Introduction

Hydrocracking (HCK) catalytic process requires to control the balance between the hydrogenation function and the acidic function [1]. For that purpose, various types of catalytic supports exhibiting a tuneable acidity scale (mesoporous alumina, amorphous silica-alumina (ASA) or zeolites) are industrially used in combination with a transition metal sulfide or even a metallic active phase. Depending on the type of the petroleum feeds to be converted, it is thus crucial to optimize the acidic function of the HCK support. ASA supports are empirically known to provide mild Brønsted acidity (intermediate between zeolites and alumina) which is profitably used to convert petroleum feeds in presence of refractory compounds. However, understanding the nature of the acid sites of this type of material, remains a challenging question. Experimental studies have proposed the existence of zeolite-like Si-(OH)-Al groups [2], whereas silanols in the vicinity of aluminum atoms are also invoked [3,4]. We have recently established the first ASA surface model, by ab initio simulation of the interface between silica derivates and the γ-Al_2O_3 (100) surface [5,6]. In the present communication, we show how the less acidic alumina surface develops a strong tendency to amorphization upon interaction with silica, and reveals some original Lewis and Brønsted acid sites thanks to the formation of an ASA phase [5]. Moreover, we have instigated the adsorption of various proble molecules such as CO, NH_3, pyridine, lutidine on these acid sites and highlighted new chemical behaviours of the so-called "pseudo-bridging silanols" [6].

Methods

DFT calculations, in the framework of the GGA-PW91 functional, were performed with the VASP 4.6 code [7]. The interaction between core and valence electrons was described by the projector augmented waves (PAW) approach [8]. DFT calculations give access to accurate surface energies of the ASA surfaces as a function of silica content. Moreover, adsorption energies of the various probe molecules have been estimated with DFT.

Force-field NVT molecular dynamics calculations were also performed with the GULP program [9,10] to explore the γ-alumina surface reconstruction in presence of the grafted silica at high temperature (T=1023 K). The dehydrated model for γ-alumina (100) surface was inherited from previous theoretical studies [11-13].

Thermodynamic stability domains were established for variable temperatures and water partial pressures (including HCK conditions) by calculating the surface energy systems as a function of the chemical potential of water according to the methodology detailed in [5].

Results and discussion

ASA surfaces

Starting from an epitaxially deposited silica film over the γ-Al_2O_3 dehydrated (100) surface (with Si coverage of 6.4 nm^{-2}) further submitted to a NVT molecular dynamics, the most stable surface found reveals the amorphization of the original γ-Al_2O_3 surface and the formation a mixed silica-alumina surface phase. This result highlights the determining role of thermal treatments in the activation of the formation of an ASA phase. In particular, the extraction of Al atoms from the γ-Al_2O_3 surface implies the appearance of an intimate mixture between alumina and silica at the surface. The extracted Al atoms, issued from bulk Al_{VI}, are finally either Al_V or Al_{IV}. This trend is fully in line with the experimental ^{27}Al NMR observation of the higher Al_{IV}/Al_{VI} ratio in ASA than in γ- Al_2O_3 [3,14] and of the appearance of new Al_V species [14].

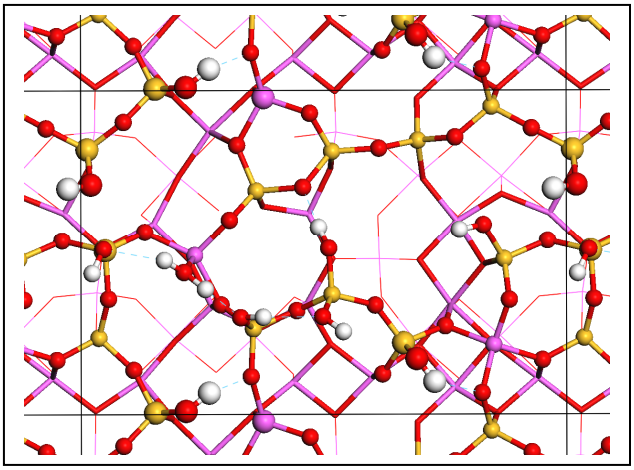

Figure 1. Diversity of the silanol groups stable on the ASA surfaces close to the HCK conditions (with an OH coverage of 5.4 nm-2). Colors legend: red balls: oxygen, white balls: hydrogen, purple balls: aluminum, yellow balls: silicon.

The behavior of this ASA surface phase towards increasing amounts of water (Figure 1), by molecular adsorption on M atoms (M=Al, Si), dissociation by M-O pairs, and hydrolysis of M1-O-M2 bridges, was then put in evidence by DFT calculations. As a first insight, this approach reveals that even for usual temperature conditions found in HCK processes, the ASA hydroxylation state remains significantly higher than the γ-alumina (100) surface, which is explained by the high stability of silanol groups. At this stage, 4 main types of silanol species have been put in evidence as a function of water coverages (as represented in figure 2) accessible under HCK conditions.

Below a coverage of 4.3 $OH.nm^{-2}$, only silanol groups (Figure 2 b) are formed, which explains why a band at 3740 cm^{-1} dominates the IR spectra of silicated alumina [3,14]. For coverages of 6.4 $OH.nm^{-2}$, our model also recover the presence of bridging Al-OH-Si silanols (Figure 2 a), as earlier discussed in the literature [2].

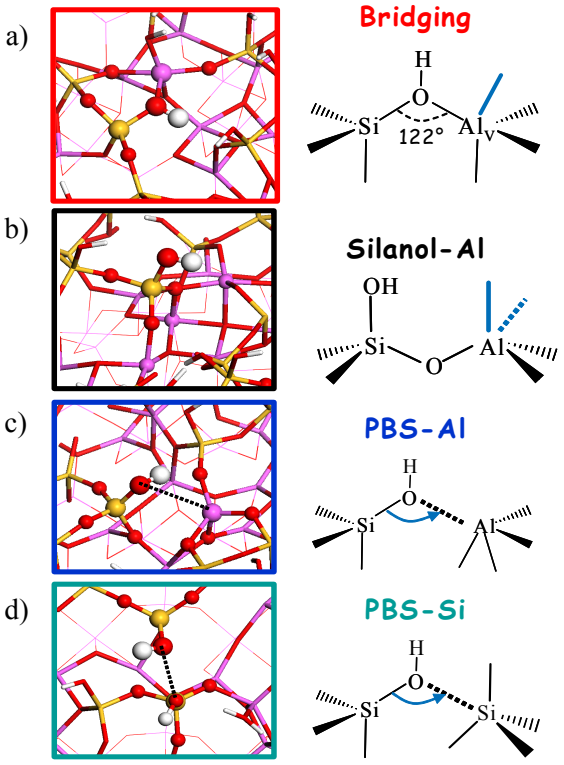

Figure 2. Ball and stick (left column) and schematic (right column) representation of the 4 main types of silanols found our ASA surface model under HCK conditions: a) bridging, b) isolated, c) PBS-Al, d) PBS-Si.

The most striking result is obtained for an intermediate coverage of 5.4 OH.nm^{-2}, where a new type of silanol species (Figure 2 c) was put in evidence. This kind of silanols keep on interacting with the neighboring Al atom and is defined "Pseudo-Bridging Silanol" (PBS). Similar PBS sites are found where silanol are also in close vicinity to neighboring Si atom (figure 2 d).

These 4 types of silanols exhibit various Si-O(H)-Al angles and Al-O(H) distances. Bridging silanols (Figure 2 a) exhibit a lattice constrained Si-O-Al angle (122°) very close to those found in zeolites, whereas PBS-Al reveal more flexible Si-O(H)-Al angles which may at the origin of their milder and tunable intrinsic acidity [3,15], a key feature of ASA surface.

In what follows, we discuss the chemical properties of these acid sites with respect to probe molecule adsorptions.

Probing the ASA Brønsted acid sites

The DFT calculation of the adsorption configurations and energies of relevant basic probe molecules (NH_3, pyridine, lutine) with various basic characters is very instructive for a better characterization of the silanol acidity. It is worth noting that such molecules are not only currently used as probes for spectroscopic analysis but are also representative of nitrogen compounds found in petroleum feeds to be treated in the HCK process.

As it can be shown in Table 1, the adsorption energies of the nitrogen probe molecules depend on the type of sites (acid strength and accessibility) as well as on the nature of the probe itself.

OH groups	Pyridine		Lutidine		Ammonia	
	E_{ads}	Species	E_{ads}	Species	E_{ads}	Species
Bridging Si-(OH)-Al	-44	Py-H$^+$	-37	Lu-H$^+$	-111	NH_4^+
Silanol-Al	-25	OH····Py	-36	OH····Lu	-41	OH····NH_3
PBS-Al	-36	OH····Py	-45	Lu-H$^+$	-51	NH_4^+
PBS-Si	-72	Py-H$^+$	-90	Lu-H$^+$	-81	NH_4^+

Table 1. Adsorption energies (kJ/mol) of pyridine, lutidine and ammonia as a function of silanol sites.

As expected, isolated silanol groups exhibit the lowest adsorption energies and no protonation of the probe is observed. These sites seem to behave as those found in purely amorphous silica materials.

For the ammonia molecule for which all sites are easily accessible, it is found that the bridging Si-OH-Al sites exhibit the strongest adsorption energies with the formation of an ammonium cations induced by the proton transfer. As proposed in the literature [2], these sites behave similarly as bridging silanol found in zeolites even if the adsorption energies (table 1) remain slightly smaller than energies reported in zeolites, such as mordenite (calculated between -110 and -175 kJ/mol [16]). In contrast, when increasing the bulkiness of the nitrogen molecules (pyridine and lutidine), the adsorption energies drop by a factor of 3, which means that bridging Si-OH-Al sites (even if intrinsically strongly acid) can be sterically constrained at the surface.

PBS sites exhibit a contrasting behavior. First, regarding the ammonia probe adsorption energy (between -81 and -51 kJ/mol), their Brønsted acidity is thus intrinsically weaker than bridging silanols on ASA or in zeolites. In addition, the adsorption energies reported in Table 1 are less impacted by the probe bulkyness: the adsorption energies of the lutidine are close to ammonia. Moreover, adsorption energies of pyridine and lutidine on PBS are competitive with energies found on bridging silanols. This is even more pronounced for PBS-Si sites which exhibit the highest adsorption energies. This trend can be explained by analyzing the original chemical bonding redistribution involved during the adsorption process, as illustrated in Figure 3.

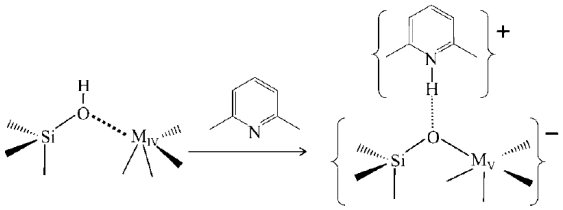

Figure 3. Schematic representation of the adsorption process of lutidine on a PBS sites: proton transfer and simultaneous formation of the M-O bond (M=Al or Si).

On the pseudo-bridging silanol site, while the proton transfer associated to the lutidinium cation formation occurs, there is a concomitant formation of a new Al-O or Si-O bond leading to the formation of a bridging [Si-O-Al]$^-$ complex. The covalency of the newly formed Al-O or Si-O bonds has been further characterized by ab initio chemical bond analysis and chemical shift calculation [6]. Hence, the adsorption process on PBS sites is also stabilized by the

energy gain induced by the formation of the new covalent M-O bond (M=Al or Si). As a consequence, we think that PBS can be considered as relevant sites featuring the versatile acidity of ASA materials of critical importance in HCK catalytic support.

Conclusion

To conclude, the present DFT study proposes the first atomic insight in the origin of the much debated Brønsted acidity of amorphous silica-alumina (ASA) surfaces. Bridging Si-(OH)-Al groups but also aluminic and silicic Pseudo-Bridging Silanols PBS are shown to be able to protonate nitrogenated molecule thanks to their ability to bridge after deprotonation. Thanks to the propensity of cations on the ASA surface for adapting their coordination number after deprotonation of a nearby PBS, their Lewis acidity is converted into Brønsted acidity of PBS. These results may provide clues for the rationalization and design of the reactivity of ASA in various catalytic processes and for the optimization of the choice of acidic solids through structure / reactivity relationships.

References

(1) C. Marcilly, Acido-Basic Catalysis, Technip, Paris, **2005.**

(2) B. Xu, C. Sievers, J. A. Lercher, J. A. R. van Veen, P. Giltay, R. Prins, J. A. van Bokhoven, *J. Phys. Chem. C* **2007**, *111*, 12075.

(3) G. Crépeau, V. Montouillout, A. Vimont, L. Mariey, T. Cseri, F. Maugé, *J. Phys. Chem. B* **2006**, *110*, 15172.

(4) M. Trombetta, G. Busca, S. Rossini, V. Piccoli, U. Cornaro, A. Guercio, R. Catani, R. J. Willey, *J. Catal.* **1998**, *179*, 581.

(5) C. Chizallet, P. Raybaud, *Angew. Chem. Int. Ed.* **2009**, *48*, 2891.

(6) C. Chizallet, P. Raybaud, *ChemPhysChem* **2010**, *11*, 105.

(7) G. Kresse, J. Hafner, *Phys. Rev. B* **1994**, *49*, 14251.

(8) G. Kresse, D. Joubert, *Phys. Rev. B* **1999**, *59*, 1758.

(9) J. D. Gale, *Philos. Mag.* **1996**, *73*, 3.

(10) J. D. Gale, *J. Chem. Soc. Faraday Trans.* **1997**, *93*, 629.

(11) X. Krokidis, P. Raybaud, A-E. Gobichon, B. Rebours, P. Euzen, H. Toulhoat, *J. Phys. Chem. B* **2001**, *105*, 5121.

(12) M. Digne, P. Sautet, P. Raybaud, P. Euzen, H. Toulhoat*, J. Catal*. **2002**, *211*, 1

(13) M. Digne, P. Raybaud, P. Sautet, D. Guillaume, H. Toulhoat, *J. Am. Chem. Soc.* **2008**, *130*, 11030.

(14) C. Dorémieux-Morin, C. Martin, J. M. Brégeault, J. Fraissard, *Appl. Catal.* **1991**, *77*, 149.

(15) W. Daniell, U. Schubert, R. Glöckler, A. Meyer, K. Noweck, H. Knözinger, *Appl. Catal. A* **2000**, *196*, 247.

(16) T. Bucko, J. Hafner, L. Benco, *J. Chem. Phys.* **2004**, *120*, 10263.

HIGH THROUGHPUT EXPERIMENTATION AS AN EFFICIENT TOOL FOR THE TESTING OF HYDROPROCESSING CATALYSTS

Josef Find, Jochen Berg, Sascha Vukojevic

hte Aktiengesellschaft
Kurpfalzring 104
69123 Heidelberg
Germany
www.hte-company.com

Increasing global demand for fuels, the tightening of environmental regulations and the optimization of refineries has led to an increasing demand for catalyst testing capacity. High throughput catalyst testing is a time-efficient approach for meeting this demand, however, in the past the increase in testing throughput was subsequently accompanied by a loss of data quality.

The demand for hydroprocessing and the testing of hydroprocessing catalysts has been growing steadily over the past years and this seems unlikely to decrease in the future. Over the last couple of years hte has developed parallel testing reactor systems for testing these catalysts under a wide range of process conditions in order to meet this demand. The latest development is capable of processing VGO, heavy VGO and bio-oil under industrially relevant conditions. Temperatures of up to 450°C can be achieved routinely, as well as pressures from 20 up to 170 bar.

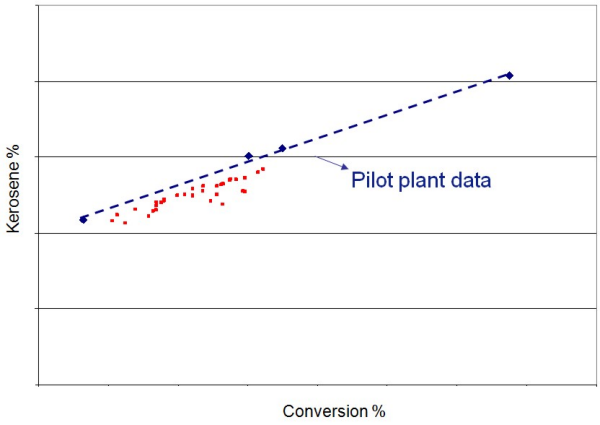

Figure 1. Correlation of high throughput HVGO-hydrocracking data (red) with data derived from a hydrocracking pilot plant (blue).

A challenging example for the parallel testing of hydroprocessing catalysts is hydrocracking. The products of this process depend strongly on the reaction conditions (temperature, pressure, catalyst activity). These products range from ethane, LPG to heavier hydrocarbons comprising mostly isoparaffins. Closing the total carbon mass balance covering gas and liquid products, under demanding reaction conditions is one of the latest major achievements for high throughput reactor systems. Figure 1 reveals that hydrocracking data derived from high throughput reactor systems can be directly correlated to results from a hydrocracking pilot plant.

The results that will be presented will show the effectiveness of parallel testing technology and the data quality standard in a reactor-to-reactor and run-to-run comparison for hydrodesulphurization and hydrocracking processes over several months feeding diesel, VGO, heavy VGO and bio-oil, as it is shown in Figure 2 for the hydrocracking of HVGO in an hte 16-fold parallel reactor system. To prove the value of the achieved data, the experimental results will be compared to pilot plant data. The latest developments in the field of high throughput reactor technology for refinery applications will also be shown, including parallel catalyst testing technology in a sub-pilot scale with higher catalyst volumes.

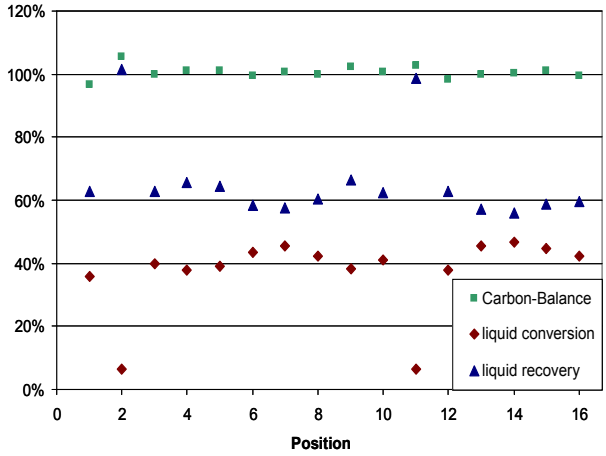

Figure 2. Carbon balance, liquid conversion and liquid recovery in a reactor-to-reactor comparison of HVGO hydrocracking in one of hte's parallel trickle-bed reactor systems.

Highly active nickel molybdate catalysts prepared for deep hydrodesulfurization of dibenzothiophene

Changlong Yin, Dong Chen, Sheng Zhang and Chenguang Liu

Key Laboratory of Catalysis, CNPC
State Key Laboratory of Heavy Oil Processing
College of Chemistry & Chemical Engineering
China University of Petroleum, Qingdao, Shandong 266555, China

Introduction

Recently the new changes in clean fuels requirements have increased the research work for reducing sulfur in petroleum products. The sulfur content in the motor fuels is continuously reduced by regulations to lower and lower levels. In the near future, highway diesel will truly be ultra-low sulfur diesel (ULSD).Thus, refiners must process diesel with sulfur content in the range of 5-10ppm. Some significant breakthroughs in catalyst developments for low-sulfur diesel have been accomplished (1-3). The new catalysts systems are specifically designed to overcome the steric hindrance in the hydrodesulfurization reactions of substituted DBTs at low content levels.

Transition-metal molybdates are well-known to be catalytically active for partial oxidation reactions, particularly for the selective oxidation of lower alkanes (4). However, earlier work had generally reported that molybdates are poor precursors of sulfided HDS catalysts (5). The industrial HDS catalysts of composition Ni(Co)-Mo/Al_2O_3 typically consist of several surface species. Among these, molybdates of the type $AMoO_4$ have been detected (6). Such compounds or mixed-oxide surface species resembling them may have practical importance, as they may help to prevent loss of the Co or Ni promoter into the lattice of the alumina support caused by oxidative treatments, especially during regeneration (7). On the other hand, these mixed phases could be optima precursors for the Ni–Mo–S structures, proposed to be the true active components of the sulfided catalysts(8).

In the present paper, a porous ammonium nickel molybdate, $(NH_4)HNi_2(OH)_2(MoO_4)_2$, was synthesized by high-temperature hydrothermal synthesis from a solution of nickel nitrate and ammonium heptamolybdate, and the activity of the hydroprocessing of the DBT was investigated. A commercial NiMo/γ-Al_2O_3 catalyst was used to compare.

Experimental

Synthesis of ammonium nickel molybdate(ANM)

The high-temperature hydrothermal synthesis is as follows. Ammonium heptamolybdate, nickel nitrate, polyethylene glycol (PEG) and the precipitating agent, urea, were used to prepare a solution containing Ni and Mo in the desired molar ratio, and the solution was added into an autoclave, where the solution was heated and stirred at 150°C for 5h, leading to the formation of a pale green precipitate. The products were isolated by vacuum filtration, washed with deionized water, and dried overnight at 110°C and atmospheric pressure. The precursors with different Ni/Mo ratios were labeled as NiMo1-1, NiMo2-1 and NiMo3-1.

Preparation of catalysts

To obtain the fixed-bed catalysts, the precursors were mixed with an alumina gel (precursor/alumina ratio=80/20) and extruded into diameter 1.6mm rods. The rods was dried in air at 110 ºC for 10h, and then calcined at 350 ºC for 4h. The catalysts were labeled as Ni_1Mo, Ni_2Mo and Ni_3Mo according to the precursors used.

Catalyst characterization

X-ray powder diffraction analysis was carried out with a Rigaku D/max-IIA diffractometer using a graphite-filter CuKα radiation at a scan rate of 2 degrees per minute. Nitrogen adsorption (BET) was used for measuring the surface area, pore diameter and pore volume of the catalyst. A FEI Quanta200 scanning electron microscope (SEM) was used to perform morphological analysis. Thermogravimetric analysis was carried out by using a thermal analysis instrument at a heating rate of 10°C min^{-1} under a high-purity nitrogen atmosphere.

Catalyst activity

Catalytic activity measurements were carried out in a high pressure micro-reactor unit of 10 mm I.D., 40cm in length. 10 ml of the catalyst extrudates were loaded in the center of the reactor. The catalyst is treated at 110°C for 1 hour and 360°C for 6 hours with a liquid stream containing 3.0w% CS_2 in cyclohexane. A mixture containing 2.0wt% dibenzothiophene (DBT) and 98wt% n-decane was then pumped into the reactor at the test temperature. The reaction conditions are pressure 3.0MPa, H_2/feed ratio 300, and LHSV $2h^{-1}$. The product was cooled and separated into gaseous and liquid products in a high-pressure separator. The liquid product was sampled after stabilizing 10 hours at each reaction condition. The compositions of the liquid products were analyzed using GC-MS and a Varian 3800 gas chromatography equipped with a FID detector and a 30m fused-silica capillary column.

Results and Discussion

Synthesis of ANM with different Ni/Mo ratio

XRD patterns of ammonium nickel molybdate with different Ni/Mo ratio before and after calcination are reported in Figure 1a and b, respectively. Before calcination the precursor with Ni/Mo=1 is trigonal with hexagonal unit cell, the structure of which is $(NH_4)HNi_2(OH)_2(MoO_4)_2$ (PDF card no. 50-1414), belonging to a member of a solid solution series of $(NH_4)H_{2x}Ni_{3-x}O(OH)(MoO_4)_2$, where $0 \leq x \leq 3/2$ (9). The peak strength weakens in the sample with Ni/Mo=2, and some amorphous material appears, while it retains the main structure of the ammonium nickel molybdate. Only an amorphous phase is detected in the precursor with Ni/Mo=3. After calcination the precursor with Ni/Mo=1 decomposes into $NiMoO_4$ (PDF card no. 33-0948), while the other two samples decompose into a different phase of $NiMoO_4$, β-$NiMoO_4$ (PDF card no. 45-0142). $NiMoO_4$ presents two polymorphic phases at atmospheric pressure: a low-temperature α phase, and a high-temperature β phase (4). The β phase undergoes a transformation to the α phase when cooled below 180°C. Although pure β-$NiMoO_4$ is unstable below 180°C, it can be stabilized at ambient temperature after calcination of mixed oxides in the composition range Ni/Mo >1, as observed in Fig.1b, the excess NiO phases are detected in the two samples with Ni/Mo=2 and Ni/Mo=3. The stable β-$NiMoO_4$ phase detected in this paper may be attributed to the formation of a solid solution with the excess Ni oxide phases (10).

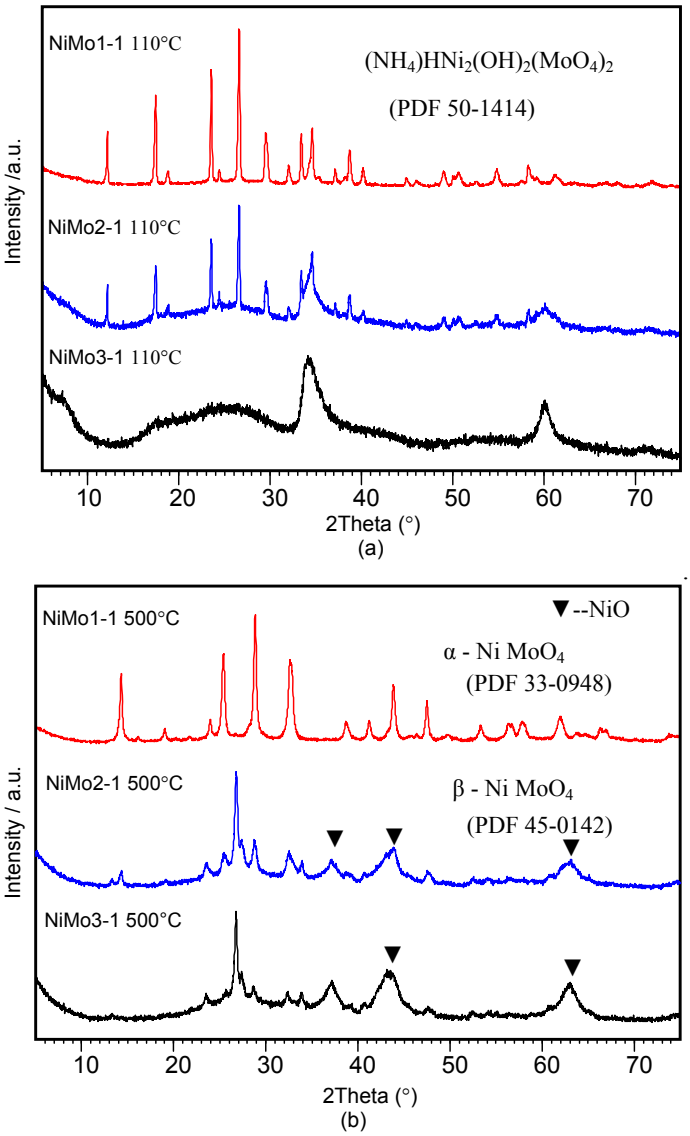

Figure 1. XRD patterns of ammonium nickel molybdate with different Ni/Mo ratio: (a) before calcination, (b) after calcination.

Thermogravimetric analysis of the precursor with Ni/Mo=1 in air shows that the weight loss occurs over a temperature range from 350°C to 425°C, as shown in Figure 2. The total weight loss ratio was 11.0%, and the weight loss could be attributed to the removal of water and ammonia from the structure. The decomposing equation is shown as follows, in which the theoretical total weight loss ratio is 10.8%.

$(NH_4)HNi_2(OH)_2(MoO_4)_2 \rightarrow 2NiMoO_4 + NH_3 + 2H_2O$

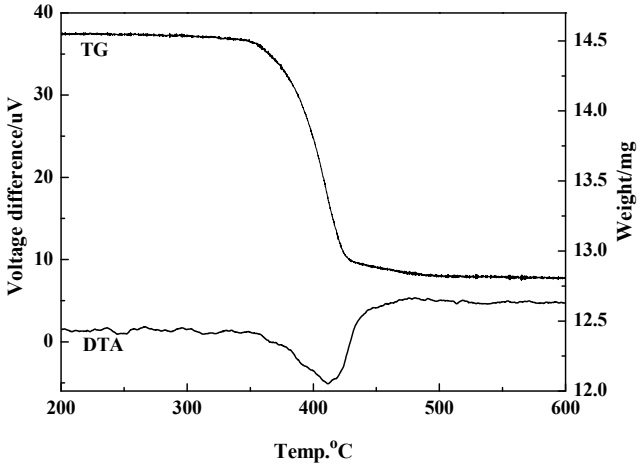

Figure 2. The TG-DTA curve of $(NH_4)HNi_2(OH)_2(MoO_4)_2$ in air.

The ammonium nickel molybdate is a good crystal, and the compound prepared with conventional methods described by Levin (9) has only a small amount pore. While the precursor with Ni/Mo=1 prepared by high-temperature hydrothermal synthesis method (HT) is porous. The BET results of ammonium nickel molybdate with two synthesis methods are shown in Table 1. The precursor prepared by HT method shows a significant increase in surface area and pore volume, whereas that prepared by literature method shows poor surface area and pore volume. Figure 3 gives the SEM photographs of the two precursors, which can explain the significant differences between them. The sample by conventional method is a dense crystalline material, and the shape of many differences. While the precursor prepared by HT method is mostly serrated cylindrical shape, and the surface is porous. The main difference between two methods is the precipitating agent, and the adding of the pore-forming reagent PEG. The decomposition of urea in aqueous media at elevated temperatures can produce ammonia and CO_2, which play the role of the precipitation agent, and at the same time increase the surface area of the product. The role of PEG is increasing the hydrophilicity of the surface and the formation of some larger holes after it decomposition.

Table 1. The BET Results of Ammonium Nickel Molybdate Prepared by Different Synthesis Methods

Methods	BET surface area ($m^2 \cdot g^{-1}$)	Pore volume ($cm^3 \cdot g^{-1}$)	Average pore diameter (nm)
Literature	15.8	0.09	7.6
HT	70.6	0.16	5.4

Catalytic activity

The surface area characteristics of the ANM catalysts and an industrial $NiMo/Al_2O_3$ are reported in Table 2. The surface area of catalysts was measured before sulfurization. The catalysts have higher surface area and larger pore volume than their precursors, mainly because the addition of alumina. A significant increase in the surface area and pore volume was observed after enhancing the Ni/Mo ratio. The results indicate that the excessive Ni can increase the surface areas and the pore volume of the ANM catalysts.

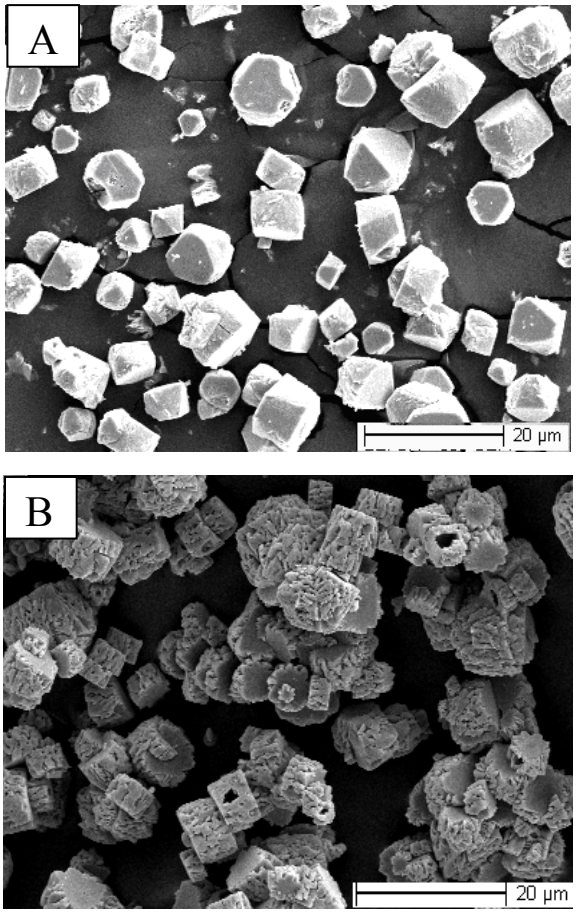

Figure 3. The SEM photographs of $(NH_4)HNi_2(OH)_2(MoO_4)_2$ prepared with different methods: (a)literature, (b)HT method.

Table 2. The BET Results of Different Catalysts

catalysts	BET surface area ($m^2 \cdot g^{-1}$)	Pore volume ($cm^3 \cdot g^{-1}$)	Average pore diameter (nm)
Ni_1Mo	105.8	0.23	7.6
Ni_2Mo	144.2	0.28	5.4
Ni_3Mo	158.9	0.31	8.9
$NiMo/Al_2O_3$	130.2	0.31	9.2

The HDS of DBT occurred through two parallel reactions: direct desulfurization (DDS) which yields biphenyl (BP) and desulfurization through hydrogenation (HYD) which gives cyclohexylbenzene (CHB). Most researchers think that BP is difficult to hydrogenation; hence the ratio of CHB/BP may denote the hydrogenation property of the catalyst. While on highly active catalysts, BP and CHB can be further hydrogenated into other products as shown in Figure 4. In this case, CHB/BP ratio can not be a good description of the hydrogenation activity of the catalyst. Therefore in this experiment we define total hydrogenation products (TH), namely, the sum of the further hydrogenation product of biphenyl and cyclohexyl benzene. For example, in Figure 4, TH= sum (2, 3, 4,...17). And TH/BP ratio may express the depth of hydrogenation catalyst activity.

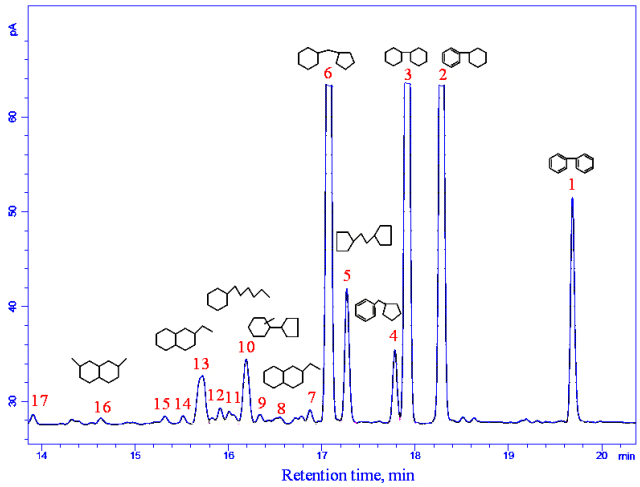

Figure 4. Gas chromatography of the DBT HDS products on Ni_2Mo catalyst at 280°C

Figure 5 shows the conversion of DBT, CHB/BP and TH/BP ratios on different catalysts at 280°C. The Ni_2Mo catalyst shows the highest DBT conversion, CHB/BP and TH/BP ratios, indicating the highly hydrogenation activity of this catalyst. Although the DBT conversion for Ni_1Mo is low, but the TH/BP ratio is high, its lower DBT conversion rate should be related with the smaller BET surface area and pore volume. The surface area and pore volume of Ni_3Mo catalyst are bigger than that of Ni_2Mo, but a smaller DBT conversion, CHB/BP and TH/BP ratios are showed on Ni_3Mo. The reason may be excessive Ni in Ni_3Mo to form an independent NiSx, whose hydrogenation activity is lower, thereby reducing the overall hydrogenation activity of the catalyst.

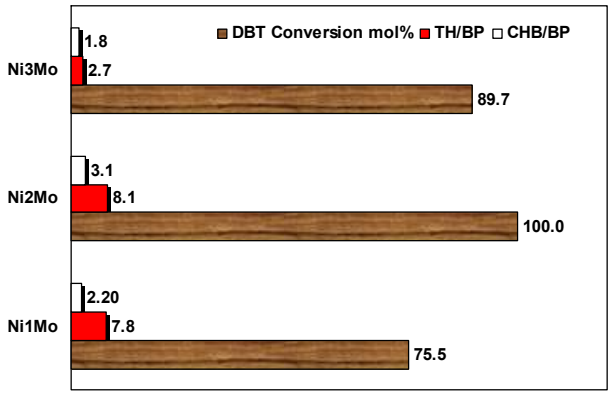

Figure 5. The conversion of DBT, CHB/BP and TH/BP ratios on different catalysts at 280°C

The conversion of DBT, CHB/BP and TH/BP ratios on Ni_2Mo at different temperatures are shown in Figure 6. With increasing reaction temperature, the TH/BP ratios have increased significantly, and the value has reached 23.4 at 300°C; but the CHB/BP ratios have not changed much. The reason is mainly due to the further hydrogenation of CHB and BP. Figure 7 shows the molar content of CHB and BP changes with the reaction temperature, from which we can clearly see that the decreasing trend of CHB is larger, indicating CHB is more easily be hydrogenated than BP.

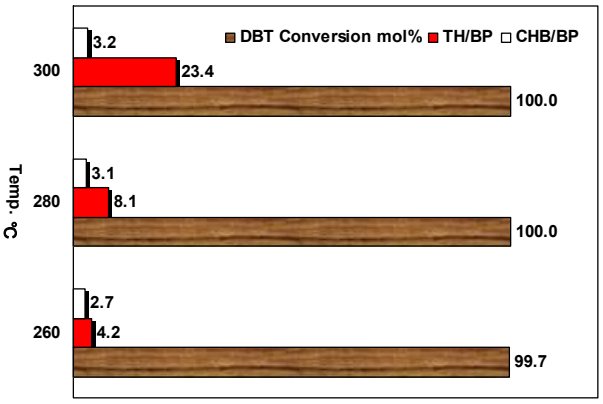

Figure 6. The conversion of DBT, CHB/BP and TH/BP ratios on Ni_2Mo at different temperatures.

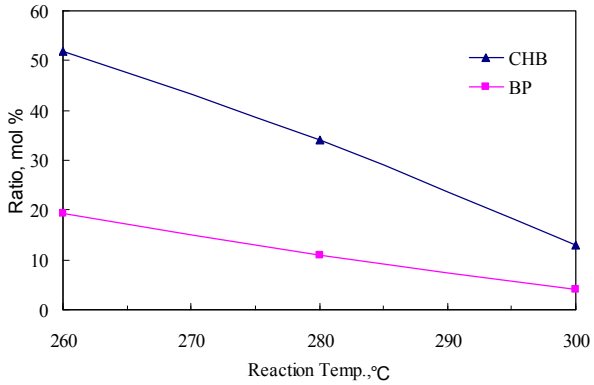

Figure 7. Contents of CHB and BP changes with the reaction temperature on Ni_2Mo.

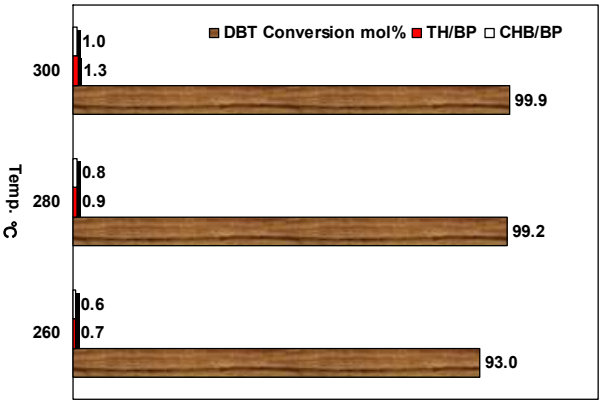

Figure 8. The conversion of DBT, CHB/BP and TH/BP ratios on $NiMo/Al_2O_3$ at different temperatures.

As a comparison, Figure 8 shows the conversion of DBT, CHB/BP and TH/BP ratios on **s**upported $NiMo/Al_2O_3$ catalyst. It can be seen from Figure 7, both DBT conversion rate and CHB/BP ratios increase with the increasing temperature. However, the CHB/BP ratio did not exceed 1.0 under the reaction temperature range, indicating the DBT HDS reaction through the DDS path is higher than the proportion of the path through the HYD on **s**upported $NiMo/Al_2O_3$ catalyst. At the same time, the TH/BP and the CHB / BP are almost the same rate, indicating only a small part of the product is further hydrogenated.

Conclusions

A series of porous sulfided bulk nickel molybdate catalysts with Ni/Mo ratios varying from 1 to 3 were prepared from the precursor of ammomium nickel molybdate and their activities for hydrodesulfurization (HDS) of dibenzothiophene (DBT) were evaluated. The experimental results reveal a significant improvement in the conversion of DBT for the bulk nickel molybdate catalyst compared to the $NiMo/Al_2O_3$ catalyst. The TH/BP ratio for the sulfided bulk nickel molybdate catalyst is 5-7 times larger than that for $NiMo/Al_2O_3$ catalyst, denoting the former has remarkably higher hydrogenation activities. The DBT conversion and the TH/BP ratio increase distinctly with the enhancement of reaction temperature. It can be concluded that the layered ammonium nickel molybdate will be a promising precursor of the highly active HDS catalyst for deep desulfurization of diesel fuel.

Acknowledgement. The National Key Fundamental Research Development Project of China (973 Project: No.2010CB226905). Financial support from PetroChina Corporation Limited is also greatly appreciated.

References

(1) Kabe T.; Ishihara A.; Tajima H. *Ind. Eng. Chem. Res.* **1992**, 31, 1577.
(2) Song C.; Ma X. *Appl. Catal. B* **2003**,41, 207.
(3) Babich I.V.; Moulijn J.A. *Fuel* **2003**,82, 607–631.
(4) Mazzocchia C.; Aboumrad C.; Diagne C. et al. *Catal. Lett.*, **1991**, 10, 181.
(5) Richardson, J. T. *Ind. Eng. Chem. Fundam.* **1964**, 3, 154.
(6) Brito, J. L.; Laine, J. *Appl. Catal.* **1991**,72, 113.
(7) Madeley, R. A.; Wanke, S. *Appl. Catal.* **1988**, 39, 295.
(8) Wivel, C.; Candia, R.; Clausen, B. S.; Topsøe, H. *J. Catal.* **1981**,68, 453.
(9) Levin D.; Soled S. L.; Ying J. Y. *Inorg. Chem.* **1996**, 35, 4191.
(10) Mazzocchia C.; DiRenzo F.; Aboumrad C.; Thomas G. *Solid State Ionics*, **1989**,32, 228.

Basic Properties of Supported Transition Metal Sulfides.

A. Travert,[1] V. Ruaux,[1] F. Maugé,[1] J.F. Paul.[2]*

1 - Laboratoire Catalyse et Spectrochimie, ENSICAEN – Université de Caen – CNRS, 6, Bd du Marechal Juin, 14050 Caen cedex, France

2 – Unité de Catalyse et Chimie du Solide – Université Lille 1 CNRS – 59650 Villeneuve d'Ascq cedex, France

Introduction

The catalytic activity of transition metal sulfides in hydrotreating reactions such as hydrodesulfurization (HDS) is usually related to their anionic vacancies (coordinatively unsaturated sites, CUS).[1] The structure and properties of these sites have been studied in-depth using chemisorption of probe molecules – in particular infrared spectroscopy of NO[2] and CO,[3] as well as *ab initio* or DFT modeling techniques.[4,5] By now, a clearer picture of these CUS sites has emerged from these studies, notably for Mo-based catalysts. Comparatively, little is known on the properties of sulfur atoms of the sulfide phase which are expected to play a key role in hydrogenation reactions (H_2 dissociation leading to SH groups, hydrogenation of adspecies…).

The aim of the present work was to specify the basic properties of supported sulfide phases. For this purpose, a series of supported sulfided phases (Mo, CoMo, Ru and Pt) was characterized using pyrrole (C_4H_4NH) and deuteriated chloroform ($CDCl_3$) as a probe molecules,[6] before and after sulfur removal by a hydrogen treatment. The sulfur basicity was assessed by comparing the corresponding infrared spectra with those obtained for solutions of $CDCl_3$ in organic sulfides: dimethyl disulfide (DMDS), dibutyl sulfide (DBS) and tetrahydrothiophène (THT). Finally, DFT calculations were carried out to model $CDCl_3$ adsorption on MoS_2 compared with the experimental IR spectra.

Experimental and Theoretical Methods

Catalysts were obtained by pore-filling impregnation of a γ-Al_2O_3 (258 m^2/g) and SiO_2 (350 m^2/g) supports with solutions of the appropriate salts. The samples were dried at 393 K overnight and calcined at 773 K for 3 h. The metal contents as determined by elemental analysis were 8.0 wt.% for Mo/Al_2O_3; 9.5 wt.% (Mo/Al_2O_3); 1.1 (Co) and 9.5 wt.% (Mo) for $CoMo/Al_2O_3$; 7.2 wt.% (Mo/SiO_2); 7.5 wt.% (Ru/SiO_2) and 11 wt.% (Pt/SiO_2).

Sulfidation was carried out in situ under flow of H_2S (100%) for Ru/SiO_2 or a H_2S/H_2 (10/90) mixture for the other catalysts at 623 K followed by evacuation. Adsorption of $CDCl_3$ was carried out at room temperature (RT). Calibrated doses of $CDCl_3$ were introduced in the IR cell up to an equilibrium pressure of 5 mbars. Adsorption of CO was carried out at low temperature (100 K) up to an equilibrium pressure of 1 mbar.

The IR spectra of $CDCl_3$/organic sulfide solutions were recorded using an ATR cell.

The DFT calculations were performed using the VASP software based on periodic density functional theory using the exchange correlation functional of Perdew and Zunger and a plane wave basis set. The calculations were performed using a 5 k points mesh, a cutoff energy of 550 eV and a convergence criterion 10^{-6} eV. The supercell contains two MoS_2 layers, four elementary MoS_2 units in the direction parallel to the surface and four in the direction perpendicular to the (100) surface, with a vacuum layer of 10 Å on top of it.

Results and discussion

Pyrrole adsorption. On Al_2O_3 and Mo/Al_2O_3 pyrrole adsorption leads to the appearance of broad and complex band in the 3600 – 2500 cm^{-1} range, mainly resulting from the formation of pyrrolate species ($C_4H_4N^-$) by dissociative adsorption of pyrrole on Al_2O_3.[6] The spectra obtained on Mo/Al_2O_3 did not show specific infrared bands that could result from pyrrole adsorption on the sulfide phase.

On SiO_2, pyrrole adsorption leads to a decrease of free SiOH groups and to the appearance of a broad νOH band centered at 3500 cm^{-1}. The pyrrole νNH vibration is located à 3474 cm^{-1}, close from that observed in diluted solution. These features are assigned to the formation of hydrogen bond from free silanol groups to the pyrrolic ring. No distinct features could be observed on the Mo/SiO_2 catalyst.

Chloroform adsorption. Adsorption of $CDCl_3$ on sulfided Al_2O_3 leads to a strong and broad νCD band extending from 2250 to 2200 cm^{-1}. This band characterizes the formation of hydrogen bonds between $CDCl_3$ and the basic sites of the Al_2O_3 support ($Cl_3CD\cdots O^{2-}$). Besides, however, supplementary bands characterizing $CHCl_3$ and formate species readily appeared. The latter species remained upon evacuation, which indicates that in our conditions $CDCl_3$ strongly reacts with the Al_2O_3 support. The possibility of chlorine deposition on the surface prevents a relevant assessment of basicity by $CDCl_3$ on Al_2O_3-based catalysts to be made.

The infrared spectra obtained upon $CDCl_3$ adsorption on SiO_2 and SiO_2 supported sulfide phase are reported on Figure 1. On all catalysts, $CDCl_3$ adsorption leads to a perturbation of the νOH band of free silanol groups (3742 cm^{-1}) and to the appearance of a broad ν(OH) band centered at 3680 cm^{-1}. The νOH frequency shift is close from that observed upon CCl_4 adsorption on SiO_2 and indicates the formation of a $SiOH\cdots Cl$ hydrogen bond. This assignment is in agreement with the position of the νCD band observed on SiO_2 (2264 cm^{-1}, Figure 1B, spectrum a) which is close from that observed in the gas phase. This clearly shows that $CDCl_3$ does not form $CD\cdots OH(Si)$ or $CD\cdots O^{2-}$ hydrogen bonds with the silica support.

Figure 1B shows that $CDCl_3$ adsorption on all supported sulfide catalysts (spectra b-e) leads to a supplementary νCD band at ~2235 cm^{-1}. This band is not observed on pure SiO_2 and characterizes the interaction of $CDCl_3$ with the sulfided phase.

The appearance of this band (2235 cm^{-1}) is totally reversible: $CDCl_3$ desorption upon evacuation at room temperature leads to the complete disappearance of this band.

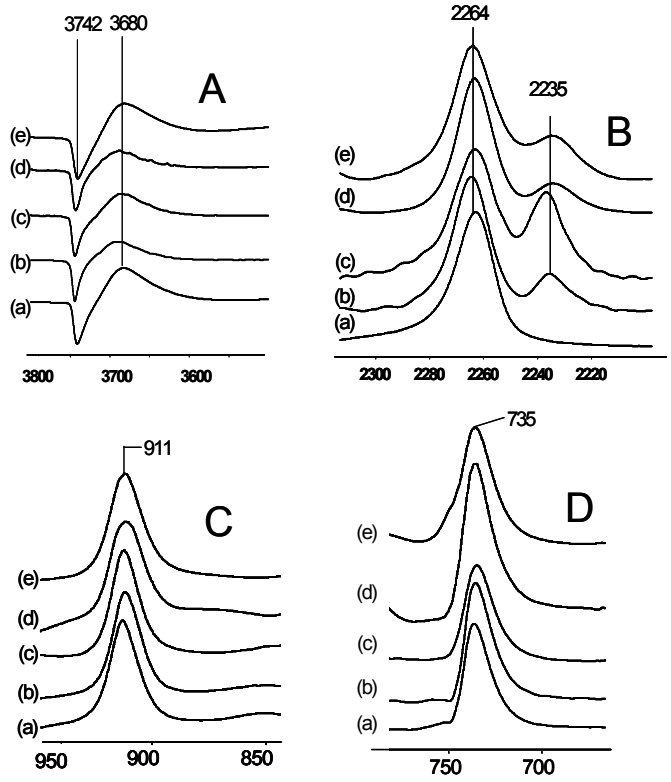

Figure 1 : Adsorption of $CDCl_3$ (5 mbars at equilibrium) on (a) SiO_2 ; (b) Mo/SiO_2 ; (c) $CoMo/SiO_2$; (d) Ru/SiO_2 ; (e) Pt/SiO_2. A: νOH vibration; B: νCD vibration; C: δCDvibration ; D: $\nu_{as}CCl_3$ vibration

δCD and νCCl vibration ranges, respectively. No strong differences between the spectra obtained on SiO_2 and on SiO_2 supported catalysts are observed. Moreover, no supplementary bands were observed on these catalysts, showing that in our conditions, no dissociative adsorption of $CDCl_3$ occurs on the sulfide phase.

Hence, the νCD band observed at 2235 cm^{-1} is related to the molecular adsorption of $CDCl_3$ on the supported phase of these catalysts. Similar experiments carried out on the oxidic form of these catalysts did not lead to the appearance of this band led and the IR spectra were almost identical to that observed on SiO_2. This allows one to exclude the assignment of the band at 2235 cm^{-1} to the adsorption of $CDCl_3$ on an oxysulfide phase. Thus, considering an adsorption on a fully sulfided phase, the band at 2235 cm^{-1} could result from either an interaction with the CUS sites or the formation of a hydrogen bond with the sulfur atoms of the sulfide phase.

Influence of sulfur coverage. Hydrogen treatments at 400°C (100 mbars, 1h) were carried out on Mo/SiO_2 and $CoMo/SiO_2$ in order to reduce the sulfur coverage of the sulfide phase[7] and to examine its influence on the adsorption of $CDCl_3$.

Figure 2 (left) shows the νCO spectra obtained after CO adsorption at low temperature (100 K) on Mo/SiO_2 and $CoMo/SiO_2$ before and after the hydrogen treatment. The band at 2157 cm^{-1} corresponds to CO adsorbed on the silanol groups of the support. The bands at 2115 and 2076 cm^{-1} are assigned to CO adsorbed on non-promoted Mo sites and promoted Co or Mo sites, respectively.[3] These spectra clearly show a strong increase of the amount of CUS sites after the hydrogen treatment due to a decrease of the sulfur coverage of the edges of $(Co)MoS_2$ phases. Figure 4 (right) shows the corresponding νCD spectra obtained $CDCl_3$ on the same catalysts. It clearly appears that the hydrogen-treatment leads to a strong decrease of the band at 2235 cm^{-1} and to the appearance of a new νCD component at 2255 cm^{-1}. This component increases with the number of CUS sites and its position close from that observed in the gas

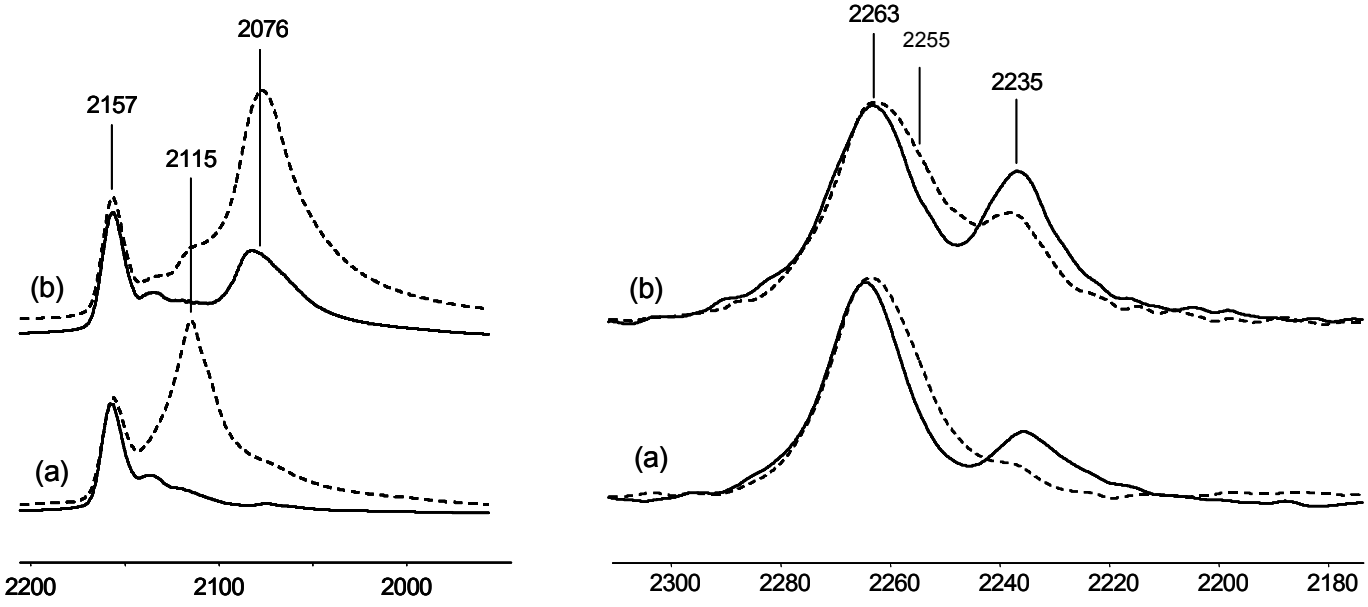

Figure 2 : Left : CO adsorption (1 mbar at equilibrium) on (a) Mo/SiO_2 and (b) $CoMo/SiO_2$ before (full lines) and after (dotted lines) H_2 treatment at 623K. Right : $CDCl_3$ adsorption (5 mbar at equilibrium) on (a) Mo/SiO_2 and (b) $CoMo/SiO_2$.

phase (Δν = -9 cm-1). It is thus assigned to $CDCl_3$ adsorbed through one of its a chlorine atoms on the CUS sites of the sulfide phase (Scheme 1A). On the other hand, the strong decrease of the intensity of the band at 2235 cm^{-1} allows to discard the assignment of this band to $CDCl_3$ adsorbed on CUS sites. This band is thus assigned to $CDCl_3$ adsorbed on sulfur atoms of the sulfide phase through hydrogen bond (Scheme 1B)

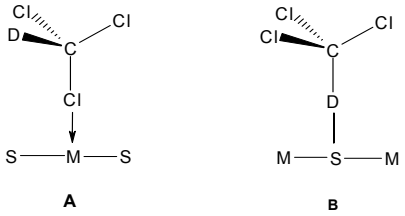

Scheme 1

Interaction of $CDCl_3$ with organic sulfides. While several studies have reported the adsorption of $CDCl_3$ on metal oxides or its interaction with oxygenated compounds through the formation of hydrogen bonds,[6] to our knowledge no study have characterized its interaction with sulfur atoms. In order to ascertain our assignment of the band at 2135 cm^{-1}, we have carried out a study of $CDCl_3$ with organic sulfides: dimethyldisulfide (DMDS), tetrahydrothiophène (THT) and dibutylsulfide (DBS). To this aim, IR spectra of $CDCl_3$ / organic sulfide solutions were recorded (not shown). In the presence of these molecules, we have evidenced the formation of a νCD band resulting from the formation of a hydrogen bond with this compounds at a frequency close from that observed on the sulfide catalysts: 2236 cm^{-1} for DMDS, 2232 cm^{-1} for THT and 2231 cm^{-1} for DMS. No such a band was observed in $CDCl_3$/alkane solutions, indicating that it results from the formation of a hydrogen bond with sulfur atom ($CCl_3D\cdots S$).

DFT Calculations. DFT calculations were carried out to model $CDCl_3$ adsorption on MoS_2. The starting surfaces were chosen as the stable MoS_2 edges obtained in our experimental conditions,[3,7] the M-edge consisting in 6-fold coordinated Mo atoms bridged with surface S atoms (M-edge, 4S), the S-edge consisting in tetrahedrally coordinated Mo atoms with either disulfide groups at high sulfur coverage (S-eddge, 8S) or bridged sulfur atoms lying alternatively on both sides of the Mo plane at low sulfur coverage (S-edge, 4S).

Figure 3 shows the adsorption geometry of $CDCl_3$ on the M-edge (4S) which is the dominating MoS_2 surface in our conditions of sulfidation.[7] It clearly evidences the formation of a hydrogen bond of $CDCl_3$ with a sulfur atom of this edge. Similar adsorption geometries were found on the two other MoS_2 surfaces.

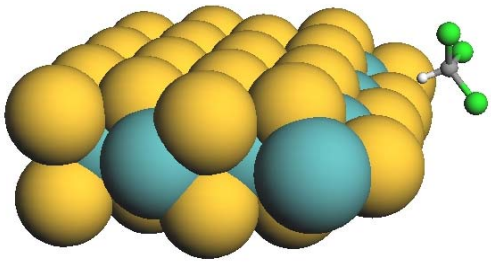

Figure 3: interaction of $CDCl_3$ with the M-edge (4S) of MoS_2

Table 1 reports the computed ΔνCD frequency shifts ($\Delta\nu CD = \nu CD_{ads} - \nu CD_{gas}$) and the sulfur-deuterium distances obtained for the various surfaces. These values clearly show that $CDCl_3$ forms hydrogen bonds with these surfaces, leading to ν (C-D) frequency shifts of 30-45 cm^{-1}, very close to those experimentally observed ($\Delta\nu CD = 31\ cm^{-1}$).

Table 1. Computed $CDCl_3$ adsorption Energies, νCD vibration frequencies and CD⋯S distances on MoS_2 edges.

MoS_2 Edge	ΔνCD / cm^{-1}	r(D⋯S) / pm
M-edge, 4S	-32	253
S-edge, 8S	-43	265
S-edge, 4S	-29	271

Assessment of sulfide phase basicity. The probe molecules used in this study, pyrrole (C_4H_4NH) and deuterated chloroform ($CDCl_3$) are classically used to characterize the basicity of metal oxides.[6] They present an N-H (or C-D) group of similar acidity, with deprotonation energies of 1500 and 1496 kJ mol^{-1}, respectively. They interact by hydrogen bond with basic centers, leading to a downward shift of the νNH (or νCD) frequencies which increases with the strength of the basic center.

These molecules adsorb dissociatively and non-dissociatively on Al_2O_3 and Al_2O_3 supported catalysts, leading to complex spectra and preventing any precise assessment of the supported sulfide phase basicity. Moreover, in the case of $CDCl_3$, chlorine deposition on the Al_2O_3 alumina support lead to strong modifications of the surface which in turn is likely to change the acid-base properties of the sulfide phase.[8] In any case, however, Al_2O_3-supported catalysts did not present significantly higher basicity than Al_2O_3, indicating that the basicity of the sulfide phase is much lower than that of Al_2O_3.

The dissociation on the support could be avoided by using SiO_2-supported catalysts. In the case of pyrrole, however, the formation of SiOH⋯ pyrrole hydrogen bonds leads to a broad νOH band which overlaps the νN-H band. This might explain why no clear differences were found between SiO_2 and SiO_2 supported catalysts.

Silanol groups also lead to hydrogen bond formation with the chlorine atoms of $CDCl_3$. In this case, however, the νCD vibration is located at a much lower frequency and does not overlap with other absorption bands. Moreover, $CDCl_3$ adsorbs non-dissociatively and reversibly on SiO_2 supported catalysts, thus allowing a reliable evaluation of the basicity of the sulfide phase.

$CDCl_3$ was found to form a hydrogen bond with the sulfur atoms of the sulfided phases, leading to a downward shift of ~ -31 cm^{-1}. Surprisingly, the nature of the sulfide phase (Mo, CoMo, Ru or Pt) does not significantly affect position of the ν(C-D) band indicating that sulfur basicity is not strongly affected by variations in sulfur-metal bond energies.[9] It should be noted, however, that $CDCl_3$ is not very selective with respect to moderate changes in sulfur basicity:[6] further work is certainly needed to characterize more finely the basicity these systems.

In any case, the νCD frequency shift observed on these catalysts clearly indicates that the sulfur atoms of the sulfide phase present a basic character which is confirmed by our DFT calculations. This frequency shift (31 cm^{-1}) is lower than that observed on classical basic catalysts. Thus, $CDCl_3$ adsorption on basic zeolites (NaY, KY, RbY and CsY) leads to νCD in the order of 40-60 cm^{-1}.[10]

Finally, the νCD band shift obtained on the supported sulfide phases is comparable to that observed for organic sulfides in solution, indicating that the basicity of these metal sulfides is close from that of these compounds which proton affinity lies in the range of 845±30 kJ mol^{-1} (DMDS: 815 kJ mol^{-1}, THT: 849 kJ mol^{-1} and DBS: 872 kJ mol^{-1}). These values indicate that sulfur basicity is weak. Such a weak basicity indicates that the dissociation of hydrogen on these surfaces should lead to acidic –SH groups, as suggested by DFT calculations[11] and previously observed by infrared spectroscopy[12,13] and recent STM studies.[14]

Conclusions .

This study reports the first characterization of the basic properties of supported sulfide phases (Mo, CoMo, Ru and Pt). While no basic sites are detected on the SiO_2 support alone, $CDCl_3$ adsorption on supported catalysts leads to the formation of a (C-D•••S) hydrogen bond which is clearly evidenced by a new νC-D band, downward shifted by ~31 cm^{-1} as compared to the gas phase. The formation of the hydrogen bond was confirmed by comparing these IR spectra with those obtained in $CDCl_3$-organic sulfide solutions and by modeling $CDCl_3$ by DFT, leading to computed νCD frequency shifts of 25-40 cm^{-1}, consistent with those experimentally observed. Such a νCD band indicates that the metal sulfides examined in the present study present a rather weak basicity and should lead to acid –SH groups upon hydrogen dissociation.

Acknowledgement.

We acknowledge Centre de Ressources Informatiques of Université Lille 1 for CPU time allocations.

References

(1) Topsoe, H.; Clausen, B. S.; Massoth, F. E. *Hydrotreating Catalysis, Sciences and Technology* Springer-Verlag: Berlin/New York, 1996.

(2) Topsøe, N.-Y.; Topsøe, H. *Journal of Catalysis* **1983**, *84*, 386-401.

(3) Travert, A.; Dujardin, C.; Mauge, F.; Veilly, E.; Cristol, S.; Paul, J. F.; Payen, E. *Journal of Physical Chemistry B* **2006**, *110*, 1261-1270.

(4) Raybaud, P. *Applied Catalysis A: General* **2007**, *322*, 76-91.

(5) Paul, J.-F.; Cristol, S.; Payen, E. *Catalysis Today* **2008**, *130*, 139-148.

(6) Lavalley, J. C. *Catalysis Today* **1996**, *27*, 377-401.

(7) Travert, A.; Dujardin, C.; Mauge, F.; Cristol, S.; Paul, J. F.; Payen, E.; Bougeard, D. *Catalysis Today* **2001**, *70*, 255-269.

(8) Maugé, F.; Crepeau, G.; Travert, A.; Cseri, T. *ACS Preprint, Fuel Chemistry Division* **2003**, *48*, 131.

(9) Toulhoat, H.; Raybaud, P.; Kasztelan, S.; Kresse, G.; Hafner, J. *Catalysis Today* **1999**, *50*, 629-636.

(10) Scokart, P. O.; Rouxhet, P. G. *J.Chem.Soc., Farad.Trans. 1* **1980**, *76*, 1476.

(11) Travert, A.; Nakamura, N.; van Santen, R. A.; Cristol, S.; Paul, J.-F.; Payen, E. *Journal of American Chemical Society* **2002**, *124*, 7084-7092.

(12) Topsoe, N. Y.; Topsoe, H. *Journal of Catalysis* **1993**, *139*, 641-651.

(13) Travert, A.; Maugé, F. *Studies in Surface Science and Catalysis* **1999**, *127* 269-277

(14) Temel, B.; Tuxen, A. K.; Kibsgaard, J.; Topsøe, N.-Y.; Hinnemann, B.; Knudsen, K. G.; Topsøe, H.; Lauritsen, J. V.; Besenbacher, F. *Journal of Catalysis*, *In Press, Corrected Proof*.

Criterion CENTERA® Hydroprocessing Catalysts: Improved Active Site Architecture Provides Improved ULSD HDS Activity

John A. Smegal[(a)], Thomas T. Weber[(b)], & Lawrence (Larry) S. Kraus[(c)]

[(a)]Criterion Catalysts & Technologies, Westhollow Technology Center, 3333 Highway 6 South, Houston, Texas 77082, USA
[(b)]Shell Global Solutions International B.V., Shell Technology Centre Amsterdam, Grasweg 31, 1031 HW Amsterdam, The Netherlands
[(c)]Criterion Catalysts & Technologies, 16825 Northchase Drive, Suite 1000, Houston, Texas 77060, USA

Abstract

Criterion CENTERA® hydroprocessing catalysts provide substantial activity improvements over current state-of-the-art hydroprocessing catalysts. CENTERA® catalysts are Type II catalyst grades (NiMo – DN-3630, CoMo – DC-2618). Pilot plant results are presented showing that CENTERA® catalysts achieve 2 – 20ºF (1 – 11ºC) Ultra Low Sulfur Diesel Hydrodesulfurization (ULSD HDS) activity improvements over previous generations of commercial hydrotreating catalysts. Characterization of DN-3630 using Transmission Electron Microscopy (TEM), Extended X-Ray Absorption Fine Structure (EXAFS), and Fourier Transform Infrared (FTIR)/Nitric Oxide (NO) Adsorption shows that these activity improvements are achieved from improved active metals dispersion, complete Mo sulfidation/Mo-S coordination, and enhanced promoter metal (Ni) utilization (enhanced Ni edge decoration).

Introduction

CENTERA® catalysts are the newest family of commercial hydrotreating catalysts from Criterion Catalysts & Technologies and are available in NiMo (DN-3630) and CoMo (DC-2618) versions for Ultra Low Sulfur Diesel Hydrodesulfurization (ULSD HDS) applications. CENTERA® catalysts are more active for ULSD HDS than previous generations of Criterion catalysts. This paper presents catalyst characterization data illustrating the differences between CENTERA® catalysts and previous catalyst families and identifying the source of the improved CENTERA® activity. Pilot plant testing data is presented showing the CENTERA® ULSD HDS activity improvements over other commercial catalysts in low and high pressure operation.

Catalyst Characterization

Commercial CENTERA® DN-3630 catalyst was characterized using Transmission Electron Microscopy (TEM), Extended X-Ray Absorption Fine Structure (EXAFS), and Fourier Transform Infrared (FTIR)/Nitric Oxide (NO) Adsorption. TEM and EXAFS analyses indicate a reduction of average metal particle size from the 4.5 nm and 3.5 nm values measured for Criterion CENTINEL and CENTINEL GOLD NiMo Type II commercial catalysts, respectively, to 2.5 – 3.5 nm for CENTERA® catalysts. The TEM images for these three catalyst systems are shown in Figure 1.

CENTERA® L_{avg}, nm = 3.5; n_{avg} = 1.5 to 2.1

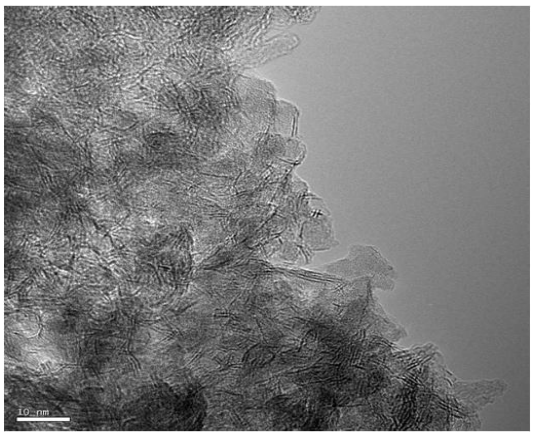

Centinel Gold: L_{avg} ,nm = 3.5; n_{avg} = 1.5 to 1.6

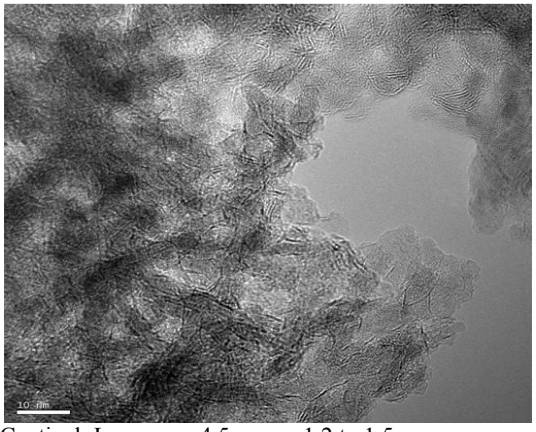

Centinel: L_{avg} ,nm = 4.5; n_{avg} = 1.2 to 1.5

Figure 1. CENTERA®, Centinel Gold, and Centinel Catalyst TEM Images

Transmission Electron Microscopy (TEM) measurements were done at the Technical University of Delft (The Netherlands). All samples were rigorously kept under inert atmosphere to avoid exposure to air during sample preparation and transfer to the microscope. Quantification of the slab length (L_{avg}) and degree of stacking (n_{avg}) of the slabs was performed by examining about 400 individual slabs per sample. For each parameter an average value was determined for each sample.

Evaluation of the CENTERA® TEM image shows that the sample consists of supported (75%) and unsupported (25%) domains, each having particle sizes around 3.5 nm. The average degree of stacking is 1.5 for the supported particles and 2.1 for the unsupported particles. Similar analyses of the CENTINEL GOLD and CENTINEL TEM images yield average particle sizes of 3.5 nm and 4.5 nm, respectively. The average degree of stacking has also increased with subsequent generations of catalysts indicative of the increased Type II character achieved with each new generation.

The extent of the Mo-S interactions can be detailed utilizing EXAFS. The Mo K edge full EXAFS spectra of the catalyst samples studied were measured at the SuperXAS beamline of SLS at the Paul Scherrer Institute (PSI), Villigen, Switzerland. The inset in Figure 2 displays the Fourier Transform of the respective *X* functions.

The first shell at about 2 Å is due to Mo-S contributions. It is identical with that of bulk MoS_2 and corresponds to the ideal coordination number (CN) of 6, i.e. every Mo center is surrounded by 6 sulfur atoms in a trigonal prismatic fashion. Correspondingly,

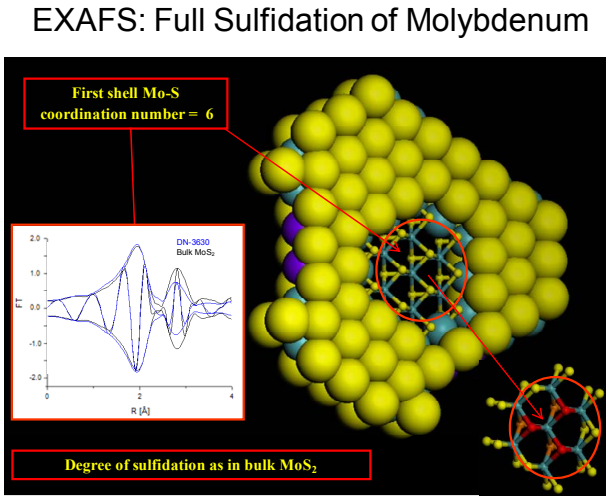

Figure 2. EXAFS Analysis of CENTERA® DN-3630 and Bulk MoS_2

Mo-S distances (R) in sulfided DN-3630 are very close to that of 2H-MoS_2 (2.415 Å). The second shell is due to Mo-Mo contributions and reflects a coordination number of 4.4 (6.0 in 2H-MoS_2). Again, the corresponding Mo-Mo distances are comparable and close to the original value of 3.16 Å. Using the size-correlation correction as suggested by Shido and Prins[(1)], the diameter of the MoS_2 slabs in DN-3630 can be determined to be ~2.5 nm. This compares favorably to the average diameter of 3.5 nm determined from TEM.

FTIR analysis of NO adsorption on DN-3630 and a CENTINEL NiMo catalyst was used to characterize the surface of the catalysts in their sulfided states. The N-O stretching vibrational frequency of NO adsorbed on hydrotreating catalysts shows characteristic differences when adsorbed on Ni, Co, or Mo. Figure 3 shows the depiction of the MoS_2 edge surfaces using molecular models based on the interpretation of the FTIR spectra of NO adsorbed on sulfided DN-3630 and CENTINEL NiMo catalysts.

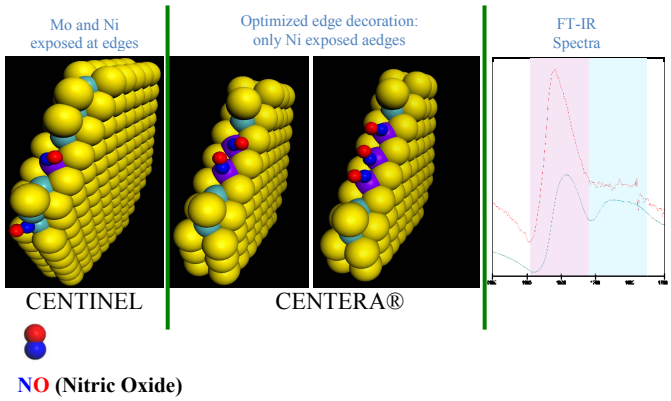

Figure 3. CENTERA® DN-3630 and Centinel NiMo NO Adsorption FTIR Spectra

The DN-3630 spectrum (top spectrum) shows that only coordinately unsaturated Ni centers are present on the edge of DN-3630 active metal particles as indicated by the single peak indicative of NO adsorbed on nickel (pink area) and the lack of a peak indicative of NO adsorbed on Mo (blue area) as found in the CENTINEL NiMo spectrum (bottom spectrum).

This finding leads to the conclusion that the edge surface of sulfided DN-3630 only contains coordinatively unsaturated Ni and does not contain any coordinatively unsaturated Mo. This is in contrast to the spectrum observed with CENTINEL NiMo that shows measureable NO adsorption on unsaturated Mo and therefore less efficient edge decoration of the MoS_2 crystallites with the promoter nickel.

In addition, an unusually high N-O stretching vibration associated with the nickel edge in DN-3630 suggests unique new surface structural properties as compared to CENTINEL. DFT molecular modeling calculations indicate that this shift to higher frequency can be explained by the presence of two to three adjacent unsaturated Ni centers (see Figure 3). It is the full presence of these specific active structures and the absence of less active unsaturated Mo-based edge structures that is believed responsible for the increased activity of the CENTERA® catalyst compared to the CENTINEL catalyst.

These FTIR/NO Adsorption experiments utilized a specially designed IR cell allowing for in-situ sample preparation, sulfiding, and analysis. NO Spectra were measured with a high resolution spectrometer, equipped with an MCT detector. Final stated results are based upon 1000 individual scans, to improve signal-to-noise ratios.

Catalyst Activity Testing

Low Pressure Pilot Plant Testing. Low pressure (300 – 600 psig, 21 – 41 barg) hydrodesulfurization (HDS) testing of DC-2618 was performed using Middle East Straight Run Gas Oil (ME SRGO), Americas (AM) SRGO, ME SRGO/Light Coker Gas Oil (SRGO/LKGO), and AM SRGO/Light Cycle Oil (SRGO/LCO) feeds and compared to results obtained with a reference conventional CoMo (REF CoMo), a high activity conventional CoMo (HAC CoMo), and a CENTINEL CoMo (CENTINEL CoMo). All tests were performed in a downflow, isothermal reactor. The objectives of this test were to determine the temperature requirements for each catalyst to achieve product S = 10 wppm and product N = 5 wppm. The properties of the test feeds are found in Table 1.

Table 1. DC-2618 Pilot Plant Test Feeds Properties

Properties	ME SRGO	AM SRGO	ME SRGO / LKGO	AM SRGO/ LCO
API Gravity (°)	36.9	34.5	33.9	29.7
Density (g / cc)	0.8413	0.8535	0.8563	0.8788
Total Sulfur (wppm)	11400	17100	19300	13900
Total Nitrogen (wppm)	52	276	430	377
Br Number (g / 100 g)	3	6	13	5
UV Aromatics (wt%)				
Mono-	5.25	5.83	6.56	6.04
Poly-	5.24	6.17	6.68	15.95
Total	10.49	12.00	13.24	21.99
D-2887 Distillation (ºF / ºC)				
90 wt%	649 / 343	652 / 344	651 / 344	672 / 356
FBP	707 / 375	776 / 413	811 / 433	841 / 449

The process conditions used in these tests are shown in Table 2. These process conditions were chosen to replicate the process conditions used in actual commercial hydrotreating operations.

Table 2. DC-2618 Pilot Plant Test Conditions

Test	1	2	3	4
Feed	ME SRGO	AM SRGO	ME SRGO / LKGO	AM SRGO / LCO
Pressure (psig / barg)	300 / 21	435 / 30	600 / 41	600 / 41
LHSV (hr^{-1})	0.50	0.70	0.80	0.75
H_2 Feedrate (SCFB / Nl/l)	1200 / 202	1200 / 202	2000 / 336	2000 / 336

The hydrodesulfurization (HDS) and hydrodenitrogenation (HDN) results with the various catalysts tested are shown in Tables 3 and 4, respectively. The data in these tables is presented as the reduction in the temperature requirement to achieve product S = 10 wppm and product N = 5 wppm with the various catalysts tested using REF CoMo as a reference. For example, when processing the ME SRGO feed under the process conditions specified in Table 2, DC-2618 had a 20ºF (11ºC) lower temperature requirement than REF CoMo to achieve product S = 10 wppm. The data in these tables are presented graphically in Figures 4 and 5. H_2 consumption data for the catalysts tested are shown in Table 5.

Table 3 and Figure 4 show the relative temperature requirements of the catalysts tested to achieve product S = 10 wppm with the four test feeds. From this data it is seen that DC-2618 has 7 - 20ºF (4 - 11ºC) greater activity than REF CoMo, 2 - 12ºF (1 - 7ºC) greater activity than HAC CoMo, and 8 - 12 ºF (4 - 7ºC) greater activity than CENTINEL CoMo for the feed and process conditions employed. This additional ULSD HDS activity allows for several possible commercial processing advantages, such as increasing unit throughput, extending unit cycle length, or processing more difficult feeds.

Table 3. DC-2618 Pilot Plant Test Results Temperature Requirements: Product S = 10 wppm

Test	1	2	3	4
Catalyst	ΔTemperature Requirement: Product S = 10 wppm (ºF / ºC)			
REF CoMo	Base	Base	Base	Base
HAC CoMo	8 / 4	6 / 3	5 / 3	4 / 2
CENTINEL CoMo	8 / 4	2 / 1	-2 / -1	2 / 1
CENTERA® DC-2618	20 / 11	10 / 6	7 / 4	10 / 6

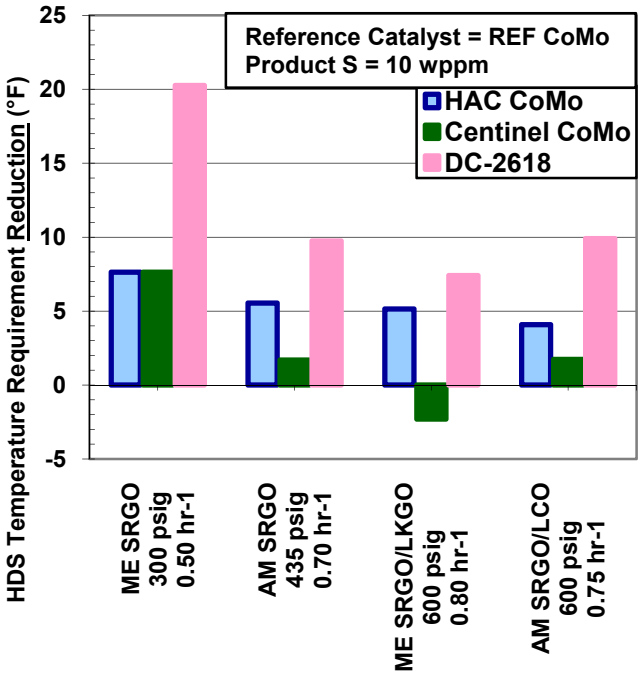

Figure 4. DC-2618 Pilot Plant Test Results Temperature Requirements: Product S = 10 wppm

The relative temperature requirements for achieving product N = 5 wppm are shown in Table 4 and Figure 5. Here it is seen that DC-2618 has higher HDN activity than REF CoMo, HAC CoMo, and CENTINEL CoMo by 11- 23ºF (6 - 13ºC), 7 - 24ºF (4 - 13ºC), and 2 - 17ºF (1 - 9ºC), respectively. This substantial improvement in HDN activity makes DC-2618 more effective at removing the nitrogen molecules that function as catalyst inhibitors and limit ULSD HDS activity/performance[2,3]. Also, the higher HDN activity of DC-2618 make it more robust to processing higher nitrogen content or higher endpoint feeds.

Table 4. DC-2618 Pilot Plant Test Results
Temperature Requirements: Product N = 5 wppm

Test	1	2	3	4
Catalyst	ΔTemperature Requirement: Product N = 5 wppm (ºF / ºC)			
REF CoMo	Base	Base	Base	Base
HAC CoMo	-1 / ~-1	4 / 2	4 / 2	-2 / -1
CENTINEL CoMo	6 / 3	6 / 3	3 / 2	12 / 7
CENTERA® DC-2618	23 / 13	11 / 6	12 / 7	14 / 8

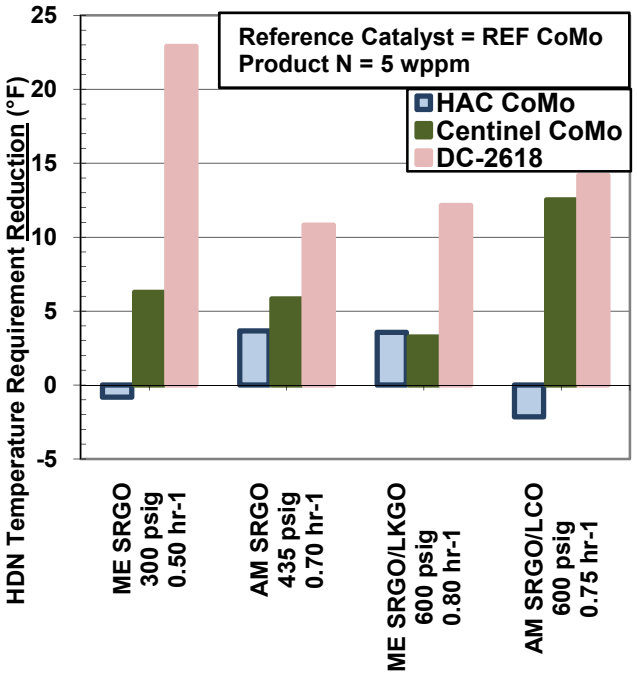

Figure 5. DC-2618 Pilot Plant Test Results Temperature Requirements: Product N = 5 wppm

Table 5 contains the H_2 consumption data associated with producing S = 10 wppm product. The H_2 consumptions with the ME SRGO/LKGO and AM SRGO/LCO straight run/cracked stock feed blends are substantially higher than those observed with the ME SRGO and AM SRGO feeds because of the higher olefin and aromatics contents of these straight run/cracked stock blends. The data in Table 5 show that the DC-2618 ULSD HDS activity improvements over previous generations of CoMo catalysts are achieved with a 0 – 14% increase in H_2 consumption when processing straight run feeds and a 4 – 9% increase in H_2 consumption when processing straight run/cracked feed blends. Since the most efficient route for ULSD HDS production is through the indirect HDS mechanism that involves saturation of an aromatic ring in refractory (sterically hindered) sulfur species[4-9] an increase in overall H_2 consumption is expected to accompany and is consistent with higher ULSD HDS activity.

Table 5. DC-2618 Pilot Plant Test Results
H_2 Consumption: Product S = 10 wppm

Test	1	2	3	4
Catalyst	H_2 Consumption: Product S = 10 wppm (SCFB / Nl/l)			
REF CoMo	175 / 30	270 / 46	435 / 73	510 / 86
HAC CoMo	180 / 30	295 / 50	435 / 73	520 / 88
CENTINEL CoMo	180 / 30	285 / 48	430 / 73	535 / 90
CENTERA DC-2618	200 / 34	295 / 50	465 / 78	555 / 94

High Pressure Pilot Plant Testing. High pressure (1050 psig, 72 barg) HDS testing of DN-3630 was performed using a SRGO/LCO/LKGO (50/25/25 – Volume % Basis) feed blend. The results of this test were compared with an identical test using CENTINEL GOLD DN-3330 (NiMo Type II Catalyst). The properties of the feed blend tested are shown in Table 6.

The process conditions used are shown in Table 7. The processing objective of these tests was to achieve product S = 8 wppm. These tests were run for an extended duration (~1500 hours) to compare the stability of the two catalysts. All tests were performed in a downflow, isothermal reactor.

Table 6. DN-3630 Pilot Plant Test Feed Properties

Properties	SRGO / LCO / LKGO Blend (50 / 25 / 25 – Volume % Basis)
API Gravity (°)	28.4
Density (g / cc)	0.8849
Total Sulfur (wppm)	19900
Total Nitrogen (wppm)	634
Br Number (g / 100 g)	15
UV Aromatics (wt%)	
Mono-	7.04
Poly-	15.38
Total	22.42
D-2887 Distillation (ºF / ºC)	
90 wt%	669 / 354
FBP	839 / 448

Table 7. DN-3630 Pilot Plant Test Conditions

Test	1
Feed	SRGO / LCO / LKGO Blend (50 / 25 / 25 – Volume % Basis)
Pressure (psig / barg)	1050 / 72
LHSV (hr^{-1})	1.0
H_2 Feedrate (SCFB / Nl/l)	4000 / 672

The feed processed in this test is a high sulfur, high nitrogen, high aromatics feed and is representative of the more difficult feeds processed by many U.S. refiners to produce ULSD. The pressure used in this study is at the low end of the range of unit pressures (1000 – 1300 psig, 69 – 90 barg) typically employed for processing these types of feed. A space velocity of 1.0 is typical for these units. NiMo catalysts are typically used in these applications to maximize HDN activity and utilize the high pressure of the units for maximum aromatic saturation and ULSD HDS performance. The results of this study are shown in Figure 6.

These data show a ~12ºF (~7ºC) advantage for DN-3630 over DN-3330 in the steady state operation period (1100 – 1500 hrs). Periodic checks of the H_2 consumption for both catalysts were within 5% of each other (insignificant). With the DN-3630 catalyst the H_2 consumption ranged from 870 – 950 SCFB (145 – 160 Nl/l) over the course of the testing period. These data demonstrate that the activity improvements of CENTERA® DN-3630 over previous generations of high activity NiMo ULSD catalyst are achieved without a sacrifice in stability or a significant increase in H_2 consumption.

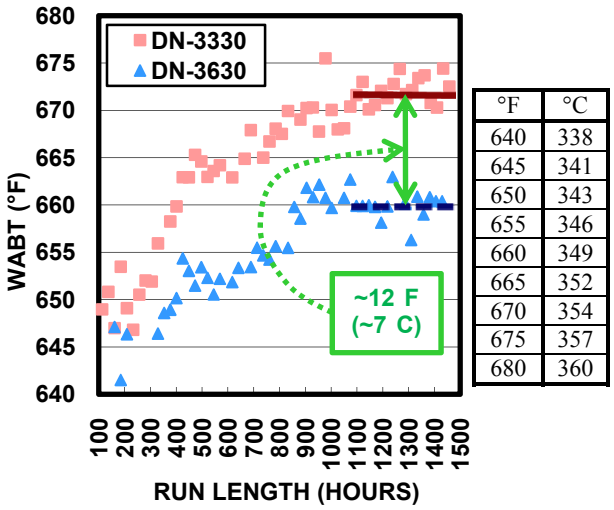

°F	°C
640	338
645	341
650	343
655	346
660	349
665	352
670	354
675	357
680	360

Figure 6. Comparison of DN-3630 and DN-3330 ULSD HDS Activities: SRGO/LCO/LKGO Feed Blend

Conclusions

Criterion CENTERA® catalysts show significant, up to 20°F (11°C), ULSD HDS activity improvements over previous generations of catalysts in both low (300 – 600 psig, 21 – 41 barg) and high pressure (1050 psig, 72 barg) testing. These activity improvements are accompanied by only modest increases in H_2 consumption: 0 – 14%. CENTERA® catalysts achieve greater ULSD HDS activity than previous generations of catalysts while maintaining catalyst stability. TEM, EXAFS, and FTIR/NO Adsorption experiments show that these improvements are due to increased active metal dispersion, complete Mo sulfiding/Mo-S coordination, and more efficient decoration of the active sites with coordinately unsaturated promoter atoms.

Acknowledgements. Nick Flinn, CRI/Criterion Ltd., Fareham, UK; Alexei Gabrielov, CRI/Criterion, Inc., Westhollow Techology Center, Houston, USA; Sal Torrisi, Criterion Catalysts & Technologies, Two Greenspoint Plaza, Houston USA

References

(1) Shido, T. and Prins, R., *J. Phys. Chem B,* **1998,** *102*, 8426.
(2) Ho, T.C., *Catalysis Today*, **2004**, *98*, 3.
(3) Koltai, T., Macaud, M. Guevara, A., Schulz, E. Lemaire, M., Bacaud, R. and Vrinat, M., *Applied. Catalysis. A: General*, **2002**, *231*, 253.
(4) Froment, G.F., Depauw, G.A. and Vanrysselberghe, V., *Ind. Eng. Chem. Res.,* **1994**, *33*, 2975.
(5) Kabe, T., Ishihara, A. and Qian, W., *Hydrodesulfurization and Hydrodenitrogenation*, Kodansha Ltd./Wiley-VCH, Tokyo/Weinheim, 1999.
(6) Prins, R., in: G. Ertl, H. Knözinger, F. Schüth, and J. Weitkamp (Eds.), *Handbook of Heterogeneous Catalysis, 2nd Edition, Volume 6,* Wiley-VCH, Weinheim, 2008, pp. 2695.
(7) Egorova, M. and Prins, R., *J. Catal*., **2004**, *225*, 417.
(8) Li, X., Wang, A., Egorova, M., and Prins, R., *J. Catal.,* **2007**, *250*, 283.
(9) Wang, H. and Prins, R., *J. Catal.,* **2009**, *264*, 31.

THE SUPPORT EFFECT IN HYDRODEOXYGENATION

D. Laurenti, C. Geantet

Institut de Recherches sur la Catalyse et l'Environnement de Lyon (IRCELYON), UMR 5256 CNRS-Université Lyon 1
2 avenue A. Einstein, 69626, Villeurbanne, France.

Introduction:

The need to reach lower sulphur content in fossil fuels has induced a lot of studies devoted to a better understanding of hydrotreating catalysts. The most commonly used HDT catalysts are NiMoS or CoMoS phases supported on γ-alumina. The different key parameters to improve the performances of these systems are the nature of the active phase, the nature of the support, the method of preparation and sulfidation, and also the use of additives. The support effect associated with HDT catalysts has been deeply studied especially in hydrodesulfurization (HDS) [1,2]. Among the possible oxides, titania and zirconia supports were intensively investigated in order to understand the promoting effect obtained for CoMo catalysts which was still lower on these carriers than over γ-alumina although the unpromoted counterparts were much more active when supported on titania and zirconia [3,4,5]. Nowadays, second generation bio-fuels coming from ligno-cellulosic biomass are expected to afford a solution to the increasing demand for fuel. The bio-oils obtained from biomass liquefaction need to be deoxygenized in order to be compatible with conventional fuels and this upgrading can be realized by hydrodeoxygenation (HDO) process [6]. CoMoS and NiMoS supported catalysts which have been found to be efficient for HDO are also interesting because of the possibility to co-process bio-oil together with gas-oil [7]. However, among the different studies undertaken in this area [8,9,10] the support effect over the performance of the catalysts in HDO reaction and in HDO/HDS competition reaction has never been clearly evidenced. In this work, a model reaction of HDO has been carried out with supported CoMoS catalysts in order to evaluate the support effect in this reaction, complementary to the study on promoting effect realized previously. In relation with HDS studies, zirconia and titania appeared as good candidates to be evaluated in HDO and compared to γ-alumina. Guaiacol (GUA) has been chosen as model reactant representative of the O-compounds coming from ligno-cellulosic biomass.

The reaction scheme of the GUA transformation involved several steps (Figure 1): the conversion of GUA to catechol (CAT) by demethylation (DME) or the direct transformation of GUA into phenol (PHE) and methanol by demethoxylation (DMO). Starting from PHE, two routes have to be considered: a direct deoxygenation (DDO) to form benzene or a hydrogenation (HYD) to form cyclohexene and then cyclohexane. When GUA is converted into CAT, the positively charged eliminated methyl group can be further involved in a methyl substitution on the aromatic ring to form a new family of methyl-products. This-side reaction principally occurred with supports and does not need the presence of metallic phase [11]. Starting from PHE, a direct analogy can be made with HDS of (benzo)thiophenic compounds transformed via two main routes: DDS and HYD. Considering the results obtained with the three catalytic systems a novel reaction scheme has been proposed for each of them.

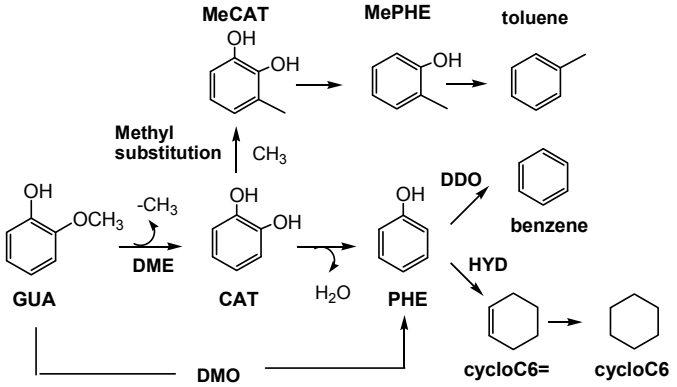

Figure 1. General GUA HDO reaction scheme

Experimental:

Catalysts: The catalysts were prepared by classical incipient wetness co-impregnation method with aqueous solutions of $NH_4Mo_7O_{24}.4H_2O$ and $Co(NO_3)_2.6H_2O$. The alumina used is γ-type with 200 m^2/g surface area. Zirconia and titania are commercial supports (Norpro, Saint-Gobain) with a surface area of 120 m^2/g and 100 m^2/g respectively. The supports were crushed and sieved to 80-125 μm size before impregnation. After impregnation and maturation overnight, the solids were dried at 383K under vacuum condition for 3h and calcined at 773K for 3h under air flow (4 L/h). Before each catalytic experiment, the catalysts were sulfided ex-situ under H_2S/H_2 15% (v/v) flow at 673K for 4h (10K/min, flow rate: 4L/h). At the end of the sulfidation, the catalysts were cooled down under nitrogen flow and stored under argon to avoid any oxydation.

Catalysts characterization: For each support, the loading of CoMo has been optimized in order to avoid $CoMoO_4$ and MoO_3 in oxidic phase. Several preparations have been made increasing the loading of Mo and Co with the atomic ratio Co/(Co+Mo) still equal to 0.3, and for all the systems, the appearance of $CoMoO_4$ and MoO_3 has been controlled by Raman spectroscopy mapping. Textural and elemental analyses of the catalytic systems have been undertaken, as well as High Resolution Electronic Microscopy (HREM) and X-ray Photoelectron Spectroscopy (XPS). The main characteristics of the catalysts used in this work are summarized in Table 1. From XPS and TEM (not given), we can observed that the dispersion, the slabs dimensions, or the sulfidation state for the three catalysts were quite similar. The stacking and length of the slabs for $CoMoS/TiO_2$ compared to the others systems were found slightly smaller (2.5 nm and 2.1 respectively) in accordance with previously published results. Isopropanol dehydration has been carried out to evaluate the acidity of the supports which decreased in the order: $\gamma\text{-}Al_2O_3 > TiO_2 > ZrO_2$.

Table 1. Main characteristics of the catalysts

Catalysts	Mo at/nm^2	BET m^2/g	Co/(Co+Mo)
$CoMoS/\gamma\text{-}Al_2O_3$	2.7	190	0.29
$CoMoS/TiO_2$	4.1	90	0.31
$CoMoS/ZrO_2$	3.7	112	0.29

Catalytic evaluation: The catalytic experiments were carried out in a fixed bed tubular reactor equipped with a Pyrex envelope. The

operating conditions were chosen in order to avoid any diffusion limitations. The temperature of the reaction was 573K and the total pressure of hydrogen was 4MPa. The reactant (GUA) was introduced with H_2 through a saturator/condenser system at a partial pressure of 2,67 kPa. Hydrogen sulfide (H_2S) was added to reach a partial pressure of 400 Pa (100 ppm) in order to maintain the catalyst in a sulfided state during HDO reaction. The total flow was varied between 50 and 500 ml/min. Catalytic activities were measured at steady state after 12 hours on stream. The accuracy of catalytic activity determination is better than 10%. The products were analyzed online by gas chromatography HP 5890 equipped with a flame ionization detector (FID) with CP-Sil5 capillary column (50 m x 0.32 mm x 5 μm). All the products have been identified by GC-MS.

Results and discussion:

Many compounds were formed during the transformation of Guaiacol (GUA) in the described conditions. With the three catalytic systems the appearance of products in function of the total conversion has been measured and displays an image of the reaction scheme. The intrinsic reaction rates calculated for total GUA conversion ($ri_{(GUA)}$) showed that the $CoMoS/ZrO_2$ catalyst was very efficient compared to the two other systems since the total conversion rate reached a value 7-times higher (Table 2). However, some products were not deoxygenated like catechol (CAT), Phenol (PHE) and to have a more precise idea of the deoxygenation performances, an intrinsic HDO rate has been calculated $ri_{(HDO)}$ per Mo atom. $CoMoS/ZrO_2$ was also found to be the most active catalyst for deoxygenation as $ri_{(HDO)}$ was 6 times higher than for the two others catalysts. Such a difference in catalytic activity per Mo atom between CoMo catalysts supported on titania, alumina and zirconia has never been reported previously in HDT. It should be noted that for the considered three catalysts the sulfidation state and the dispersion observed with XPS and HREM can not explain the different performances.

The selectivity found for the three catalytic systems showed that different pathways have to be considered for each catalytic system. The reaction scheme could be analyzed in two steps: the first is the GUA conversion to CAT and PHE, the second is the conversion of PHE to O-free compounds

Table 2. Total and deoxygenation intrinsic rates in GUA HDO over ZrO_2, TiO_2 and Al_2O_3-supported CoMo catalysts

Catalysts	$ri_{(GUA)}\ 10^{-4}$ molec.Mo $at^{-1}.s^{-1}$	$ri_{(HDO)}10^{-4}$ *molec.Mo* $at^{-1}.s^{-1}$
$CoMoS/\gamma\text{-}Al_2O_3$	93	*7.8*
$CoMoS/TiO_2$	131	*12.6*
$CoMoS/ZrO_2$	*736*	*65.0*

For alumina-supported catalyst, CAT and PHE appeared as the primary products of GUA conversion followed by methyl-catechol (Me-CAT) and methyl-phenol (Me-PHE). Then from phenol or Me-PHE, DDO and HYD were observed leading to benzene and cyclohexene as well as methylated analogs like toluene. In gas phase, methane and methanol have been also identified. In addition of those, $CoMoS/Al_2O_3$ lead to more than 40 products including condensation (cyclohexylbenzene) or polymethylated compounds (tetramethylbenzene). With titania-supported CoMo catalyst, DME to form CAT and methane (observed in gas phase) was the principal way of the transformation of GUA. PHE was formed exclusively from CAT and then HYD route with the formation of cyclohexene, or DDO with benzene appeared. Only toluene was observed as methylated O-free product indicating that HYD was inhibited by methyl in ortho position.

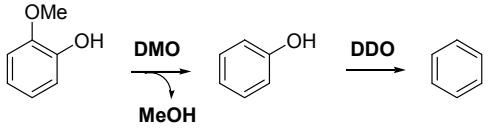

Figure 2. Reaction scheme of GUA HDO over $CoMoS/ZrO_2$

With zirconia-supported catalyst, few products have been formed and the reaction scheme is very simple (Figure 2): PHE was formed directly from GUA by DMO and then benzene was obtained by DDO. The advantage of this catalytic reaction scheme is the lower consumption of hydrogen during the process. Independently of that, and contrary to previous studies, these experiments show that the GUA transformation is very dependant of the nature of the support and the support can change drastically the selectivity of the transformation. Previously, Centeno et al. demonstrated that carbon support compared to alumina, lead to a higher PHE/CAT ratio but the catalytic activity with carbon support was lower [12]. PHE/CAT ratio found in this work for the GUA transformation over the three catalysts has been illustrated in Figure 3. In the case of zirconia-supported system, the ratio CAT/PHE was totally different from the ones observed with TiO_2 and Al_2O_3 catalyst. Thus, for $CoMoS/ZrO_2$, the GUA was quickly demethoxylated to PHE and methanol. Gas analysis has confirmed that methanol was the main gaseous product observed.

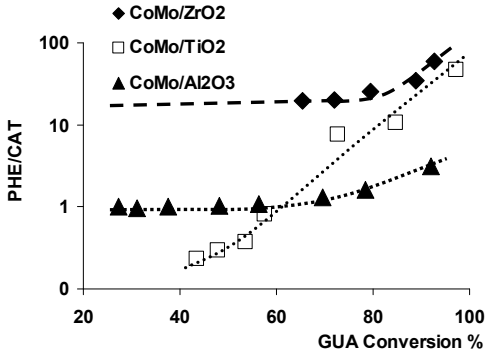

Figure 3. PHE/CAT ratio in function of GUA conversion with ZrO_2, TiO_2 and Al_2O_3-supported CoMo catalysts

The first step of GUA transformation (conversion GUA to PHE) may have a dramatic influence over the total transformation. Effectively, with alumina-supported system, three different pathways were observed in parallel:
- GUA to PHE with CAT as intermediate (DME)
- GUA to PHE (DMO)
- GUA to CAT and methyl substitution to Me-CAT, Me-PHE.

In this last case the substitution of methyl group occurred preferentially in ortho position and this steric hindrance slowed down the deoxygenation [13].
The DME route used with this catalyst (GUA to CAT and then to PHE) is also the main pathway observed with $CoMoS/TiO_2$. It

consists in two dehydroxylation reactions certainly happening according a hydrogenation\dehydration sequence.

The direct DMO to PHE happens very quickly compared to these two successive dehydroxylations and could explain the higher rate observed for the whole process with $CoMoS/ZrO_2$. Nethertheless, the selectivity for the conversion of PHE to O-free compounds should also play a great role: the HYD route goes through many intermediates as cyclohexanone and cyclohexanol while the DDO route affords directly to benzene. The adsorption mode of GUA onto the catalytic system must play an important role in this reaction scheme and ZrO_2 appeared to favor activation of O-compounds on the support surface as recently published [14].

In which concerns HDS of dibenzothiophenic compounds, CoMo catalysts supported on ZrO_2 or TiO_2 can be as active as γ-Al_2O_3 but they have never reached such high level of catalytic activity although the active site required to realize the transformation can be considered to be the same [15] for both reactions. This last assumption has to be moderated to the PHE transformation into deoxygenated compounds. Effectively, as previously explained only this part of the GUA reaction scheme can be directly compared to HDS of dibenzothiophenic (DBT) compounds. Of course the reactivity of these molecules should differ greatly from phenol because of the difference between C-S and C-O bond strength, but analogy between HDO of PHE and HDS of DBT seems significant. The importance of the adsorption mode has been well-established and hydrogenolysis of C-X (X=O, S) bond is strongly favored by a perpendicular adsorption through the X atom (η^1). The similar selectivity obtained in thiophenic compounds HDS with CoMoS catalysts supported on alumina, titania or zirconia [16] indicates that the adsorption mode must be the same on these supports which is not the case for HDO. The stronger hydrogenolysis character evidenced for C-O bond with $CoMoS/ZrO_2$ catalyst, in this work, can be initiated by a specific adsorption and activation on zirconia support of O-compounds.

Conclusion:

The use of $CoMoS/ZrO_2$ catalyst in the model HDO reaction of GUA showed that the direct hydrogenolysis of C_{arom}-O bond was mainly observed and lead very efficiently and selectively to deoxygenates. A very simple reaction scheme, where both support and active phase play important roles can be proposed, with a low consumption of hydrogen. On the contrary, with $CoMoS/TiO_2$ and $CoMoS/Al_2O_3$ catalytic systems, parallel reactions and HYD slowed down the whole HDO process and the reaction schemes are more complicated. Compared to HDS studies, the adsorption mode and activation of O-compounds must play a major role in the HDO transformation of GUA. In order to upgrade bio-oils in co-process with gas-oil or independently, $CoMoS/ZrO_2$ appears as a candidate of choice and more investigations are carried out.

References

(1) Muralidhar G., Massoth F. E., Shabtai J. J. Catal., 1984, 85, 44-52.

(2) Breysse M., Portefaix J. L., Vrinat M., Catal. Today, 1991, 10, 489-505.

(3) Ramirez J., Fuentes S., Diaz G., Vrinat M., Breisse M., Lacroix M., Appl. Catal. 1989, 52, 211-224.

(4) Duchet J.C., Tilliette M. J., Cornet, D., Vivier L., Perot G., Bekakra L., Moreau C., Szabo G., Catal. Today, 1991, 10, 579-592.

(5) Luck F., Bull. Soc. Chim. Belg., 1991, 100, 781.

(6) Furimsky E., Appl. Catal. A: General, 2000, 199, 147.

(7) Bui V. N., Toussaint G., Laurenti D., Mirodatos C., Geantet C., Catal. Today, 2009, 143, 172-178.

(8) Laurent E., Delmon B., Applied Catal. A: General, 1994, 109, 77.

(9) Bunch, A. Y., Ozkan, U. S., J. Catal., 2002, 206, 177-187.

(10) Laurent E., Delmon B., Appl. Catal. A : General, 1994, 109, 77-96.

(11) Bredenberg J.B.-s., Huuska, M., Toropainen P., J. Catal. 1989, 120, 401-408.

(12) Centeno A., Laurent E., Delmon B., J. Catal. 1995, 154, 288-298.

(13) Odebunmi E. O., Ollis D. F., J. Catal. 1983, 80, 56.

(14) Yakovlev V. A., Khromova S. A., Sherstyuk O. V., Dundich V. O., Ermakov D. Yu, Novopashina V. M., Lebedev M. Yu, Bulavchenko O., Parmon V. N., Catal. Today 2009, 144, 362-366.

(15) Viljava T.-R., Saari E. R. M., Krause A. O. I., Appl. Catal. A: General, 2001, 209, 33-43.

(16) Ji Y., Afanasiev P., Vrinat M., Li W., Li C., Appl. Catal. A: General, 2004, 257, 157-164.

THERMOLYTIC SOLVENT EXTRACTION OF BIOMASS TO PRODUCE HEAVY OILS IN HIGH YIELD WITH LOW OXYGEN CONTENTS

Colin E. Snape, Hui Deng, Will Meredith and Clement Uguna*

Department of Chemical and Environmental Engineering, Faculty of Engineering, University of Nottingham, University Park, NG7 2RD, UK *Colin.snape@nottingham.ac.uk

Introduction

It is recognized that bio-oils obtained by fast pyrolysis processes are not compatible with existing petroleum products due to their hydrophilic and acidic nature arising from their oxygen contents. The thermolytic solvent extraction of biomass offers a promising route for producing oils in high yield that are compatible with petroleum streams without the need to employ high pressure catalytic hydrogenation to facilitate high levels of oxygen removal. A number of solvents have been investigated in early studies. For example, Vanasse *et al*.[1] used creosote oil and ethylene glycol to achive oil yields over 40 % from Populus Deltoides. Yan[2] investigated the thermal liquefaction of paper, oak and fir using a number of process solvents and reported high conversions to pyridine-solubles. Czarena *et al*.[3] studied mild solvent extraction of white and red oak at different temperatures and, at 350°C using anthracene oil, conversions of 99% were achieved but with significant solvent loss. Li et al.[4] studied liquefaction of rice straw in sub- and supercritical 1,4-dioxane-water mixtures at temperatures of 260-340°C and reported oil yields of 30-50%. To date, there have been no studies have reported in model hydrogen-donor solvents, Therefore, in this study extractions have been conducted on miscanthus with tetralin and a selection of non-donor solvents and the effect of temperature on heavy oil (bitumen) yield has been assessed.

Experimental

The liquefaction experiments were conducted using the equipment shown in Figure 1 that comprises a Parr 4740 series stainless steel 22 ml cylindrical pressure vessel connected to a pressure gauge rated to 690 bar. Heat was applied by means of a fluidised sand bath and temperature was monitored by means of an additional K-type thermocouple connected externally to a computer which records the temperature every 10 seconds.

The liquefaction experiments were conducted on miscanthus using tetralin as a hydrogen-donor solvent and decalin, 1-methylnaphtphalene as non- donors, together with bitumen, polyethylene and polystyrene. Baseline anhydrous and hydrous experiments were also conducted. Standard condition used were a temperature of 410°C, a residence time of one hour and a solvent to feedstock mass ratio of 2.5:1. For tetralin, the temperature was varied between 380 and 460°C. For all experiments performed, the experimental set up was purged for about 20 minutes with nitrogen gas, after which nitrogen gas at 2 bar was introduced toprovie an inert atmosphere. The sand bath was pre-heated to the required temperature and left for about 10 mins. to equilibrate. The pressure vessel was then lowered onto the sand bath and the experiment left to run with a constant air flow through the sand bath. After the duration of the experiment, the reactor was removed from the sand bath immediately and allowed to cool to room temperature before product recovery.

Gases were collected using a gas tight syringe, transferred into a gas bag and immediately analysed on a Carlo Erba HRGC 5300 gas chromatograph. The contents of the reactor were recovered in toluene to determine the yield of toluene-insolubles. The toluene-solubles were distilled first to remove toluene and, then in the case of tetralin distilled further to remove both tetralin and naphthalene. The residue was weighed and is referred to as bitumen.

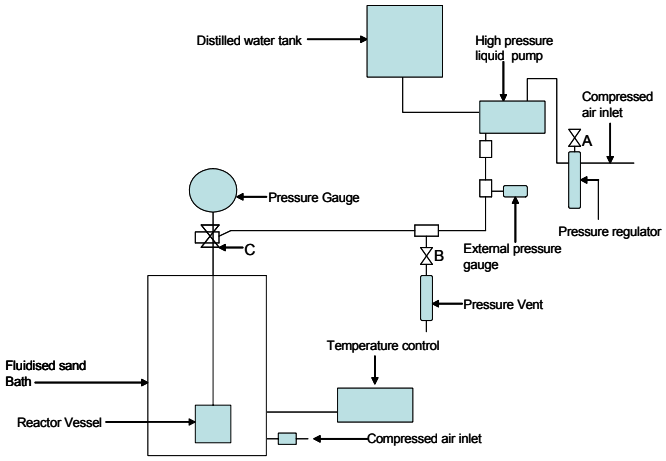

Figure 1 Schematic diagram of liquefaction equipment

Results and Discussion

Conversions with different solvents Figure 2 presents the conversions to toluene-solubles obtained with the different solvents investigated. The baseline conversion obtained in water was close to 60%. As expected, the highest conversion was obtained with tetralin (90%) with intermediate conversions for the non-donor solvents, 1-methylnaphthalene and decalin both giving conversions close to 70%. No synergistic effect was observed between decalin and 1-methylnaphthalene with the conversion again being close to 70% for their 50:50 mixture. The increase in conversion from 60 to 90% in going from using no solvent to using tetralin is largely accounted for by the increase in bitumen yield.

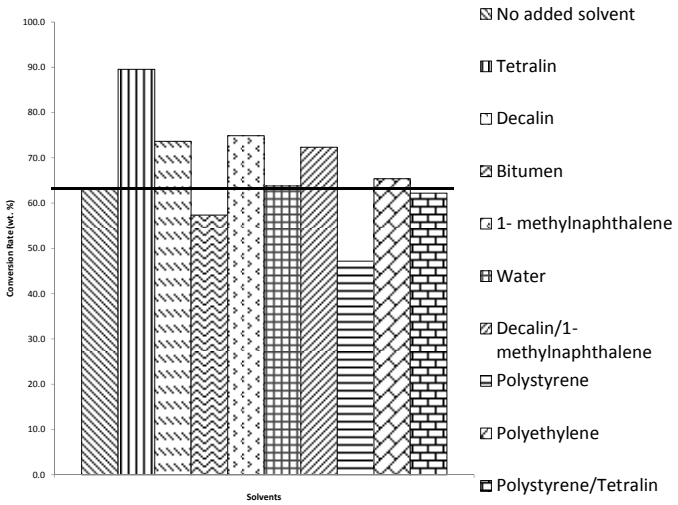

Figure 2 Conversions to toluene-solubles for miscanthus with different solvents at 410°C (daf basis, one hour with a solvent to feedstock mass ratio of 2:5: 1).

Petroleum bitumen as a solvent gave rise to only increase in overall conversion compared to the baseline conversion level of 60%. Polyethene and polystyrene gave rise to reduced conversions, the reduction being greater for polystyrene and the yield of toluene-

solubles being below 50% (Figure 1). The use of a 50:50 mixture of polystyrene and tetralin gave rise to a lower conversion than predicted. These results suggest that waste polymer streams are not going to effective solvents for liquefying biomass.

Effect of temperature on conversion Figures 3 and 4 present the total conversions to toluene-solubles and the hydrocarbon and bitumen yields as a function of temperature. It is interesting to note that conversion continue to increase with temperature and does not reach a plateau after which carbonization reactions begin to occur and reduce conversion (Figure 3).

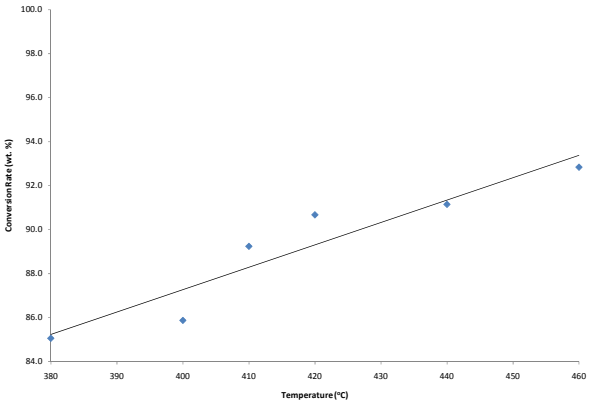

Figure 3 Effect of temperature on conversions to toluene-solubles for miscanthus (daf basis, one hour with a solvent to feedstock mass ratio of 2:5: 1).

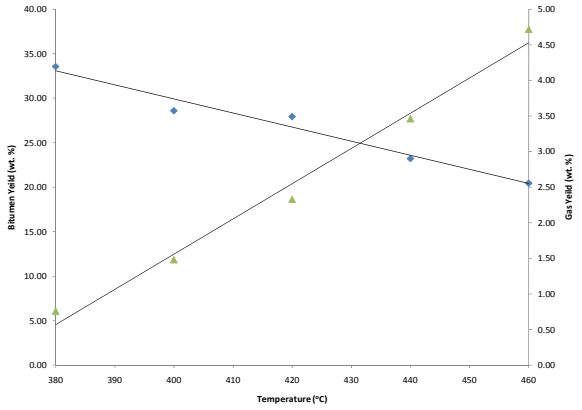

Figure 4 Effect of temperature on hydrocarbon agas nd bitumen yields for miscanthus (daf basis, one hour with a solvent to feedstock mass ratio of 2:5: 1).

In going from 380 to 460°C, the yield of hydrocarbon gases increases from *ca*. 0.5 to 4.5 %w/w while the yield of bitumen falls from *ca* 34 to 25 %w/w (Figure 4)..The discrepancy between the increase in hydrocarbon gas yield and the decrease in bitumen yield is accounted for by a combination of increased oxygen removal and some cracking to light oil.. Indeed, the tetralin and naphthalene recovered by distillation becomes more coloured with increasing temperature due to the presence of light oil. The oxygen contents of the oil measured by difference are close to 10% w/w and fall with increasing temperature.

Conclusions

1. Overall, conversions with tetralin to toluene-solubles are *ca*. 90% with heavy oil (bitumen) yields of *ca*. 35% compared to 72 and 20%, respectively with 1-methylnaphthalene and other non-hydrogen-donors.
2. The oils have oxygen contents as low as 10% and these generally decrease with increasing extraction temperature.
3. The use of thermally-decomposing polymers as solvents resulted in conversions similar or lower than the baseline level of *ca*. 60% without solvent.
4. Total conversions remain high at temperatures up to 460°C but bitumen yields decrease due to cracking giving rise hydrocarbon gases and light oil with a further loss of oxygen,

References

1. Vanasse C., Chornet E., and Overend R.P. Liquefaction of lignocellulosics in model solvents: creosote oil and ethylene glycol. *Canadian J. of Chemical Engineering 1988; 66:112–120.*
2. Yan T.Y. Liquefaction of wood and paper. *in Hydrocarbon Technology Environment, Alternate Energy ASources IV. Veroglu T.N.,Ed.. Ann Arbor: Ann Arbor Science; 1980. 79–102.*
3. Czarena; C., Montross, M D., Berkovich, A and Andrews, R. The effect of temperature on the mild solvent extraction of white and red oak. *Biomass and Bioenergy 2005, 28, 572-578.*
4. Li, H., Yuan, X., Zeng, G.; Tong, J., Yan, Y., Cao, H., Wang, L.;,Cheng, M.; Zhang, J. and Yang D.. (2009) Liquefaction of rice in sub- and supercritical 1,4-dioxane-water mixture. *Fuel Processing Technology 2009, 90: 657-663*

DEVELOPMENT OF NANO NICKEL-BASED SORBENT FOR ULTRA-DEEP DESULFURIZATION OF ULTRA LOW SULFUR DIESEL FOR FUEL CELL APPLICATIONS

Cigdem Sentorun-Shalaby, Xiaoliang Ma, Chunshan Song**

Clean Fuels and Catalysis Program, EMS Energy Institute, The Pennsylvania State University, 209 Academic Projects Building, University Park, PA, 16802.
*E-mail: mxx2@psu.edu (X.M.); csong@psu.edu (C.S.)

Introduction

Ultra-deep desulfurization of transportation fuels has become an increasingly important subject because of not only the stringent fuel specifications for the transportation fuels, but also the severe requirement of liquid hydrocarbon fuels (< 1 ppmw S) for fuel cell applications.[1-5]. Transportation fuels such as the current commercial ultra-low sulfur diesel (ULSD) with sulfur content less than 15 ppmw is a preferred liquid hydrocarbon fuel for producing H_2 for automotive, portable and resident fuel cells due to its high energy density, availability, safety, and ease for delivery and storage. Since sulfur poisons the reforming catalysts and the electrode catalysts, the sulfur in the fuel needs to be reduced to less than 1 ppmw for PEMFC[1]. Hydrodesulfurization (HDS) is the conventional process in petroleum refineries to reduce the sulfur from liquid fuels, but it is difficult or very costly to reduce the sulfur content in ULSD with 15 ppmw sulfur to less than 1 ppmw level for the fuel cell applications. According to our previous study,[2,6] for reducing the sulfur content in the current commercial ULSD from 15 ppmw to less than 1 ppmw by using the current hydrotreating technology, the catalyst bed volume or the catalyst activity must be about 68 % higher than that currently used in refineries. Therefore, it is desired to develop a novel technology for ultra-deep desulfurization of ULSD for fuel cell applications. Many new approaches for ultra-deep desulfurization of liquid hydrocarbon fuels have been reported in literature.[1,2,7] Among them the reactive adsorption on the nickel-based sorbents is promising and has attracted a significant attention due to the high capacity and selectivity without using hydrogen gas.[8-16]

The present paper reports on one of our current approaches in development of mesoporous nickel-based sorbents for the adsorptive desulfurization of ULSD. The desulfurization performance of the sorbents was evaluated in a fixed-bed flow sorption system at 200 ºC using a commercial ULSD with sulfur content of 15 ppmw. The desulfurization selectivity for the different sulfur compounds on the nickel-based sorbent was discussed on the basis of the detailed analysis of the sulfur compounds in the initial and treated ULSD.

Experimental

Sorbent Preparation. MCM-48 was prepared using a similar procedure as described in the literature[17]. The mesoporous-molecular-sieve-supported nickel sorbents were prepared by an incipient wetness impregnation (IWI) method. The desired amount of $Ni(NO_3)_2.6H_2O$ was dissolved in tetrahydrofuran (THF), and the solution was slowly added into the support material at room temperature under the ultrasonic aid in a ultrasonic bath. The mixture was kept in the ultrasonic bath for 3 h at room temperature, and then, dried in an oven at 100 ºC overnight. The dried samples were then reduced in a fixed-bed reactor under a pure hydrogen gas flow at 550 ºC for 4 h.

Sorbent Characterization. Transmission electron microscopy (TEM) was obtained by using a JEOL EM-2010F with EDS from EDAX operating at accelerating voltage of 200 kV. The samples were prepared by dispersing the sorbent powder as slurry in acetone, which was then deposited and dried on a lacey carbon film on a Cu grid.

The H_2-chemisorption was performed using a Micromeritics AutoChem II 2910 instrument. About 40 mg of the sample was first pretreated in a quartz reactor under a pure H_2 flow at 550 ºC for 2 h followed by purging with high-purity argon (Ar). After the sample was cooled to 50 ºC, a H_2-Ar mixture with 5 vol % H_2 was introduced into the reactor. The consumption of H_2 was monitored by a thermal conductivity detector (TCD).

Adsorptive desulfurization (ADS) Performance Tests. Evaluation of the ADS performance of sorbents was conducted in a fixed-bed flow sorption system with a stainless steel column (4.6 mm I.D. x 150 mm length). A commercial ULSD (or a model fuel) was fed into the column from the bottom by a HPLC pump. The adsorption conditions were controlled at 200 ˚C and a liquid hourly speed velocity (LHSV) of 4.8 h^{-1}. The effluent fuel from the top of the column was periodically sampled at an interval of 15-20 min for analysis. A commercial ULSD with 15 ppmw of total sulfur was used in this study. The composition and properties of the ULSD are listed in **Table 1**.

Table 1. Composition and properties of ULSD.

Specific Gravity	0.84
Distillation (˚C)	
IBP	166
T50	260
FBP	346
Cetane Number (engine rating)	49.7
Flash point (˚C)	63.9
Viscosity at 40˚C, (cSt)	2.5
Pour point (˚C)	-18
Cloud point (˚C)	-12
Polycyclic aromatic hydrocarbon (GC-SFC, wt %)	6.9
Element analysis	
C (wt%)	86.8
H (wt%)	12.9
N (ppmw)	12
S (ppmw)	15

Analysis of the Treated ULSD. The total sulfur concentration of the treated fuel samples was analyzed by using ANTEK 9000 series sulfur analyzer. The sulfur compounds in the treated and un-treated fuels were analyzed by using a Hewlett-Packard gas chromatograph equipped with a sulfur-selective pulsed flame photometric detector (GC-PFPD). A Hewlett Packard 5890 series II gas chromatograph with a capillary column (XTI-5, Restek, bonded 5%, 30 m × 0.25 mm i.d. × 0.25 µm film thickness) and a split mode injector (ratio: 100:1) was used with ultra high-purity helium as a carrier gas. The oven temperature was initially set at 120 °C and ramped immediately at 6 °C/min to 170 °C, followed by a ramp at 20 °C /min from 170 to 290 °C, and held at 290 °C for 5 min. The injection sample volume was 1 µL.

Results and Discussion

ADS performance of the prepared sorbent was evaluated in comparison with a commercial Raney Nickel and a Ni/SiO_2-Al_2O_3 with nickel loading of 55 wt % in the flow sorption system at 200

°C and 4.8 h^{-1} of LHSV. The breakthrough curves for Ni20/MCM-48, Raney Nickel and Ni/SiO_2-Al_2O_3 are shown in **Figure 1**. The breakthrough capacity on the basis of the sorbent weight increases in the order of Raney Nickel (0.19 mg-S/g-sorb) < Ni55/SiO_2-Al_2O_3 (0.41 mg-S/g-sorb) < Ni20/MCM-48 (2.1 mg-S/g). Ni20/MCM-48 gives the highest breakthrough capacity. If the results were compared on the basis of the sorbent volume, the order of breakthrough capacity is changed to Ni55/SiO_2-Al_2O_3 (0.32 mg-S/ml-sorb) < Raney Nickel (0.35 mg-S/ml-sorb) < Ni20/MCM-48 (0.69 mg-S/ ml-sorb), as the packing densities of the sorbents are quite different. On the basis of the sorbent volume the desulfurization performance of Ni20/MCM-48 is still the best sorbent among them. According to the present study, each kilogram of Ni20/MCM-48 is able to treat 170 L of the commercial ULSD with sulfur content of 15 ppmw to get the treated ULSD with sulfur content less than 1 ppmw. The weight-based capacity of the Ni20/MCM-48 developed in this study is higher than that by Park et al.[13] by a factor of more than 4.

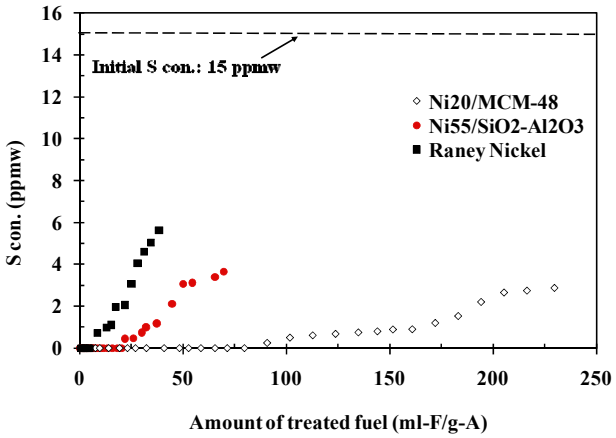

Figure 1. Breakthrough curves of ULSD over Ni20/MCM-48, Ni55/SiO_2-Al_2O_3, and Raney Nickel. Sorption condition: 200 ˚C and 4.8 h^{-1} of LHSV.

MCM-48 and Ni20/MCM-48 were also characterized by TEM. The TEM images are shown in **Figure 2**. **Figure 2a** confirms the three-dimensional network structure of the synthesized MCM-48. **Figure 2b** shows the uniform distribution of the nickel particles with an average particle size about 2.5 nm in Ni20/MCM-48. The majority of the nickel particles should be in the MCM-48 channels, which results in the high dispersion of nickel on MCM-48 support. In order to clarify further why Ni20/MCM-48 exhibited the much better ADS performance than others, the H_2 chemisorption on the Ni20/MCM-48 was conducted, and the measured metal dispersion was 35%. The results reveal that large number of the exposed nickel atoms in Ni20/MCM-48 due to the high dispersion of nickel lead to the high breakthrough capacity of Ni20/MCM-48.

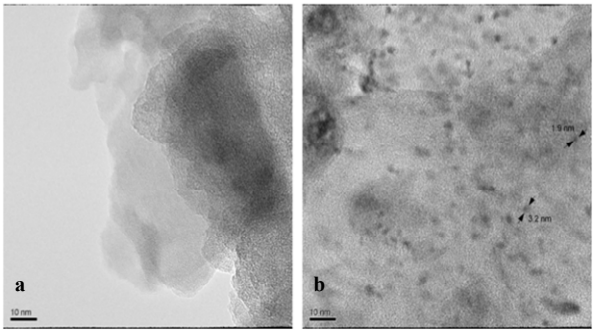

Figure 2.TEM images of MCM-48(a) and Ni20/MCM-48(b).

The GC-PFPD chromatograms of the initial ULSD and the treated ULSD with the assigned peaks are shown in **Figure 3**.

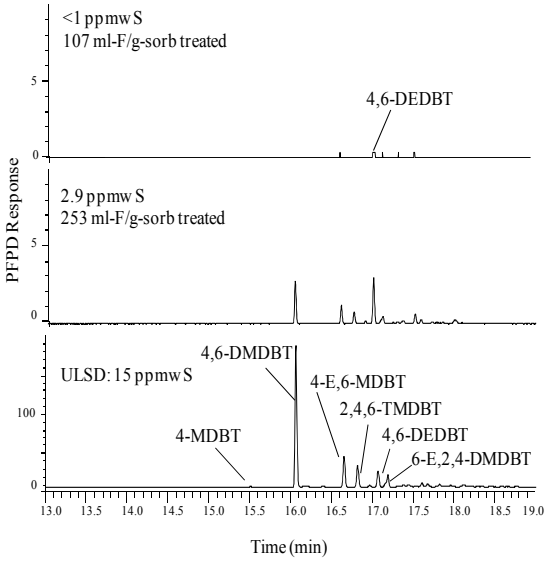

Figure 3. GC-PFPD chromatographs of initial ULSD and the desulfurized ULSD samples over Ni20/MCM-48 at 200 ˚C, 4.8 h-1 of LHSV.

The major sulfur compounds in the ULSD are the alkyl DBTs with two alkyl substituents at the 4- and 6-positions respectively, such as 4,6-DMDBT, 4-ethyl,6-methyl-dibenzothiophene (4-E,6-MDBT), 2,4,6-trimethyldibenzo-thiophene (2,4,6-TMDBT), 4,6-diethyldibenzothiophene (4,6-DEDBT) and 6-ethyl,2,4-methyldibenzothiophene (6-E,2,4-DMDBT). It was found that among these sulfur compounds, the first breakthrough sulfur compound was 4,6-DEDBT. By comparison of the GC-PFPD peak area of the sulfur compounds in the treated and initial fuels, it appears that the desulfurization selectivity of Ni20/MCM-48 decreases in the order of 4-MDBT > 4,6-DMDBT ≈ 2,4,6-TMDBT > 4-E,6-MDBT ≈ 6-E,2,4-DMDBT, > 4,6-DEDBT. It indicates that the desulfurization selectivity is dependent not only on the number of the alkyl substitutes at the 4- and 6-positions, but also on the size of the alkyl substituents at the 4- and 6-positions. The lowest selectivity for 4,6-DEDBT can be ascribed to the two largest alkyl substituents (ethyl groups) at the 4- and 6-positions, respectively.

Conclusion

A new nickel-based sorbent for the reactive adsorption desulfurization of commercial ULSD was developed by the incipient wetness impregnation of nickel on mesoporous silica, MCM-48. The prepared sorbent with 20 % nickel loading on MCM-48 (Ni20/MCM-48) showed the excellent sorption performance, as the loaded nickel highly dispersed on the MCM-48 with the average nickel particle size of 2.5 nm. A breakthrough capacity of 2.1 mg-S/g-sorb at a breakthrough sulfur level of 1 ppmw was obtained for sulfur removal from the commercial ULSD with 15 ppmw of sulfur. The desulfurization reactivity of the alkyl DBTs on the nickel-based sorbents is dependent not only on the number, but also on the size of the alkyl substituents at the 4- and 6-positions of DBTs. Among all sulfur compounds in the ULSD, 4,6-DEDBT has the lowest reactivity, which can be ascribed to the strong steric hindrance of the two ethyl groups at the 4- and 6-positions.

Acknowledgement.

This work was supported in part by the U.S. Department of Energy, National Energy Technology Laboratory under Contract No. DE-FC26-08NT0004396.

References

(1) Song, C. S. *Catal. Today* **2003**, 86, 211-263.
(2) Song, C.S.; Ma, X.L. *Appl. Catal. B. Env.* **2003**, 41, 207-38.
(3) Ma, X.L.; Sun, L.; Song, C.S. *Catal. Today* **2002,** 77, 107-16.
(4) Song, C.S. *Catal. Today* **2002**, 77, 17-49.
(5) Farrauto, R.; Hwang, S.; Shore, L.; Ruettinger, W.; Lampert, J.; Giroux, T.; Liu, Y.; Ilinich, O. *Annu. Rev. Mater. Res*. **2003**, 33, 1–27.
(6) Ma, X.L.; Sakanishi, K.; Mochida, I. *Ind. Eng. Chem.* **1994**, 33, 218–222.
(7) Ito, E.; van Veen, J.A.R. *Catal. Today* **2006**, 116, 446–60.
(8) Nagai, M.; Urimot, H.; Uetake, K.; Sakikawa, N.; Goonzales, R.D. *Polynuclear Aromatic Compounds*, Am. Chem. Soc. **1988**.
(9) Ma, X.L.; Sprague, M.; Song, C.S. *Ind. Eng. Chem. Res.* **2005**, 44, 5768-75.
(10) Velu, S.; Ma, X.L.; Song, C.S.; Namazian, M.; Sethuraman, S.; Venkataraman, G. *Energy & Fuels* **2005**, 19(3), 1116-25.
(11) Ma, X.L.; Velu, S.; Kim, J.H.; Song, C.S. Appl. Catal. B: Environ. **2005**, 56(1-2), 137-47.
(12) Ko, C.H.; Park, J.G.; Park, J.C.; Song, H.; Han, S.; Cho, S.; Kim, J. *Appl. Surf. Sci.* **2007**, 253, 5864–67.
(13) Park, J.G.; Ko, C.H.; Yi, K.B.; Park, J.; Han, S.; Cho, S.; Kim, J. *Appl. Catal. B: Environ.* **2008**, 81, 244-50.
(14) van Rheinberg, O.; Lucka, K.; Köhne, H.; Schade, T.; Andersson, J.T. *Fuel* **2008**, 87, 2988–96.
(15) Hernández, S.; Solarino, L.; Orsellob, G.; Russo, N.; Fino, D.; Saracco, G.; Specchia V. *International Journal of Hydrogen Energy* **2008**, 33, 3209–14.
(16) Landau, M.V.; Herskowitz, M.; Agnihotri, R.; Kegerreis, J.E. *Ind. Eng. Chem. Res.* **2008**, 47, 6904–16.
(17) Shao, Y.; Wang, L.; Zhang, J.; Anpo, M. *J. Phys. Chem. B.* **2005**, 109, 20835.

Effect of supercritical water on upgrading reaction of oil sand bitumen

Masato Morimoto, Yoshikazu Sugimoto, Yoshiaki Saotome, Shinya Sato, Toshimasa Takanohashi

Advanced Fuel Group, Energy Technology Research Institute, National Institute of Advanced Industrial Science and Technology, Tsukuba 305-8569, Japan

Introduction

Oil sand bitumen is an important energy resource because of its abundant supply. The proven reserve in Canada is estimated to be about 173 billion barrels. Steam assisted gravity drainage (SAGD) is a new mining method that enables recovery of the bitumen in deep layers by injection of steam into the ground. Because the amount of bitumen minable by conventional surface mining methods is estimated to be only about 20% of the total reserve, in situ methods such as SAGD are increasingly important. The viscosity of bitumen mined using SAGD is not sufficiently low to enable transport by pipeline without any treatment. Therefore, development of an effective on-site upgrading process for bitumen is essential. Because hot bitumen and high-pressure water are already available at SAGD mine sites, treatment of the bitumen using supercritical water (SCW) could be a viable solution.[1]

The objective of this work was to clarify the effect of SCW during bitumen upgrading. We treated the bitumen with water, nitrogen, and toluene at 450°C. Nitrogen and toluene were selected as inert and reactive media, respectively, for comparison with water. Then, we conducted analyses and comparisons of the products.

Experimental

Experimental procedure Canadian bitumen (C: 83.5, H: 10.6, N: 0.47, S: 4.17, O: 1.00, Others: 0.30 wt %) mined by SAGD method was used. Two steal balls (7.0 mm-D) and 4.0 g of SAGD-bitumen were put into an autoclave (SUS316, 50 ml, 14 mm-ID × 320 mm), and packed with 8.0 g of water, 8.0 MPa of nitrogen, or 22 g of toluene. The autoclave was heated up to 450°C at a heating rate of about 25 K/min, using a tiltable electric furnace applied about 39 times per min. The inner pressure of every experiment was about 30 MPa. After a given time (60 or 120 min) from the time point that the autoclave was inserted into the furnace, the autoclave was pulled out and cooled down. Product remained in the autoclave was recovered by washing with hot toluene.

The toluene-insoluble fraction (coke) was separated by filtration. The toluene-soluble product obtained was distillated using a glass tube oven at 250°C and 0.001 MPa, which corresponds to 420°C at 0.1 MPa. Using this distillation, the liquid product was separated into two fractions: middle distillate (MD) and distillation residue (DR).

The products prepared at 450°C are referred to by the experimental conditions under which they were produced: reaction medium (W for water, N for nitrogen, or T for toluene) subscript (reaction time 60 or 120 min)-product (MD, DR, or coke). For example, W_{60}-MD is the MD prepared with water at 450°C for 60 min. The MD and the DR contained in the bitumen are abbreviated as B-MD and B-DR, respectively.

Product analysis The amounts of gaseous products, C_1 to C_3 and CO_2, were determined using a GC. MDs were analyzed in terms of boiling point distribution (ASTM D2887), molecular weight distribution (GPC), elemental composition (CHNS), hydrogen and carbon type distribution (NMR) , and compound distribution (GC-FID, GC-SCD, GC-NPD, and GC-MS). The DR was analyzed in terms of molecular weight distribution, elemental composition, hydrogen type distribution, carbon type distribution, and Conradson carbon residue (CCR, ASTM D189). The average molecular structure of the DR was analyzed using our method[2] based on the Brown−Ladner method. The number average molecular weight (M_n) was determined using GPC with calibration standards our proposed.[3]

The coke was analyzed in terms of elemental composition and carbon aromaticity (f_a), which were determined using a solid-state ^{13}C CP/MAS NMR at a ^{13}C frequency of 75.46 MHz and MAS rate of 10 kHz, with a contact time of 1 ms and a pulse repetition time of 4 s for 3600 scan times.

Result and discussion

Effect of reaction media on conversion Tables 1 and 2 show the recovery ratios of MD and DR. The bitumen contained 23 wt% of MD, 77 wt% of DR, and no toluene-insoluble fraction. As the reaction time increased, the yield of coke increased and that of DR decreased. The conversion shown in those tables was defined as the ratio of fraction converted into the light product from the original DR, i.e. one minus (sum of the yields of DR and coke) divided by (the yield of DR contained in the bitumen). At both 60 and 120 min, the conversions in water were the highest of all the reaction media.

MD comparisons All MD samples consisted mainly of compounds with boiling points of less than 500°C. The boiling point distributions of W_{60}-MD and N_{60}-MD were similar, whereas T_{60}-MD contained a larger amount of compounds with low boiling points. Figure 1 shows the GC-FID, GC-SCD, and GC-NPD traces of MDs treated at 450°C for 60 min with water, nitrogen, and toluene. No significant differences among those traces were observed except for T_{60}-MD. T_{60}-MD showed several specific peaks, which were identified by GC-MS analysis as being related to derivatives of alkyl toluenes and their dimers. This indicated that toluene reacted with decomposed products formed during the pyrolysis. The GPC traces of W_{60}-MD and N_{60}-MD were similar, whereas T_{60}-MD contained larger amount of compounds with low molecular weights. Table 1 shows the elemental compositions of MDs. The H/C atomic ratios of W_{60}-MD and N_{60}-MD were both about 1.4, and that of T_{60}-MD was slightly less. The ^1H and ^{13}C NMR spectra of W_{60}-MD and N_{60}-MD were almost the same as those of ^1H and ^{13}C at all ranges of chemical shift. These tendencies for MDs prepared at 60 min were same as those for at 120 min.

DR comparisons Judging from the GPC traces, N_{60}-DR contained a larger amount of higher molecular weight compounds than the others did. M_ns of W_{60}-DR and N_{60}-DR were 608 and 655, respectively, and those of W_{120}-DR and

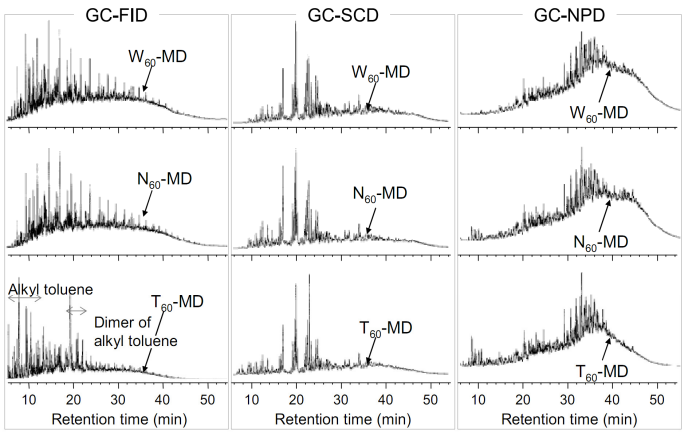

Figure 1. GC-FID, GC-SCD, and GC-NPD traces of MD prepared at 450°C for 60 min with water, nitrogen, and toluene.

N_{120}-DR were 589 and 610, respectively. DR prepared in SCW consisted of compounds with a lower molecular weight than those prepared with nitrogen. Table 2 summarizes the elemental compositions, M_n, and distributions of hydrogen and carbon type of W_{60}-DR, W_{120}-DR, N_{60}-DR, and N_{120}-DR. Although the H/C ratio of both W_{60}-DR and N_{60}-DR were about 0.92, that of W_{120}-DR (0.73) was much lower than that of N_{120}-DR (0.85). W_{120}-DR also contained a larger amount of aromatic carbon. As a result, the DR prepared with water and nitrogen exhibited different hydrogen and carbon type distributions. The CCRs of DRs were considered to reflect the differences in DR structure and molecular weight distribution.

The average molecule in the DR had 9–11 rings. The numbers of units of W_{60}-DR and W_{120}-DR were 1.4 and 1.1, and the numbers in N_{60}-DR and N_{120}-DR were 1.2 and 1.5, respectively. Here, unit means the structure consisting of one fused ring system and several side chains. The units in DR prepared with both media were combined with two to four alkyl chains, whose average lengths were less than two. The DRs prepared with water had more condensed structure and shorter average chain lengths than those prepared with nitrogen.

Coke comparison Table 3 shows the elemental composition and aromaticity of coke prepared at 450°C for 60 and 120 min with water and nitrogen. The coke prepared with water had lower values of H/C and higher f_a than that prepared with nitrogen for both treatment times.

Summary and Conclusion

SCW gave the highest conversion of all the reaction media used. The MD prepared with water and nitrogen showed similar properties for analyses of the boiling point distribution, molecular weight distribution, elemental composition, distribution of hydrogen and carbon type, and compound distribution. The DR produced with water had lower molecular weight distribution, lower H/C value, higher aromaticity, and more condensed structure than those produced in nitrogen. The coke prepared in SCW also had higher aromaticity.

The upgrading of bitumen by SCW reaction was primarily considered to be physical in nature, because all properties of the MDs prepared with water and nitrogen were similar to each other. As a result, it is possible to highly disperse the bitumen by SCW. This dispersion effect led to intramolecular dehydrogenation of the heavier component and prevention of recombination reactions. Consequently, the DR prepared in SCW consisted of lower molecular weight compounds, which had more condensed structures than that prepared in nitrogen. And, SCW gave the highest conversion, a greater amount of lighter products, and a lower yield of coke.

Table 1. Elemental composition and aromaticity of MDs prepared at 450°C for 60 and 120 min with water, nitrogen, and toluene

	B-MD	W_{60}-MD	N_{60}-MD	T_{60}-MD	W_{120}-MD	N_{120}-MD	T_{120}-MD
Recovery (wt %)	23.0	37.2	32.5	46.3	33.5	25.7	42.9
Conversion	0.00	0.65	0.61	0.58	0.71	0.60	0.57
C (wt %)	84.4	85.6	85.3	86.8	83.6	83.6	85.6
H (wt %)	11.8	9.9	10.1	9.7	8.4	8.5	8.0
N (wt %)	0.0	0.6	0.6	0.6	0.3	0.4	0.1
S (wt %)	2.8	3.8	3.7	2.7	6.0	5.8	3.3
Diff. (wt %)	0.9	0.0	0.3	0.2	1.7	1.7	3.0
H/C	1.66	1.37	1.41	1.33	1.20	1.21	1.12
f_a	0.19	0.40	0.40	0.46	0.58	0.56	0.65

Table 2. Elemental composition, aromaticity, M_n, CCR, and distribution of hydrogen type of DRs prepared at 450°C for 60 and 120 min with water and nitrogen

	B-DR	W_{60}-DR	N_{60}-DR	W_{120}-DR	N_{120}-DR
Recovery (wt %)	77.0	14.3	14.0	8.3	7.5
Conversion	0.00	0.65	0.61	0.71	0.60
C (wt %)	82.4	84.2	84.7	84.7	84.5
H (wt %)	9.2	6.5	6.6	5.2	6.1
N (wt %)	0.5	1.0	0.9	1.0	0.8
S (wt %)	7.1	7.0	7.3	8.8	8.4
Diff. (wt %)	0.8	1.4	0.4	0.3	0.2
H/C	1.33	0.92	0.93	0.73	0.85
f_a	0.30	0.69	0.68	0.81	0.73
Mn	992	608	655	589	610
CCR (wt %)	16.1	23.8	31.7	34.3	25.1
^{1}H NMR (%)					
H_a	7.8	26.6	24.7	35.8	30.1
H_α	13.0	33.3	29.9	35.2	29.1
H_β	58.1	31.5	35.0	21.5	30.8
H_γ	20.7	8.6	10.3	7.5	10.0

Table 3. Elemental composition and aromaticity of coke prepared at 450°C for 60 and 120 min with water and nitrogen

	W_{60}-Coke	N_{60}-Coke	W_{120}-Coke	N_{120}-Coke
Recovery (wt %)	12.3	15.9	14.0	23.0
Conversion	0.65	0.61	0.71	0.60
C (wt %)	84.8	84.7	83.7	85.2
H (wt %)	4.0	4.2	3.6	3.6
N (wt %)	1.6	1.5	1.6	1.4
S (wt %)	7.0	7.5	6.4	6.0
Diff. (wt %)	2.5	2.1	4.7	3.9
H/C	0.56	0.60	0.51	0.50
f_a	0.86	0.83	0.90	0.88

Acknowledgement This research was supported by the Japan Petroleum Energy Center (JPEC) as part of a technological development project financially supported by the Japanese Ministry of Economy, Trade, and Industry.

References

(1) Kamimura, H., et al. *ACS Fuel Div.* **1998**, *216*, 153−153.
(2) Sato, S. *J. Jpn. Pet. Inst.* **1997**, *40*, 46−51.
(3) Sato, S., et al. *Energy Fuels* **2005**, *19*, 1991–1994.

DESULFURAZATION OF FUEL FRACTIONS ON MODIFIED ADSORBENTS

M. M. Sugungun, A. Fayomi and E. Umukoro

Nigeria National Petroleum Corporation
Research and Development Division
49, Moscow Road
Port Harcourt, Nigeria
FAX: +234 84 237 001
Email: Mustafa.Sugungun@NNPCGroup.com

INTRODUCTION

Conventionally, sulfur compounds are removed from fuels and fractions employing various hydrotreating processes that involve use of Co-Ni-Mo and other mixed transition metal oxides catalysts under excessive hydrogen pressure. These processes defending on severity, removes sulfur compounds catalytically and consistently transforming these compounds to hydrogen sulfides and oxides of sulfur that are further treated to non-toxic form. However, bulks of the refractory sulfur compounds are difficult to remove using these convectional technologies and the limits of sulfur tolerance in fuels is aggressively lowering with advent of ultra-deep sulfur reduction requirements on transporting fuels. These stringent environmental requirements are pushing sulfur tolerance to 10-ppm limit and aiming for even lesser sulfur content in fuels. Current sulfur removal technologies will not be able to meet those demands without equipment modification, increased process severity and heavy investments on improved catalyst design. This in turn, will increase processing costs per unit of treated feedstock.

Removal of sulfur and sulfur refractory sulfur compounds can also be achieved using other non-convectional techniques like oxidation, microwave application and adsorption on molecular sieves and adsorbents. In order to accomplish the objectives of ultra low sulfur reduction, deep desulfurization of fuels is fast becoming a prominent topic in the refining industry. Selective adsorption of sulfur compounds, especially refractory sulfur and other hetro-atoms is gaining popularity as an alternative method for sulfur reduction in fuels. Several studies and patents have indeed reported removal of mecaptans, sulfides and disulfides from petroleum fractions using adsorbents and other molecular sieves; specially synthesized zeolites and mesapores are reported to successfully adsorb sulfur-containing compounds from petroleum fractions.

In this study, removal of sulfur using adsorbents, molecular sieves and modified adsorbents is investigated. Adsorption selectivity, operating conditions and fuel loss consequent to adsorption were established. The study is primarily aimed at targeting adsorbent selection and screening.

EXPERIMENTAL

The reference refinery AGO sample was initially fractionated into eight (8) boiling range fractions at interval of 30 degrees Celsius each in order to locate fraction containing higher bulk sulfur. Characteristics of the reference AGO are shown in table 1 below. The fractionated samples of the reference fuel are then individually analyzed individually for bulk sulfur using TwinX sulfur analyzer XRF spectrophotometer by wavelength dispersive x-ray spectrometry (ASTM D2622).

Adsorbents were prepared by impregnation of $CoCl_2.xH_2O$ and $Ni(NO_3)_2$ salts in accordance to literature. The modified natural adsorbents and prepared adsorbents with metal loadings were utilized in the adsorbent screening and testing experimentations. A simplified sketch of the experimental setup is depicted in figure 1 below. The adsorption experiments were conducted in a fixed bed of adsorbents using a tubular reactor operating at temperature interval of (25 – 150) ^oC. All experiments were conducted under atmospheric pressure. Both modified and metal loaded adsorbents were pre-treated thermally at 150 ^oC for 2 hrs and followed by controlled treatment for 4 hrs in nitrogen stream at 400^oC before loading into the fixed bed of the tubular reactor. The collected samples of the desulfurized fuel existing the reactor were equally analyzed by wavelength dispersive x-ray spectrometry.

RESULTS AND DISCUSSION

We have carried out investigative study for screening of adsorbents for potential use in desulfurization of fuels fraction under mild operating conditions. Three (3) naturally occurring adsorbents were pre-treated and modified for use in the adsorption experiments. Experimental results for adsorption on these adsorbents are shown in table 2 below. Additionally, the adsorbent with higher potential is subjected to further treatment with metals loading and investigated further for increase in adsorption intensity. The study did not investigate any chemical transformation the fuel underwent in the course of the adsorption. The adsorption experiments were conducted at varying temperature ranges from room temperature (25^oC) to 150^oC utilizing different fractions of the reference fuel.

Sulfur adsorption is noticed to reduce with increasing temperature as witnessed in figure 2 below. This is possibly as a consequent to reverse process (de-sorption) that seems to occur at the higher temperatures. Higher adsorption intensity is also noticed in adsorbent with metal loadings consequent to a probable catalytic incision of C-S bonds that the desulfurization metals exhibits. The effect of the metal loadings on the adsorbents is depicted in table table 2 below.

Table 1. Properties of the Reference Refinery AGO

Property	Value
Density, @20/4 ^oC, kg/m^3	849.2
ASTM Color (D-1500)	L1.0
Water and sediments, v %	0
Ash content, w %	< 0.001
Copper strip corrosion (3h, 50^oC)	1
D86 Distillation, ^oC, %v/v	
IBP	122.4
5%	162
10%	173.1
30%	220.2
50%	261.2
70%	308.1
80%	338.1
90%	375.7
Kinematic viscosity @ 40^oC, cSt	2.682
Total Sulfur, mg/kg	335
TAN, mgKOH/g	0.12
Cetane number	43.0

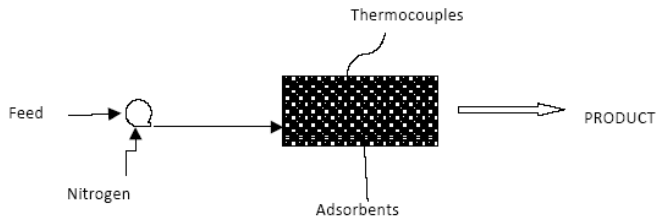

Figure 1. Simplified sketch of the adsorption experimental setup

Table 2. Adsorption Ratings of Modified Adsorbents and Percentage Fuel Recovery (fuel fraction boiling range: 280°C – 310°C, initial sulfur concentration 377ppm, fixed bed reactor volume: 105.5 cm^3, fixed bed temperature 27°C)

Adsorbent	Percentage of bulk sulfur adsorbed, %	Percentage of fuel recovery, %
Ad-A1	17.20	59.0
Ad-A2	19.36	72.0
Ad-A3	8.48	97.0
Ad-A4 (metal loaded)	45.62	70.0

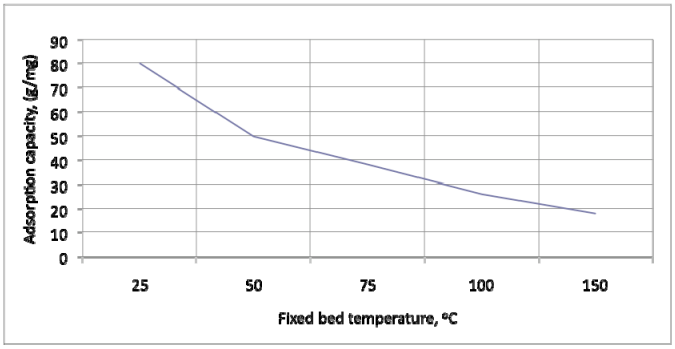

Fig. 2 The effect of temperature on the adsorption capacity of the modified adsorbent Ad-A2 fixed bed volume 105.5cm^3 fuel fraction 280°C -310°C, 377ppm sulfur.

CONCLUSION

Adsorbents screening for non-hydrogen desulfurization of fuels fractions is investigated. Modified naturally occurring adsorbent (Ad-A2) exhibits potential for sulfur removal from petroleum fractions. Impregnation of desulfurization metals to the adsorbent greatly enhances the sulfur removal ability of the adsorbent lowering the initial bulk sulfur concentration by 45.65 percent under mild ambient conditions.

REFERENCES

(1) Takashi Fujikawa, Journal of Japan Petroleum Inst, 50(5), 249 261 (**2007**)

(2) C. Song, Am Chem Soc Div Fuel Chem, Prep, (**2001**), 46(1) 8-13

(3) J. R. Benner, L. T. Thomson, Catalysis Today, 21 (**1994**), 101-112

(4) R. G. Leliveld, A. J. van Dillen, J. W. Geus and D. C. Koningsberger, Journal of Catalysis, 175, 108-116 (**1998)**

(5) C. Song and K. M. Reddy, Am Chem Soc Div Fuel, prep, **1996** 41(3), 567-573

(6) M. Campanati, G. Fornasari, A. Vaccari, Catalysis Today, 77 (**2003**), 299-314

(7) Celia Marin, Jose Escobar, Ernesto Galvan, Florentino Murrieta, Rene Zarate, Canadian Journ of Chem Engineering, Vol 80, (**2002)**

DEVELOPMENT OF HIGH-PERFORMANCE ADSORBENT VIA OXIDATING MODIFICATION OF ACTIVATED CARBON FOR ADSORPTIVE DENITROGENATION OF LIQUID HYDROCARBON STREAMS

Na Li,[a,b] Xiaoliang Ma,[a] Qingfang Zha[b] and Chunshan Song[a]*

[a]: EMS Energy Institute, The Pennsylvania State University
209 Academic Project Building, University Park, PA 16802, USA
[b]: College of Chemistry and Chemical Engineering, China University of Petroleum, Dongying, Shandong 257061, China
*Email: mxx2@psu.edu

Introduction

Deep denitrogenation of liquid hydrocarbon streams is becoming a more and more important subject, because 1) the nitrogen compounds coexisting in the liquid hydrocarbon streams inhibit strongly the ultra-deep hydrodesulfurization (HDS) and the removal of such nitrogen compounds from the streams can improve the ultra-deep HDS performance significantly;[1, 2] 2) nitrogen compounds in the liquid hydrocarbons and the intermediates and NH_3 produced from them during the subsequent processes poison the catalysts in the subsequent processes, such as hydrodearomatization, reforming for hydrogen production and BTX production, ring-opening catalysts for improving the cetane number of diesel and the anode catalysts in fuel cells;[3] 3) the current commercial hydrotreating processes for deep HDS of petroleum distillates may not be suitable for the upgrading of the liquid hydrocarbon distillates from coal liquefaction and pyrolysis because of their high nitrogen content, and the hydrodenitrogenation of such distillates needs to be conducted at severe conditions with high hydrogen consumption. It is desirable to develop new approaches to deep denitrogenation that are more energy efficient, economical and environmental friendly. Currently, removal of nitrogen from various liquid hydrocarbon streams is carried out via the catalytic hydrotreating process in refineries. However, hydrodenitrogenation (HDN) is more difficult than HDS, as much severer reaction condition and higher hydrogen consumption are required for HDN. Therefore, adsorptive denitrogenation (ADN) of liquid hydrocarbon streams by using highly selective adsorbent has been attracting a great attention.[4, 5] Some investigations on ADN of liquid hydrocarbons on activated carbons have been reported recently in the literature.[4, 6, 7] It was found that some activated carbons are promising adsorbents for selective removal of the nitrogen compounds, due to their high adsorption capacity, selectivity and good regenerability. In general, the adsorption behavior of carbon materials depends on both their physical and chemical properties. In our previous studies in the structure-performance correlation, we found that the surface chemistry of the activated carbons, including the type and content of the oxygen-containing functional groups on the surface, plays an important role in determination of their ADN performance. A significant improvement in the ADN performance of the carbon-based adsorbent may be achieved by introducing more nitrogen-compound-philic oxygen-containing functional groups onto the carbon surface.

The oxygen-containing functional groups, including their types and concentration, on the carbon surfaces can be tailored by thermal or chemical treatments. Different oxygen-containing functional groups (e.g., carboxylic acids, anhydrides, lactones, carbonyl, quinones and phenols) can be introduced on the carbon surface by using oxidizing agents, such as HNO_3, H_2SO_4, H_2O_2, O_3, air, NO_2, and NaClO. Recently, $(NH_4)_2S_2O_8$ (Ammonium persulfate, APS)[8-10] has been reported to be an excellent oxidant for modifying the surface properties of carbon materials, as APS is able to introduce more oxygen-containing groups onto the surface under mild reaction conditions than the concentrated nitric acid oxidation.

The objective of this study is to maximize the oxygen-containing functional groups on the activated carbon surface by the oxidative modification using $(NH_4)_2S_2O_8$ as an oxidant in order to increase the adsorption capacity of the activated carbon for ADN of liquid hydrocarbon streams. The effects of APS concentration, oxidation temperature, and oxidation time on the concentration of the oxygen-containing functional groups on the activated carbon were examined in detail. The various functional groups on the activated carbon samples were identified and quantified by the temperature programmed desorption method (TPD-MS), which has been well developed.[11,12] The adsorption isotherms and the important adsorption parameters of the modified adsorbent for removing quinoline were measured and compared with those of the initial activated carbon. The surface chemical structure and the ADN performance of the adsorbents were correlated and discussed.

Experimental Section

Carbon Material. A commercial activated carbon, denoted as PAC, was used as a starting material. PAC with a surface area of 2311 m^2/g was prepared from petroleum coke and chemical activated. Prior to the use in experiments, PAC was washed by the distilled water, and then tried at 110 °C in a vacuum oven overnight for removal of moisture and other adsorbed contaminants.

Oxidative Modification of PAC. $(NH_4)_2S_2O_8$(APS) was used as an oxidant for oxidative modification of PAC . The oxidation process was conducted by adding 20ml of the APS solution with different concentrations from 0.1-2.5mol/L in 1M H_2SO_4 to 1g of PAC sample placed in a glass conical flask with a magnetic stirrer. The mixture was stirred at the desired temperatures for the desired periods of time. After oxidation, the treated PAC was separated from the solution by filtration and washed several times with the distilled water until a stable PH value was reached. The filter cake was dried at 110 ºC in a vacuum oven for 24h, and then, kept in a glass bottle with a cover before use. The treated PAC samples were denoted as Px-y-z, where x is concentration of APS in the solution, y is reaction temperature (°C) and z is oxidation time (h).

Characterization of AC Samples. The surface areas of AC samples were measured by the nitrogen adsorption at 77 K, and the pore size distribution was calculated by applying the Barrett-Joyner-Halenda (BJH) method on the desorption branch of isotherm curves. The oxygen-containing functional groups on the carbon surface were analyzed by TPD-Mass. About 100 mg of the sample was placed in a quartz reactor. The reactor was then connected to the instrument. After drying the sample, the temperature was increased from room temperature to 1050 ºC at a rate of 5ºC/min under a He flow of 50 ml/min (STP). The evolved CO, CO_2, and H_2O, were continuously measured by a mass spectrometer. The identification and quantification of various oxygen-containing functional groups on AC samples were conducted on the basis of the evolution profiles of CO, CO_2, and H_2O, which has been reported in our previous paper[13].

Adsorption Experiments and Analysis of Treated Oil Samples. A solution with 20.0 μmol/g quinoline in decane was prepared for use in evaluation of the adsorptive performance of the AC samples. The adsorption with different solution/adsorbent weight ratio was conducted in a batch adsorption system with an electromagnetic stirring at 300 rpm at room temperature for 4 h. After the desired adsorption time, the mixture was filtered, and the total

nitrogen concentration in the treated solution was analyzed by using ANTEK 9000 series nitrogen analyzer.

Results and Discussion

Effect of oxidation conditions on the concentration of O-containing groups on AC. The surface modification of PAC by oxidation with $(NH_4)_2S_2O_8$ solution at different concentration from 0.1 to 2.5 mol/L was conducted at 60 °C for 3 h. The measured physical properties and the O-containing functional group concentration are listed in **Table 1**. With increase of $(NH_4)_2S_2O_8$ concentration from 0.1 to 2.0 mol/L in the solution, the concentration of the O-containing functional groups increased from 6.2 to 25.9 mmol/g. Further increase in the $(NH_4)_2S_2O_8$ concentration to 2.5 mol/L resulted in the decrease of the concentration of the O-containing functional groups due to the collapse of the AC porous structure, as indicated by the significant reduction of the surface area and pore volume (see **Table 1**). The effects of the oxidation temperatures and times were also examined, and the results are also listed in **Table 1**. It is interesting to note that high temperature and long time did not lead to the increase of the O-containing functional groups on AC due to the collapse of the AC porous structure. The best oxidation condition for maximizing the O-containing functional groups on AC was found to be at 60 °C, 3 h with 2.0 mol/L concentration of APS solution. At this condtion, the concentration of the O-containing functional groups in the AC can be increased to 25.9 mmol-O/g-A (or 18.1 μmol-O/m^2), which is higher than that of the initial AC (PAC) by a factor of 4.2.

Characterization of O-containing functional groups. The TPD-Mass was used to identify and quantify the various O-containing functional groups in the AC samples. The deconvolution of CO_2 and CO evolution profiles of the AC samples using a multiple Gaussian function method is shown in **Figure 1**. The identified the functional groups on the surface include carboxyl (SA, WA), anhydride (CA), lactone (LD, LC), phenol (Ph), carbonyl (Cl) and quinine (Qu) groups and the estimated concentrations corresponding to each group are listed **Table 2**. It is clear that the oxidative modification significantly increased the concentration of various O-containing functional groups, especially phenol, weak acid carboxyl and carboxyl anhydride groups, increasing by 2.07, 1.74 and 1.49 mmol/g, respectively.

Table 1. Physical and Chemical properties of AC samples

Sample	APS (mol/L)	S_{BET} (m^2/g)	S_{MES} (m^2/g)	S_{MIC} (m^2/g)	Total O (mmol/g)
PAC	0	2311	1142	1168	6.2
P0.1-60-3	0.1	1671	751	921	9.2
P0.5-60-3	0.5	-	-	-	14.8
P1-60-3	1	-	-	-	21.3
P1.5-60-3	1.5	1096	337	759	24.3
P2-60-3	2	1433	538	896	25.9
P2-60-24	2	182	58	125	19.4
P2-25-3	2	1487	570	917	13.7
P2-90-3	2	1325	551	774	21.9
P2.5-60-3	2.5	848	313	535	24.0

Table 2. Results of the Deconvolution of the CO and CO_2-Evoluion Profiles of various AC samples.

ID	Total O	Ph mmol/g	Cl mmol/g	Qu mmol/g	SA mmol/g	WA mmol/g	CA mmol/g	LD mmol/g	LC mmol/g
PAC	6.25	1.00	1.39	0.35	0.30	0.08	0.18	0.13	0.07
P4-60-3h	24.35	3.07	2.11	1.27	0.99	1.82	1.67	0.41	0.1
Increase	18.1	2.07	0.72	0.92	0.69	1.74	1.49	0.28	0.03

Table 3. Adsorption Parameters for Quinoline over AC on the Basis of Langmuir Isotherms

Carbon	S_{BET}(m^2/g)	q_m (mgN/g)	Q_m (mgN/m^2)	K g/ug	Equilibrium capacity (mg-N/g-A) at 50ppm
PAC	2311	13.4	0.0058	0.07	10.4
P4-60-3	1096	29.4	0.0268	0.68	28.6

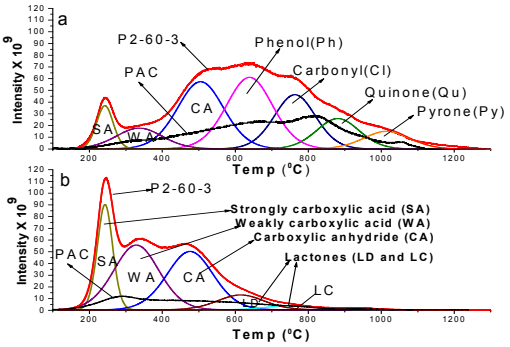

Figure 1. Deconvolution of (a) CO and (b) CO_2 profiles for P2-60-3 in comparison with PAC

Adsorption isotherms and Langmuir adsorption parameters. Adsorption isotherms, as shown in **Figure 2**, were obtained by mixing the adsorbent and the solution with different weight ratio in the batch adsorption system at room temperature for 3 h. The ADN capacity of P2-60-3 is significantly higher than that of PAC. At an equilibrium concentration of 50 ppmw-N, the ADN capacity of P2-60-3 is 28.6 mg-N/g-A, which is higher than that of PAC by a factor of 2.8.

Further analysis of the adsorption isotherms shows that the adsorption of quinoline on PAC and P2-60-3 obeys the Langmuir adsorption isotherm:

$$q = \frac{K\, q_m C_e}{1 + K\, C_e} \qquad (1)$$

where C_e and q are the concentrations of nitrogen in the liquid phase and adsorbed phase at equilibrium, respectively; K is the adsorption equilibrium constant; q_m is the maximum adsorption capacity of nitrogen corresponding to the saturation coverage of the surface. The linear regression between C_e/q and C_e was conducted to estimate the parameter values of K and q_m in the Langmuir adsorption equation. The estimated parameters are listed in **Table 3**. Comparison of these parameters for PAC and P2-60-3 indicates that the much high ADN capacity of P2-60-3 than that of PAC is because the oxidative modification increased the maximum density ($Q_m = q_m/S$; S is the surface area) of the adsorption sites on the surface by 4.6 times and the adsorption equilibrium constant (K) by 9.7 times. The further analysis and correlation of the TPD-Mass characterization data and the measured adsorption parameters imply that the increase of the adsorption sites can be ascribed to the increase in the O-containing functional groups on AC, while the increase in the K value is due to the increasing portion of acidic functional groups on the surface, which enhances the adsorption affinity for the basic quinoline molecules.

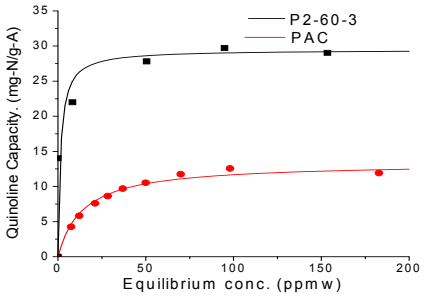

Figure 2. Adsorption isotherms of PAC and P2-60-3 for quinoline at room temperature

Conclusion

In order to increase the ADN capacity of AC, the amounts of O-containing functional groups on the surface was enhanced by oxidation using $(NH_4)_2S_2O_8$ as an oxidant. The best oxidation condition for maximizing the O-containing functional groups on AC was found to be at 60 °C, 3 h with 2.0 mol/L concentration of APS solution. At this condition, concentration of the O-containing functional groups on AC was increased from initial 6.2 mmol-O/g-A (or 2.68 μmol-O/m^2) to 25.9 mmol-O/g-A (or 18.1 μmol-O/m^2) by a factor of 4.2. At an equilibrium concentration of 50 ppmw-N, the ADN capacity of the AC after the oxidation increased to 28.6 mg-N/g-A, which is higher than that of initial one by a factor of 2.8. The further analysis and correlation of the concentration of the O-containing functional groups and the measured adsorption parameters imply that the increase of adsorption sites can be ascribed to the increase in the O-containing functional groups on the AC, while the increase in the K value is due to the increasing portion of acidic O-containing functional groups on the surface, which enhances the adsorption affinity for the basic quinoline molecules.

Acknowledgment. This work was partially supported by the US Department of Energy through CPCPC Grant No: DE-FC26-03NT41874, Subcontract No: 3551-TPSU-DOE-1874. The China Scholarship Council is gratefully acknowledged for supporting Na Li at Pennsylvania State University.

References:

1.Song, C., *Catalysis Today* **2003,** *86* (1-4), 211-263.
2.Zeuthen, P.; Knudsen, K. G.; Whitehurst, D. D., *Catalysis Today* **2001,** *65* (2-4), 307-314.
3.Furimsky, E.; Massoth, F. E., *Catalysis Today* **1999,** *52* (4), 381-495.
4.Sano, Y.; Choi, K.-H.; Korai, Y.; Mochida, I., *Applied Catalysis B: Environmental* **2004,** *49* (4), 219-225.
5.Hernandez-Maldonado, A. J.; Yang, R. T., *Angew. Chem., Int. Ed.* **2004,** *43*, 1004.
6.Kim, J. H.; Ma, X.; Zhou, A.; Song, C., *Catalysis Today* **2006,** *111* (1-2), 74-83.
7.Sano, Y.; Choi, K.-H.; Korai, Y.; Mochida, I., *Energy & Fuels* **2004,** *18* (3), 644-651.
8.Jiang, Z.; Liu, Y.; Sun, X.; Tian, F.; Sun, F.; Liang, C.; You, W.; Han, C.; Li, C., *Langmuir* **2003,** *19* (3), 731-736.
9.Pradhan, B. K.; Sandle, N. K., *Carbon* **1999,** *37* (8), 1323-1332.
10.Moreno-Castilla, C.; López-Ramón, M. V.; Carrasco-Marín, F., *Carbon* **2000,** *38* (14), 1995-2001.
11.Figueiredo, J. L.; Pereira, M. F. R., *Catalysis Today* **2010,** *150* (1-2), 2-7.
12.Figueiredo, J. L.; Pereira, M. F. R.; Freitas, M. M. A.; Orfao, J. J. M., *Carbon* **1999,** *37* (9), 1379-1389.
13.Almarri, M.; Ma, X. L.; Song, C. S., *Industrial & Engineering Chemistry Research* **2009,** *48* (2), 951-960.

Hydrotreating performance of novel catalyst on the support of Beta zeolite in-situ synthesis from kaolin clay

Aijun Duan[1], Guofu Wan[2], Ying Zhang[3], Dengqian Zhang[1], Zhen Zhao[1]*, Ruili Li[1]*

[1] State Key Laboratory of Heavy Oil Processing, China University of Petroleum, Beijing, 102249, China;
[2]College of Mechanical and Energy Engineering, Jiangsu Polytechnic University, 213164
[3]Department of Materials Science and Engineering, China University of Petroleum, Beijing, 102249, China ;
* duanaijun@cup.edu.cn; zhenzhao@cup.edu.cn,
fax: 86-10-69724721

1. Introduction:

Due to the increasing attentions on the environmental protection, the specifications of ultra clean fuels becoming more and more strict than before. Hydrotreating technique is an important choice to produce high-quality ultra clean fuels, in which the catalyst play an essential role in the removal of heteroatomic compounds from the sulphureous feedstocks. It is paid more attention on the design and development of novel hydrotreating catalyst, especially in the synthesis of new kind of materials to be the support. Zeolite beta is a typically porous zeolite with a three-dimensional large-pore structure[1], which were always used in the industrial processes of hydrocracking, hydroisomerization, alkylation and other petrochemical reactions. It also has the characteristics of suitable acidity, higher hydro-isomerization and aromatization activity. The conventional synthesis method of zeolite beta is hydrothermal crystallization method at mild conditions, and others involve vapour-phase transport method, steam-assisted crystallization method and etc[2~4]. In this paper, a micro/mesoporous zeolite beta was synthezed by in-situ hydrothermal crystallization method using kaolin clay as the unique sources of silica and alumina, and the synthesis fators such as preparation conditions of kaolin clay, the ratios of H_2O/SiO_2, the optimal temperature and crystallizaiton time were studied. Using this composite material of Beta as a part of support, $NiMo/Al_2O_3$-Beta catalyst was prepared and used in the HDS process of FCC diesel feedstock to investigate its catalytic performance.

2. Experimental

Kaolin clay from Suzhou was calcined at 720 ℃ for 5 h to obtain metakaolin at first, then it was pretreated with different kinds of acids, i.e., H_2SO_4, HCl and H_3PO_R solutions at various condition to remove the hydroxyl group and alumina radical. The acid concentrations and the preparation conditions were optimized to obtain a suitable SiO_2/Al_2O_3 ratio and the highest crystallinity. In the synthesis process, a mixture solution of TEAOH and NaOH was used to treat the metakaolin, and the formative mixtures are with different molar ratios of $Na_2O:Al_2O_3:SiO_2$:TEAOH:H_2O. Then the composite solutions were put into a high-pressure oven to proceed the crystallization under different temperatures and various times. The final solid products of zeolite beta were filtered, washed, dried and calcined at 550 ℃ for 6h.

Using the above micro/mesoporous Beta zeolites and Al_2O_3 as the supports, the NiMo catalysts were prepared by using series impregnation and incipient-wetness impregnation method with an aqueous solution of nickle nitrate and ammonia hepta-molybdate(10 m% MoO_3, 3.5 m% NiO).

Porosity and surface area of samples were analyzed on a Micromeritics ASAP 2020 automated gas adsorption system. Powder X-ray diffraction (XRD) patterns were collected with a XRD-6000 diffractometer using Cu Kα radiation under 40 kV, 30 mA, scan range from 5 to 80° at a rate of 4°•min^{-1}.

HDS performances were evaluated in a high-pressure fixed-bed micro-hydrotreater with diesel feestock(S content of 1300ppm), and the HDS efficiency was calculated and compared with each other.

3. Results and discussion

3.1 Effects of acid leached conditions:

After calcined, Suzhou Kaolin was pretreated with different acid solutions, i.e., H_2SO_4, HCl and H_3PO_4 at 90 ℃ for 3 h in order to remove the hydroxyl group and alumina radical, the results are shown in Figure 1. It is found that HCl pretreatment resulted in higher SiO_2/Al_2O_3 ratios than other acids.

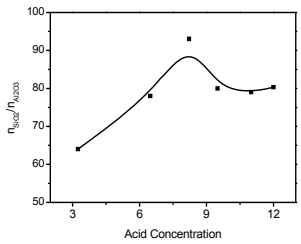

Figure1. The effect of acid type on the SiO_2/Al_2O_3 ratio of acid-treated metakaolin

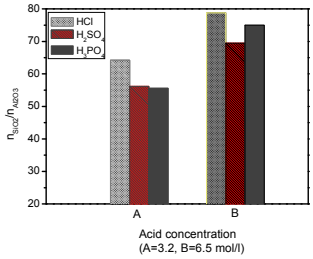

Figure 2. The effect of acid concentration on the SiO_2/Al_2O_3 ratio of acid-treated metakaolin

Using HCl as the acid resource to process the metakaolin, the effects of acid concentrations on SiO_2/Al_2O_3 ratio were researched as shown in Figure 2, which indicate that the suitable conentrations of HCl is 8.2 mol/L and the highest SiO_2/Al_2O_3 ratio reaches to 93.5.

Figure 3 gives the effects of preparation temperature on the SiO_2/Al_2O_3 ratio(with HCl of 8.2 mol/L), demonstrated that high temperature favor to compose zeolite beta with higher SiO_2/Al_2O_3 ratio.

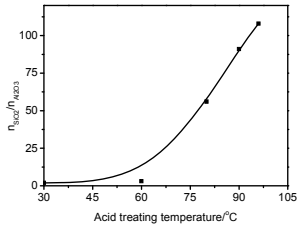

Figure 3. The effect of temperature on the SiO_2/Al_2O_3 ratio of acid-treated metakaolin

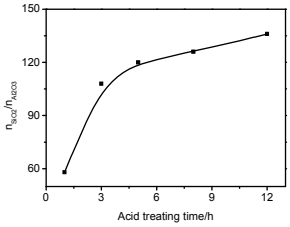

Figure 4. The effect of treating time on the SiO_2/Al_2O_3 ratio of acid treated metakaolin

Figure 4 gives the effects of acid treating time on the SiO_2/Al_2O_3 ratio(with HCl of 8.2 mol/L, at 96℃), and the results prove that the acid treating time keeps at 3 h producing zeolite beta with SiO_2/Al_2O_3 ratio of 90.

Based on the above analysis, the preparation conditions of acid treatment should be controlled to obtain zeolite beta with a suitable SiO_2/Al_2O_3 ratio. The optimal conditions to compose beta with SiO_2/Al_2O_3 ratio of 90 are with 8.2 mol/L HCl as the acid resource at 96℃ for 3 h.

3.2 Effects of crystallization conditions

Figure 5 is the XRD analysis results of different beta samples synthesized with different initial H_2O/SiO_2 ratios. The results indicate that the maximal relative crystallinity of samples is 98.3 as the H_2O/SiO_2 ratio is 3.0.

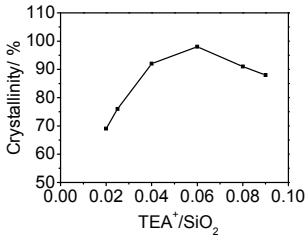

Figure 5. XRD patterns of zeolite β obtained at different H_2O/SiO_2 ratios

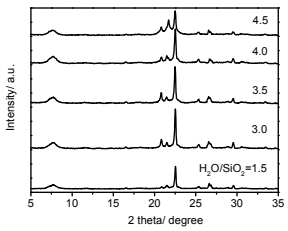

Figure 6. Crystallinity of zeolite β obtained from different $TEAOH/SiO_2$ ratios

The effect of TEAOH addition on the relative crystallinity of zeolite beta is shown in Figure 6, which testify the optimal TEA^+/SiO_2 ratio to be 0.055.

Figure 7 is the relative crystallinity tendency of zeolite beta derived from different Na_2O/SiO_2 ratios. The data show that the minimal alkaline amount required to fully dissolve acid-leached metakaolin is expected to that amount with the Na_2O/SiO_2 ratio of 0.05.

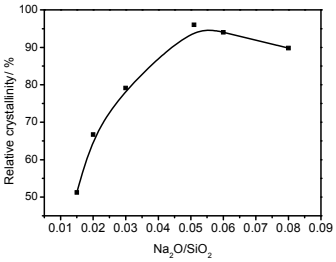

Figure 7. Crystallinity of zeolite β obtained from different Na_2O/SiO_2 ratios

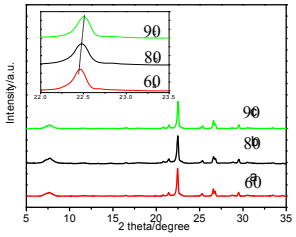

Figure 8. XRD patterns of zeolite β obtained from different SiO_2/Al_2O_3 ratios in initial feed

The effect of crystallization temperature on the crystallinity of beta is given in Figure 9, clarifing that the crystallinity reach a higher ratio at 170 ℃。

Figure 10 is the effects of crystallization time on the crystallinity of beta. From Figure 10, the crystallization curve exhibits a typical S-shaped trend indicated that the induction period is very short, and after 16h the crystallinity becomes stable.

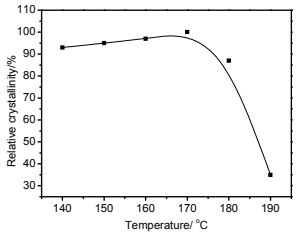

Figure 9. Crystallinity of zeolite β obtained at different crystallization temperatures

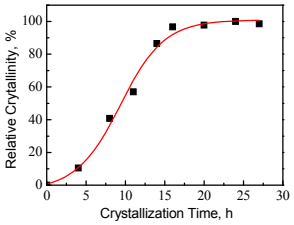

Figure 10. Crystallinity of zeolite β obtained at different crystallization times

Table 1 lists the typical physicochemistry properties of zeolite beta, the support and the relative catalyst.

Table 1. Typical physicochemistry properties

	S_{BET}/m^2g^{-1}	Micropore surface area/m^2g^{-1}	pore volume/m^3g^{-1}	Micropore volume/m^3g^{-1}	Mesopore diameter/nm
Kaolin	28.5	0.0	0.30	0.05	3.7
zeolite beta	550.6	440.1	0.30	0.21	3.7
Beta/Al_2O_3-16	237.0	210.3	0.29	0.18	4.4
Beta/Al_2O_3-32	270.9	236.1	0.29	0.21	3.9

As shown in Table 1, the obtained beta zeolite has a higher surface area, while the average pore diameter is ~3.7 nm. The presence of mesopore maybe facilitate to the diffusion process of reactant molecules into the internal metallic active sites on the surface of catalyst and result in high hydrotreating activity.

Figure 11 exhibits the catalytic performance of supported NiMo/Beta-Al_2O_3 catalysts. The HDS activities in Figure 11 show that these NiMo/Beta-Al_2O_3 catalyst over the composite support of the above synthesized beta with Al_2O_3 have higher HDS efficiencies and can produce high-quality low-sulfur diesel from sulfurious feedstock(with S content of 1300μg/g). The S content in product is lower to 20 ppm, which meets the S specification of ultra clean diesel fuel in EU-IV regulation.

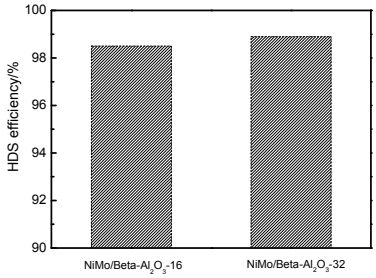

Figure 11. HDS efficiencies of catalysts

4. Conclusion:

Using kaolin clay as the unique sources of silica and alumina, through the optimization of the preparation conditions and the modulation of crystallization parameters, zeolite beta with high crytallinity and micro/mesoporous structure was synthezed by in-situ hydrothermal crystallization method. The relative NiMo/Al_2O_3-Beta catalyst performed good activities in the HDS process of diesel feed.

Acknowledgements

The authors acknowledge the financial supports from NSFC(No.20876173, 20773163 and 20833011), Ministry of Education key project of China(No.31) and CNPC- Petrochemical Research Institute project (No.2008A-3801).

References：

(1) Matsukata M, Osaki T, Ogura M, et al. *Microporous and Mesoporous Materials*. 2002. 56(1): 1-10。

(2) Camblor M A, Mifsud A and Perez–Pariente J. *Zeolites*. 1991. 11(8): 792-797.

(3) Hari Prasad Rao P R, Ueyama K and Matsukata M. *Applied Catalysis A: General*. 1998. 166: 97-103

(4) Matsukata M, Osaki T, Ogura M, etal. *Microporous and Mesoporous Materials*. 2002. 56(1): 1-10

Hydrotreating of gas oil on Ti-HMS supported heteropolyacid catalysts

Soni, K., Boahene, P.E., Dalai, A.K. *
Catalysis and Chemical Reaction Engineering Laboratories, Department of Chemical Engineering, University of Saskatchewan, Saskatoon, SK, S7N5A9 (Canada)

Introduction

In recent years, the environmental constraints have become increasingly more severe, impacting both the quality and the maximum allowable amounts of impurities for commercial on road fuels such as gasolines and diesels. For example, in the European Union (EU), the current legislation limits the total sulfur content to maximum 10 wt ppm[1,2]. Hence, refiners face the challenge of producing ultra-low sulfur diesels (ULSD) by hydrotreating (HDT). Hydrotreating is a process that uses hydrogen and a catalyst to remove contaminants, primarily sulfur, nitrogen and metals from crude oil streams.

The traditional γ-Al_2O_3 supported NiMoS and CoMoS catalysts are industrially used for the hydrotreating of petroleum fractions. However, these catalysts are unable to achieve deep HDS of alkyl-substituted dibenzothiophene (DBT). Thus, improvement of these catalysts is of relevance due stricter environmental regulations and the rather refractory nature of sulfur present in small concentrations (ppm range). In an attempt to develop improved hydrotreating catalysts, different approaches for increasing the catalytic activity of such catalysts have been explored [3-5]. For instance, the use of mixed oxide supports[3], support modification[4], and changing the catalytic precursors for the active metal components [5], have been followed.

Recently, the discovery of mesoporous materials such as MCM-41, SBA-15 and hexagonal mesoporous silica (HMS) have received immense attention due to their attractive properties such high surface area, large and uniform cylindrical mesoporous channels and high thermal stability. As compared to MCM-41 type of mesoporous materials, HMS modified by heteroatoms such as Ti, Al, Zr, etc., have proven to be efficient for the hydrodesulfurization (HDS) of DBT [6]. Their larger pore size and much thicker framework wall than MCM-41 and other desirable textural properties enhance relatively easier access of reactant molecules into its pores; thus, increasing the rate of hydrotreating reactions. Due to their redox character and strong Bronsted acidity, heteropolyacids of Keggin-type structure have been used as catalysts for acid-catalyzed reactions [7]. Precursors of heteropolyacids of molybdenum or tungsten have been used as active components for supported catalysts and applied in the HDS of thiophene [8]. For instance, Kostova et al. [9], deposited HPMo on Al-MCM-41 support and used as a catalyst to study the HDS of thiophene.

In this study, hydrotreating capabilities of HMS and Ti-containing HMS of different Si/Ti atomic ratios using real feed (CLGO) is discussed. These were used as supports for the preparation of series NiPMo catalysts. The catalysts and supports were characterized by N_2 adsorption-desorption isotherms, XRD, FT-IR, Raman, TEM, SEM, H_2-TPR. Activity studies were conducted by screening the catalysts using coker light gas oil derived from Athabasca bitumen. For comparison purposes, the conventional NiMo/γ-Al_2O_3 and NiMo/HMS catalyst were also screened at the same operating conditions.

*Corresponding author. Tel.: +1 306 966 4771; fax: +1 306 966 4777.
E-mail address: ajay.dalai@usask.ca (A.K. Dalai).

Experimental

The HMS material was synthesized by using neutral S°I° templating route, proposed by Tanev and co-workers [10,11]. The Ti-HMS material was prepared by using the procedure described by Gotier and Tuel [12] using Dodecylamine as surfactant, TEOS as silica source and Titanium butoxide as Ti source. The reaction mixture was slightly modified by using mesitylene as swelling agent. Prior to filtration of products, the reaction mixture was aged for 24 h under stirring. The reaction products were then recovered, washed with distilled water and dried at room temperature overnight; followed by drying at 120 °C for 2 h. Samples were then calcined in air at 550 °C for 5 h at a heating rate of 2 °C/min.

Results and Discussion

The presence of a low angle diffraction peaks and a high surface area demonstrates that the materials prepared by the neutral template route have a mesoporous crystalline structure. The low angle X-ray diffraction of HMS materials showed an intensive reflection first-order peak at small angles that is characteristic of HMS material. This single low angle peak indicated that HMS displayed a short range hexagonal symmetry with uniform pore diameter. The calcined NiPMo/Ti-HMS (20) sample also showed a single first-order peak but the higher order diffraction peaks was not seen as observed in HMS support, confirming the preservation of the hexagonal structure with lack of long-range order. The lack of higher order of the reflections corresponds to the small size of the scattering domain.

N_2 physisorption data show that the MPA-based catalysts have good textural properties and less pore blockage on the entrances of the mesopores compared to the traditional catalysts **(Table 1).** The Transmission electron microscopy image provides insights into the porous framework of Ti-HMS and NiPMo/Ti-HMS materials. Typical wormhole-like pores of Ti-HMS materials with network channels and uniform pore sizes exist in all samples; although long range ordering was absent, which was also confirmed by low angle XRD patterns.

Table 1 Physical properties of HMS, NiMo/HMS, Ti-HMS and NiPMo/Ti-HMS with different Si/Ti ratios determined from N_2 sorption and XRD

IR and Raman spectra of oxide catalysts indicate that the characteristic Keggin structure of the HPMo precursors was preserved during the impregnation of Ti-HMS and subsequent drying and calcination steps. The TPR profile of HPMo/Ti-HMS sample displays only one well-defined

peak at 508ºC which can be assigned to the first reduction step of octahedrally coordinated Mo^{6+} in polymolybdate structure. It can be observed that the use of $H_3PMo_{12}O_{40}$ as catalytic precursor provides a more homogeneous distribution of octahedral Mo species on the support compared to NiMo/HMS. Ni addition to HPMo/Ti-HMS catalyst leads to a decrease in the reduction temperatures of molybdenum species. DRIFT spectroscopy of CO adsorption shows that the intensity of band for NiMoS sites increased steadily when the Si/Ti ratio decreases from 80 to 20. It clearly indicates that while increasing the Ti content in the framework of HMS the number of promoted MoS_2 sites is increased accordingly.

The catalytic activity data was obtained after the catalysts stabilization. The catalysts were stabilized by precoking using CLGO at the temperature, pressure, LHSV and H_2/feed ratio of 370 ºC, 8.8 MPa, 2 h^{-1} and 600 ml/ml, respectively for 5 days. The catalyst stabilization curve of all the NiMo/γ-Al_2O_3, NiMo/HMS and NiPMo/Ti-HMS catalysts in terms of N and S conversions, are shown in **figure1.** . The initial high value in HDN and HDS activities of these catalysts shows that there is high number of active sites at initial stage of hydrotreating. The N and S conversions of CLGO catalysts decreases with time on stream and reached steady state after 3 days, probably due to coking of the most acidic sites. On the contrary, N and S conversion over the catalyst with lower acidity (NiMo/γ-Al_2O_3) is relatively stable.

Figure1. HDS (■) and HDN (▲) activities of HMS, Ti-HMS and γ-Al_2O_3 supported catalysts during pre-coking with CLGO at 375ºC (catalyst = 5 cm^3, P = 8.8 MPa, LHSV = 2 h^{-1} and H_2/oil ratio = 600 (v/v)).

The HPA loaded catalysts shows higher catalytic activities compared to reference catalysts under similar reaction conditions. The N–S conversion confirm the following order of activity: NiPMo/Ti-HMS(20) > NiPMo/Ti-HMS(40) > NiPMo/Ti-HMS(80) > NiMo/ HMS > NiMo/γ-Al_2O_3. When the reaction temperature is low (330 and 350ºC), the better performance of NiPMo/Ti-HMS catalyst over NiMo/γ-Al_2O_3 is clearly visible. But at higher temperature (375ºC) the activities of both γ-Al_2O_3 and Ti-HMS based catalysts are almost equal. It may be due to the attainment of maximum activity of catalyst at higher temperature.

Acknowledgements

The authors are grateful to Syncrude Canada Ltd. and Natural Sciences and Engineering Research Council of Canada for financial support for this research.

References

[1] Zepeda, T.A., Pawelec, B., Fierro, J.L.G., Olivas, A., Fuentes, S., Halachev, T., Appl. Micro. & Meso. Mat. 111 (2008) 157-170.
[2] Zepeda, T.A., Pawelec, B., Fierro, J.L.G., Halachev, T., Appl. Catal. B: Env. 71 (2007) 223-236.
[3] Zdrazil, M. Catal. Today 86 (2003) 151.
[4] Sundaramurthy, V., Eswaramoorthi, I., Dalai, A.K., Adjaye, J., Micro. & Meso. Mat.111 (2008) 560-568.
[5] Vradman, L., Landan, M.V., Herskowitz, Ezersky, V., Talianka,M., Nikitenko, S., Koltypin, Y., Gedanken, A., J. Catal. 213 (2003) 163.
[6] Pawelec, B., Damyanova, S., Mariscal, R., Fierro, J.L.G., Sobrados, I., Sanz, J., Petrov, L., J. Catal. 223 (2004) 86–97.
[7] Ghanbari-Siahkali, A., Philippou, A., Dwyer, J., Anderson, M.W., Appl. Catal. A: General 192 (2000) 57–69
[8] Kostova, N.G., Spojakina, A.A., Jiratova, K., Solcova, O., Dimitrov, L.D., Petrov, L.A., Catal. Today 65 (2001) 217-223.
[9] Kostova, N.G., Alla, E.K., Spojakina, A.,Godocikova, E., Balaz, P., J. Mater Sci (2007) 42:3321–3325.
[10] Tanev P. T., Pinnavaia T. J., Science, 267 (1995) 865.
[11] Tanev P. T., Chibwe M., Pinnavaia T., Nature, 368 (1994) 321.
[12] Gotier S., Tuel A., Zeolites, 15 (1995) 601.

Direct Production of Gasoline and Diesel from Biomass using Integrated Hydropyrolysis and Hydroconversion (IH^2)

Terry Marker[(1)], Larry Felix[(1)], Martin Linck[(1)], Michael Roberts [(1)]

[(1)]Gas Technology Institute
1700 South Mount Prospect Road
Des Plaines, Il 60018

Introduction

There is considerable worldwide interest in developing technologies for converting lignocellulosic biomass into transportation fuels as a way to reduce dependence on foreign oil and reduce fossil green house gas emissions. The DOE has estimated that 1 Billion tons per year of biomass[(1)] is available for conversion in the United States. If all of that U.S. biomass was converted to liquid fuels, a large portion of imported crude used to make transportation fuels could be eliminated, as shown in Figure 1.

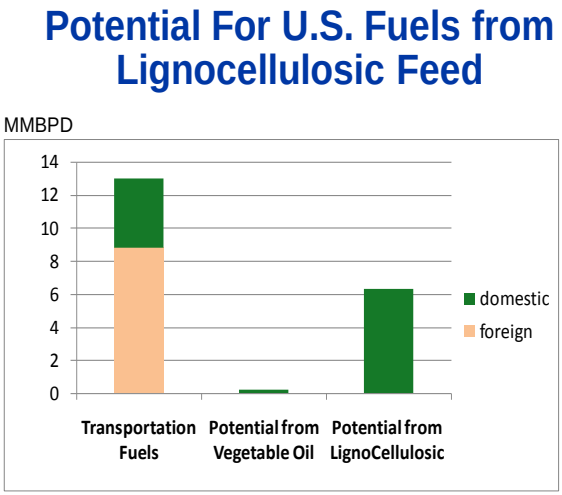

Figure 1. Potential for US Fuel Production from Lignocellulosic Biomass.

Fast pyrolysis[(2)(3)(4)] has long been advocated as a method for converting lignocellulosic biomass to liquids which could then be combusted to make electricity or be transported to oil refineries for processing into fungible fuels. However, fast pyrolysis oil possesses many undesirable properties including a high total acid number (TAN ~200), low heating value (~6560 BTU/lb), high oxygen content (~40%), chemical instability, high water content (20%) and incompatibility with petroleum fractions. Its inherently low energy density makes pyrolysis oil expensive to transport and the high TAN makes it metallurgically incompatible with conventional transport vessels and refinery hydroconversion equipment, both of which are designed for feeds with TAN<2. In addition to these undesirable properties, pyrolysis oil is not miscible with petroleum fractions and if added into existing refinery equipment (hydrotreaters or hydrocrackers) will require a separate pyrolysis-oil feed system. Thus, pyrolysis oil is chemically far from a crude oil replacement.

Upgrading pyrolysis oil[(5)(6)(7)] through hydroconversion has been demonstrated in pilot testing but is carried out at low space velocities (0.1-0.2 LHSV), high pressures (1500-2500psig) with short run times. Finally, pyrolysis oils upgraded to remove oxygen and make gasoline and diesel typically requires an additional 3-5 wt. % hydrogen, on a pyrolysis oil feed basis. Indeed, the conditions required for upgrading pyrolysis oil make it similar in cost to upgrading petroleum resid. When pyrolysis oil is upgraded to remove the oxygen, the finished hydrocarbon yield is 26-30% of the starting biomass[(7)]

A better approach for biomass conversion is the integrated hydropyrolysis and hydroconversion (IH^2) of biomass to directly produce fungible gasoline and diesel fuel or blending components. IH^2 is carried out in two integrated stages, as shown in Figure 2. The first stage is a medium pressure, catalytically-assisted, fast hydropyrolysis step completed in a fluid bed under moderate hydrogen pressure of 200-500psi. Vapors from the first stage pass directly to a second stage hydroconversion step where a hydrodeoxygenation catalyst removes all remaining oxygen and produces gasoline and diesel boiling range material. All the process steps are completed at essentially the same pressure (except for pressure drop across the equipment) so that compression costs are minimized. A unique feature of this process is that all the hydrogen required for the IH^2 process is produced by reforming the C_1-C_3 hydrocarbons so no additional hydrogen is required. Initial economic analysis suggests that the IH^2 process reduces handling, transportation, processing, and has about the same capital costs as pyrolysis alone, making it a much more attractive approach.

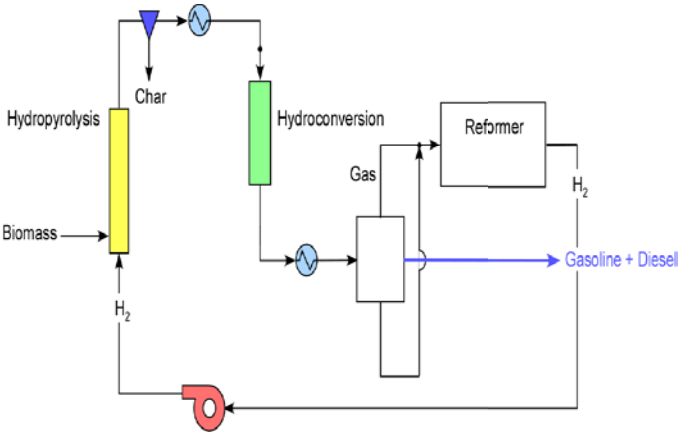

Figure 2. IH^2 system schematic, showing overall process flow.

Experimental

Analyses of the feedstocks used for the IH^2 experiments are shown in Table 1. These two biomass feeds are quite different in chemical composition and were chosen to exhibit the versatility of the IH^2 process.

IH^2 proof-of-concept testing was carried out in a pressurized fluid bed hydropyrolysis first stage that incorporated an internal char filter (2 micrometer pore size) followed by a fixed bed integrated hydroconversion second stage. An existing small-scale GTI gasifier was reconfigured for use in the hydropyrolysis R&D effort. A key modification was the addition of a hydroconversion reactor used as a fixed catalyst bed located directly downstream of the hydropyrolysis unit and process filter. Figure 3 shows the IH^2 pilot scale system.

Three different first stage hydropyrolysis catalysts have been tested. Hydropyrolysis catalyst choice was found to significantly affect the IH^2 product yield and quality, including relative amounts of gasoline and diesel that were produced.

Table 1- Analyses of Wood and Lemna Derived Feedstocks

Component	Wood	Lemna (Minor Duckweed)
%C	49.7	46.3
%H	5.9	5.8
%O (by difference)	43.0	35.7
%N	0.22	3.7
%S	0.07	0.3
%ash	1.1	8.2
% Cellulose	40	-
% Hemicellulose	32	-
% Lignin	28	-
% Carbohydrate	-	52.2
% protein	-	28.7
% lipid	-	1.0
% fiber	-	8.0

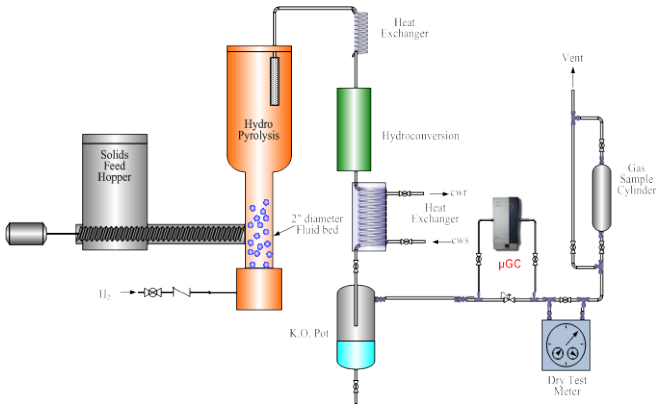

Figure 3. The GTI IH^2 proof-of-concept unit.

The catalyst used in the second stage fixed bed hydroconversion reactor was a sulfided CRI/Criterion Inc. CoMo catalyst. The CRI/Criterion Inc. catalyst worked well to deoxygenate the hydropyrolysis vapors and showed no sign of deactivation across all the testing.

Several encouraging experimental observations should be noted. Significantly, no increase in pressure drop was observed across the system filter as IH^2 testing progressed, suggesting that the fully hydrogenated product is a nonreactive component in the process exhaust. In tests of conventional fast pyrolysis of wood, a significant increase in filter pressure drop occurred during similar test periods. This shows the excellent chemical stability of the hydropyrolysis product compared to typical fast pyrolysis products (oils). The char and catalyst recovered after the experiment remain finely divided without the presence of agglomerates of char and bed material. Also, recovered water and liquid hydrocarbons form distinct separate phases and the hydrocarbon liquids produced by the IH^2 process are miscible with petroleum-based fuels.

Results and Discussion:

Data resulting from the IH^2 process development work are presented in Table 2 over a range of conditions. These data show that good yields of negligibly low oxygen content, light hydrocarbon product is produced from the IH^2 process and the proper amount of C_1-C_3 light ends is produced which can be reformed to produce all the H_2 required by the process to complete hydrogenation.

Table 2 - IH^2 Experimental Yields* –MAF

Component	Wood	Lemna (Minor Duckweed)
% C_4+ Liquid Yields	23-30	23-30
% Oxygen in Liquid	<1	<1
TAN in Liquid	<1	<1
% gasoline boiling range in liquid	53-75	55-72
% Diesel boiling range in Liquid	25-47	28-45
% Char	7-14	3-15
%COx	13-23	12-20
%C_1-C_3	8-14	4-16
% Water	31-35	30-40

* As process conditions are varied; MAF – Moisture and Ash Free

The product quality of IH^2 liquid is consistently good, with low TAN, and low oxygen content as shown in Table 3. The liquid from a lemna feed does contain more nitrogen because higher nitrogen is present in the feed biomass. With further process optimization it should be possible to reduce nitrogen in liquids from high nitrogen biomass just by operating under more severe process conditions and switching to a NiMo catalyst in the second stage.

Table 3 – Typical Product Quality of IH2 C4+ Liquid

Component	Wood	Lemna (Minor Duckweed)
%Oxygen	<0.3	<.5
%Carbon	88.27	84.62
%Hydrogen	11.86	13.70
%Sulfur	0.006	0.005
%Nitrogen	0.05	1.23
TAN	0.4	0.2
H/C	1.61	1.94
Density, gm/cm^3	0.84	0.77

The water analysis is shown in Table 4. The water produced by the IH^2 process varies with feed biomass. The wood feed produced water with low carbon contamination which should simplify cleanup and reuse. Although further testing is required, it is expected that after cleanup, the water from the wood process can be recycled to the reformer, making the process completely self sufficient in water as well as in hydrogen. Water from the lemna feed is rich in ammonia which may best be recycled back to the lemna ponds as fertilizer.

Table 4 –Typical Analysis of Water from IH^2

Component	Wood Feed	Lemna Feed
% Carbon	<1	4-5
PH	9	11
%Nitrogen	0.1	5-6 (mostly NH_3)
%Sulfur	0.03	Not measured

The analysis of the C_1-C_3 gas produced from IH^2 is shown in Table 5. The gases produced are saturated and no olefins are detected.

Table 5–Typical C_1-C_3 Analysis-Wt%, Normalized

Component	Wood Feed	Lemna Feed
Methane	33.1	27.7
Ethane	38.2	36.9
Propane	28.7	35.2

Effect of Process Variables: Testing has just begun to define the effect of process variables in the IH^2 process and some key trends have already been identified. Raising temperature in the first stage hydropyrolysis, decreases char and increases C_1-C_3 hydrocarbon gas as is shown in Figures 4 and 5.

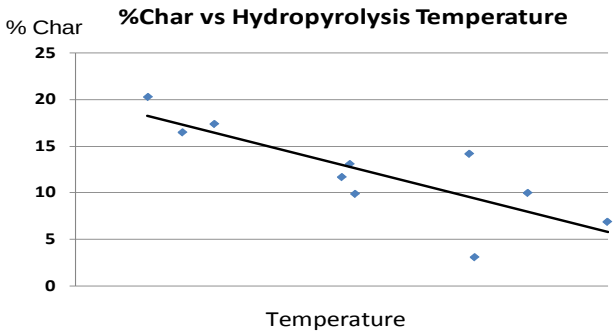

Figure 4 - % Char versus Hydropyrolysis Temperature

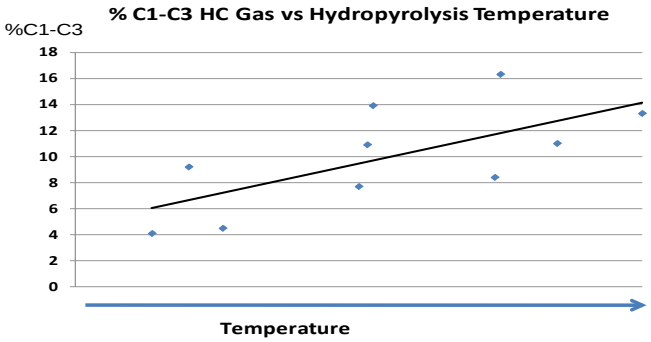

Figure 5 -%C_1-C_3 Hydrocarbon gas vs Hydropyrolysis Temperature

Life Cycle Analysis. A life-cycle analysis (LCA) of the integrated hydropyrolysis and hydroconversion process for wood was completed by Professor Shonnard based on the proof of principle results[8]. Professor Shonnard is Deputy Director of Sustainable Futures Institute, author of a widely used LCA text book, "Green Engineering: Environmentally Conscious Design of Chemical Processes," [9] and expert in LCA analysis. This analysis reveals the IH^2 process has the potential to reduce greenhouse gas emissions by over 90%, for fuels made by this process, as shown in Figure 6. Figure 6 compares the IH^2 technology to other published LCA[10] from other technology approaches.

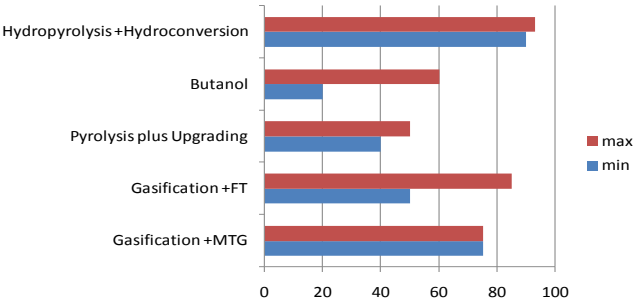

Figure 6–Comparison of % Greenhouse Gas Reduction for different technology approaches (with gasoline from petroleum as a basis).

Conclusions:

The Gas Technology Institute (GTI) has completed initial pilot plant testing which has identified a significant, new, attractive approach for converting lignocellulosic and aquatic biomass directly to fungible gasoline and diesel fuels. Additional work is needed to fully demonstrate and commercialize the process. More process variable work is planned and catalyst life testing is required before commercialization can occur.

Acknowledgement:

GTI would like to acknowledge the assistance of CRI/Criterion Inc. in providing the catalyst used in these studies and the work of Professor Shonnard of MTU in carrying out the preliminary life cycle analysis of the IH^2 process. GTI would also like to acknowledge the DOE funding of the portions of our work related to wood as a feedstock under DOE Contract DE-EE002873.

References:

1) Perlack,R,.D., Wright,L.L., Turhollow,A.F., Graham,R.L. Stokes,B.J., Erbach,D.C. "Biomass as Feedstock for a Bioenergy and Bioproducts Industry: The Technical feasibility of a Billion-Ton Annual Supply" DOE-GO-102995-2135

2) Hulet, Craig, Briens,C., Berruti, F., Chan E.W. "A Review of Short Residence Time Cracking Processes" International Journal of Chemical Reactor Engineering", Vol 3 (2005)

3) Bridgwater,A.V., Meier D.,Radlein D. " An overview of Fast Pyrolysis of Biomass." Organic Geochemistry 30,1479-1493,1999

4) Bridgwater A,V.,Peacoke G.V.C. " Fast Pyrolysis processes for biomass" Renewable and Sustainable Energy Reviews 4,1-73,2000

5) Qi,Z., ,Jie, C. Tiejun,W.,Ying, X., "Review of Biomass Pyrolysis Oil Properties and Upgrading Research' Energy Conversion and management 48 (2007) 87-92

6) Elliott,D.C., Neuenschwander, D.G. Liquid fuel by low severity hydrotreating of biocrude. Developments in thermochemical biomass conversion. London: Blackie Academic and Professional 1996 p 611-21

7) Brown, R., Holmgren J, "Fast Pyrolysis Oil and Bio-Oil Upgrading", Oct 4,2006 presentation

8) Shonnard, D, LCA Analysis of Integrated Hydropyrolsis and Hydroconversion Process , Private communication to T.Marker June 2009

9) Allen, D.T. and Shonnard, D.R., "Green Engineering: Environmentally Conscious Design of Chemical Processes", published by Prentice-Hall, 2002

10) Hsu,D.,"Biofuels Beyond Ethanol", NREL Public meeting of the Biomass Research and Development Technical Advisory committee, Sept 9, 2008

Impact of vaporization on catalyst deactivation in low pressure ultra-low sulfur diesel production

Sweers, H. Marcel; Vichailak, Montri; Kraus, Lawrence S.

Criterion Catalysts & Technologies Co. 16825 Northchase Dr. Ste 1000, Houston, TX 77060

Abstract

To comply with the recent implementation of Ultra Low Sulfur Diesel (ULSD, Product S < 10 wppm) requirements in North America and Europe, refiners have opted to either revamp existing diesel hydrotreaters, build grass-roots units, or modify unit feed properties. Many older, lower pressure (500 – 850 psig) units were revamped by adding reactor volume in order to increase residence time and facilitate the conversion of the refractory feed sulfur molecules. Grass-roots ULSD units tend to be designed for much higher operating pressure (1100+ psig).
In the past, typical operating condition requirements for hydrotreating diesel streams yielded satisfactory run lengths and basic bulk properties were sufficient to predict the performance of the catalyst. Commercial run lengths are shorter for ULSD production because the operating conditions required for ULSD are more severe. It has been found in commercial units that some combinations of feed properties and operating conditions lead to unexpected accelerated deactivation rates. These rates cannot be predicted simply by the traditional monitoring parameters and feed bulk properties used in the refining industry and are not typically due to catalyst poisons.

The conditions and mechanism for the accelerated deactivation rates have been identified by observation and evaluation of different commercial operations. Operations where co-processing of coker naphtha, heavy cat naphtha and kerosene at low operating pressure are especially prone to accelerated deactivation even though the desulfurization of the sulfur components in these lighter streams requires less energy. In ULSD operations accelerated deactivation rates are attributed to excessive vaporization of the hydrocarbon feed at high temperatures (end-of-cycle) leading to operation outside of the trickle bed regime and reduced hydrogen partial pressure. Operating outside the trickle bed regime adversely affects physical parameters such as catalyst wetting and liquid distribution. High amounts of vaporization (> 80 wt%) result in reduced hydrogen partial pressure and long residence times for heavy aromatic molecules. These factors lead to an operating environment conducive for coke formation and catalyst deactivation. The effects of vaporization, due to chemical properties of feed components and physical phenomena in the reactor at high operating temperature, of a specific commercial low pressure (~ 500 psig) ULSD unit causing the acceleration of catalyst deactivation at end-of-cycle are discussed.

Introduction.

One of the important treating processes in oil refining is hydrodesulfurization (HDS). In HDS the removal of sulfur in oil is accomplished catalytically in the presence of hydrogen and solid catalyst. Due to the negative impact of sulfur compounds on the environment the severity of this common process has been increased to reduce diesel product sulfur concentrations to ultra-local-sulfur diesel (ULSD – S < 15 wppm). This specification is practically the standard in the OECD countries and an increasing number of countries in the developing world are following suit. To comply with the recent implementation of ULSD) requirements in North America and Europe, most refiners have opted to either revamp existing diesel hydrotreaters, build new grass root units, or modify unit feed properties.

Discussion.

Background

The need for debottlenecking of existing units to meet stricter diesel and other fuel sulfur specifications is directly related to the chemical properties of the sulfur compounds that have to be removed. The order of difficulty increases as follows aliphatic < cyclic (naphthenic) < aromatic sulfur compounds. The concentration of the respective types of molecules increases with increasing final boiling point of the different oil fractions to be treated, i.e. kerosene, diesel, etc. A typical diesel stream contains disulfides, thiophenes, benzothiophenes, and dibenzothiophenes., all of which can be substituted with alkyl groups. The relative reactivity of these different species correlates with their boiling points as illustrated in Figure 1.

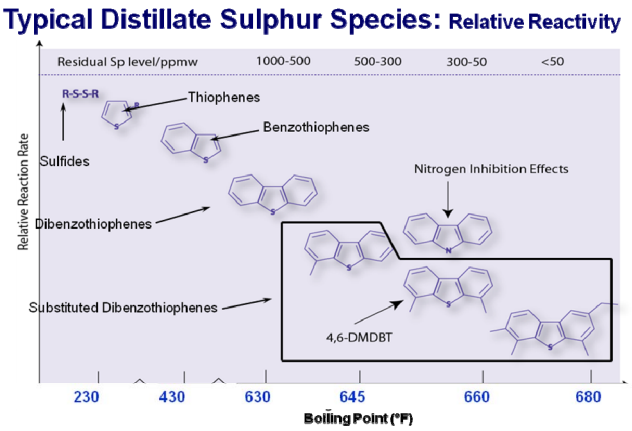

Figure 1. Reactivity and Boiling Point Properties of Typical Distillate Sulfur Species.

From Figure 1 it can be seen that only substituted dibenzothiophenes (DBT) and heavier remained in the product when producing 500 wppm sulfur diesel. It is important to note that the relative reactivity of the distillate stream depends on the composition of the stream. In refineries with cracking processes installed such as fluid catalytic cracking units (FCCUs) and delayed coking units (DCUs), it is necessary to treat refractory distillate streams such as FCCU Light Cycle Oil (LCO) and DCU coker distillate. Both of these stream are high in nitrogen and olefin contents. LCO is very aromatic (70 – 90+%). The high olefin contents of these streams make them very reactive and result in high lead bed ΔT's. In cracked streams the concentration of substituted DBT and heavier sulfur molecules increases dramatically. In all diesel streams, the concentration of sterically hindered DBT species increases with increasing endpoint (EP). As can be seen from Figure 2 substitution in the 4 and 6 position of the DBT molecules dramatically reduces the reactivity of these molecules. Increasing the size of the moieties adjacent to the sulfur atom reduces the reactivity, further indicating that steric hindrance affects the sulfur removal process. The lower relative reactivities of the heavier sulfur molecules requires longer residence

times and/or higher H_2 pressures. It is well established that sulfur removal from DBT molecules involves two competing mechanistic pathways: a) a direct desulfurization pathway (DDS) and b) an indirect pathway (HYD) where (partial) hydrogenation of the DBT molecule precedes the actual hydrogenolysis step (1-4).

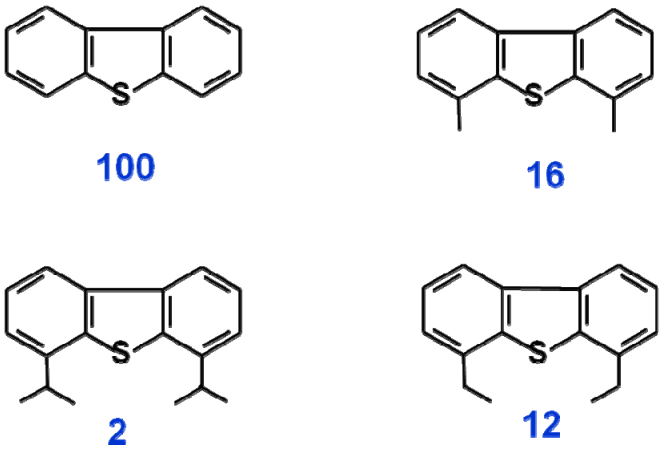

Figure 2. Relative Rates of Desulfurization for Substituted Dibenzothiophene Species.

When processing a typical feed containing 1 wt% sulfur , the production of 5000 wppm sulfur in the product corresponds to a conversion of 50 wt%. Production of distillate containing 500 wppm sulfur (low sulfur diesel - LSD) requires 95% conversion, and finally 15 wppm sulfur (ULSD) in the product corresponds to 99.85 % conversion. From Figure 1 it can be seen that with increasing HDS the sulfur species remaining in the oil are the more difficult to convert sulfur (sterically hindered DBT) molecules remain in the oil.

Many older, mostly lower pressure (400 – 650 psig) units were revamped by adding reactor volume in order to increase residence time and facilitate the conversion of the refractory (substituted) DBT feed sulfur molecules. New grass roots units tend to be designed for much higher operating pressure (1100+ psig).

Typically, deactivation rates are monitored by referencing the actual operating conditions to a reference case that takes into account sulfur concentration in the feed and product as well as the space velocity. Sometimes the equations used in this data normalization process include terms to allow for correction for H_2 purity, specific feed properties (such as feed nitrogen or T-98) and other factors that may affect the reaction rate.

Commercial run lengths are generally shorter for ULSD production than LSD production because the operating conditions required for ULSD production are more severe. In the past, typical operating condition requirements for hydrotreating diesel streams yielded satisfactory run lengths (i.e. low deactivation rates) and basic bulk properties were sufficient to predict the performance of the catalyst. However, in ULSD operations, it has been found in some commercial units that certain combinations of feed properties and operating conditions lead to unexpected accelerated deactivation rates. These rates cannot be accurately predicted by the traditional monitoring parameters (i.e. bulk sulfur content and space velocity) and are not typically due to catalyst poisons.

Conventional distillate hydrotreating units have been designed to operate as trickle bed phase. A Trickle Bed Reactor (TBR) is a three phase reactor where the catalyst pellet is covered with a film of oil and the gas phase flows concurrently with the oil, usually in down flow operation. Operation of a TBR outside the trickle bed regime of operation can result in poor feed distribution and, as we shall discuss in this paper, accelerated rates of deactivation. Deviation from trickle bed flow because of feed properties or operating conditions can be a major ULSD unit limitation.

There are several kinetic limitations of low pressure ULSD production. One is a limitation based on the two possible mechanistic routes in the conversion of DBT molecules: 1) the direct desulfurization mode (DDS route) and 2) the indirect route that requires partial hydrogenation of the DBT molecule before hydrogenolysis occurs (HYD route). The two routes are summarized (5) in Figure 3.

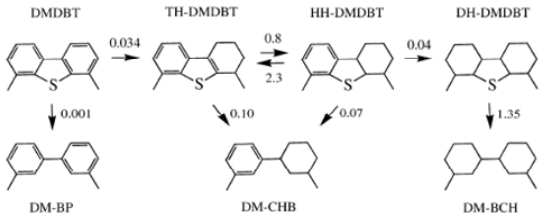

Figure 3. Mechanism of 4,6 Dimethyl Dibenzothiophene HDS and Relative Reaction Rates.

In this work, the different reaction intermediates show above were synthesized: tetrahydro dimethyldibenzothiophene (TH-DMBT), hexahydro DMBT (HH-DMBT) and dodecahydro DMBT (DH-DMBT). The DDS route is considered to be the direct conversion of 4,6-DMDBT (DMDBT) to dimethyl biphenyl (DM-BP). All other reactions are part of the HYD route and lead mainly to dimethyl cyclohexylbenzene (DM-CHB) and dimethyl bicyclohexane (DM-BCH). Two important conclusions can be drawn from this work: 1) the hydrogenolysis reaction of the HYD pathway is ~2 orders of magnitude faster than the DDS route and 2) the hydrogenolysis of 4,6-DMDBT is irreversible and, therefore, not equilibrium constrained. This indicates that it is in principal possible to remove all sulfur by kinetic control. However, other authors (6) have indicated the presence of a "sulfur floor", indicating a certain mechanistic limitation which defines the maximum HDS capability of the process. The "sulfur floor" cannot be explained by the proposed mechanisms. It was found that when treating TH-DMDBT at elevated temperatures only traces of DM-BP were detected, indicating that the DDS route is indeed very unlikely to take place under the experimental conditions.

We have been able to demonstrate the influence of reaction temperature on the rate of HYD pathway in commercial units. Reducing the operating temperature in the lag bed of Unit A below the operating temperature in the lead bed observably increases the HDS and HDN in the lag bed. This could be due to the changes in equilibrium constants at different temperatures and reactor conditions that favor the overall HDS and HDN rate.

It is well known that nitrogen molecules inhibit the HDS reaction. Nitrogen molecules are generally believed to undergo HDN through a hydrogenation mechanistic route similar to the ULSD HDS

mechanism. The hydrogenolysis of partially saturated intermediate nitrogen species is more difficult than the analogous partially saturated sulfur species. Assuming HDN of a DMBT analog, such as carbazole, undergoes a similar hydrogenation pathway as described in Figure 3, the reaction rates will be significantly lower. The net result of the presence of nitrogen is to increase process severity requirements.

Commercial Experience

The catalyst deactivation rates under TBR conditions for straight run distillate (SRD) processing are typically on the order 1-2 °F/month. However, in commercial units we have observed deactivation rates of 5-6 °F/month with feed blends containing coker naphtha, kerosene, and heavy cat naphtha (HCN) that are considerably lighter than SRD. This is counter intuitive because sulfur and nitrogen concentrations are reduced and "easier" sulfur and nitrogen molecules are being added to the feed blend via the light feed streams. However, an investigation of the performance of a commercial unit (Unit A -- two reactors in series with inter-reactor quench) reveals a strong correlation with the endpoint (EP) of the SRD, rather than total feed blend bulk sulfur or other bulk feed properties, and the severity required to obtain the desired HDS. Commonly used monitoring equations do not differentiate between the type of sulfur. They simply lump all sulfur as being equal. Further, these monitoring equations do not account for feed stream boiling properties and their effect on vaporization. Therefore, conventional unit monitoring/normalization equations and methods do not explain the accelerated deactivation rate. In Unit A, the only way to reduce the deactivation rate was to reduce SRD EP. This indicates that concentration of DMDBT molecules can exceed the process capability of Unit A to process the feed blend and obtain the desired catalyst cycle length. The progress of typical Unit A performance parameters is shown in Figure 4. In this graph the maximum measured bed temperature (Tmax), the weighted average bed temperature (WABT), the 98% distillation point (T98) of the total feed, and the liquid hourly space velocity (LHSV) are plotted simultaneously to show the correlation between these four parameters. From this commercial example it is seen that the feed T98 correlates well with temperature requirements and space velocity requirements until ~ 290 days on stream. After this point the WABT requirement to maintain product sulfur specification increases sharply, even with reductions in feed T98 and LHSV.

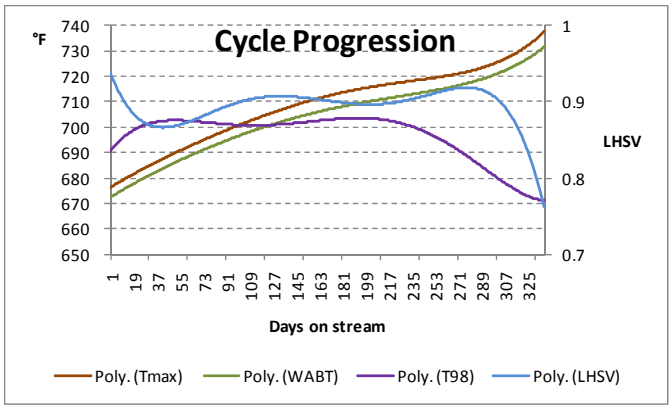

Figure 4. Operating Parameters in Commercial Unit A.

From a mechanistic point of view increasing temperature when under kinetic control should increase the reaction rate. Kinetic behavior is observed at start-of-run where ΔT increases with increasing WABT. However, at end-of-run conditions the lag reactor ΔT is negative. This is due to the dehydrogenation of the non-heterocyclic aromatic molecules in the feed, which are subject to thermodynamic limitations and are present in far greater concentrations (~ 20-25 vol%) than heterocyclic aromatic molecules.

When the impact of catalyst poisons can be neglected, it becomes necessary to evaluate the different hydrotreating reactions to explain catalyst deactivation. It is known that coke formation during hydroprocessing is a major contributor to catalyst deactivation. Coke formation is an inevitable side reaction that is suppressed by maintaining the unit hydrogen partial pressure (ppH_2) with proper minimum H_2/oil ratio. It is known that the heavier end of the distillate fraction contains increasing amounts of polynuclear aromatic (PNA) compounds which are known to form coke by condensation reactions. At low operating pressure (400 – 650 psig) and typical treat gas circulation rates(> 1000 SCFB), temperature changes play a significant role in the ratio of the vapor/liquid (V/L) equilibrium.

In Figure 5 the percent hydrocarbon feed vaporization and the T_{max} are plotted for the commercial unit discussed in this paper (Unit A). From these data it is seen that within the first 3 months ~ 80% feed vaporization was reached.

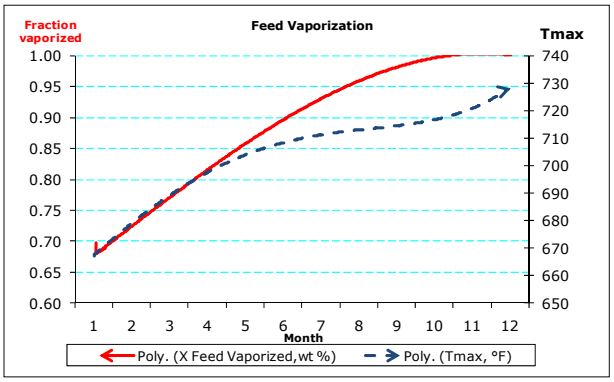

Figure 5. Percent Feed Vaporization vs. Maximum Reactor Temperature in Commercial Unit A

Hydrotreating is generally an overall exothermic process with the temperature being increased periodically to compensate for the inevitable deactivation of the catalyst caused by coke formation on the catalyst surface. In the case of Unit A co-processing of low-boiling coker naphtha causes a significant temperature increase in the top part of the reactor and increases the vapor fraction inside the reactor. The increase of hydrocarbon vaporization has several effects: a) it dilutes the H_2 vapor, which reduces the ppH_2, b) it decreases the liquid hourly space velocity (LHSV) of the oil and the liquid mass flux, c) it increases the concentration of the heavier molecules in the oil , d) it increases the concentration of sulfur molecules in the vapor phase, and e) it increases the vapor/gas space velocity. The general consequence of all the above factors is an increased processing severity requirement to effect the desired reactions (HDS, HDN, etc.) and increased catalyst coking.

The effect of vaporization of oil in hydrotreating units has been studied for vacuum gas oil and it was shown that coking increased with increasing oil vaporization until dropping drastically upon complete vaporization (7). The explanation of this behavior is the progressive concentration of heavy PNA molecules in the oil with increasing vaporization until they themselves are completely vaporized and their resulting short residence time in the gas phase limits their ability to form coke. We believe that this model can be applied to observations described in this paper, because only since the introduction of stricter sulfur specifications and the need to remove more refractory sulfur compounds has it become necessary to apply higher operating temperatures at an earlier stage in the catalyst cycle.

The coke deposit data were collected for the low pressure unit in question (Unit A) and are plotted in Figure 6. The coke deposit increases with the increase in average bed temperature. This is visible in the lead reactor where the vaporization takes place and according to flash calculations eventually complete vaporization is achieved.

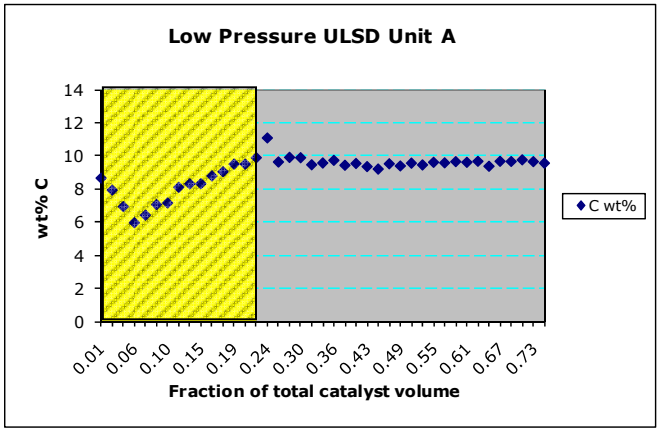

Figure 6. Coke Deposit in Low Pressure ULSD Unit A.

The yellow area with diagonal lines corresponds to the lead reactor and the grey area to the lag reactor. It was found in this particular unit that at start of run (SOR) conditions vaporization at the reactor inlet was about 70% at a WABT of 675 °F and complete vaporization occurred at a WABT of 700 °F. The expected EOR WABT is 720 °F, implying that temperatures corresponding to complete vaporization are reached well in advance of EOR conditions. Assuming that the outer surface area of the catalyst particle makes up about 5% of the total surface area it can be inferred from the quantity of coke found on the non-regenerated catalyst, that most carbon deposits on the outer surface of the catalyst leading to pore mouth plugging. This makes the interior of the catalyst less accessible to the reactants. The coke characteristics were not analyzed in detail and no information could be obtained about when the coke was deposited, but based on the above hypothesis it is likely that coke deposits initially at the bottom of the reactor and then progressively deposits more towards the inlet of the reactor as temperature and extent of vaporization increase. Evaluations of coke deposits in other low pressure units have yielded similar coke deposit profiles. In low pressure ULSD units with unexpected short cycle lengths it was shown that complete vaporization was reached early in the cycle.

To illustrate the effect of maintaining TBR conditions on coke formation, Figure 7 shows the coke profile in a VGO unit where excessive vaporization does not occur and coke deposits increase parallel to temperature increase.

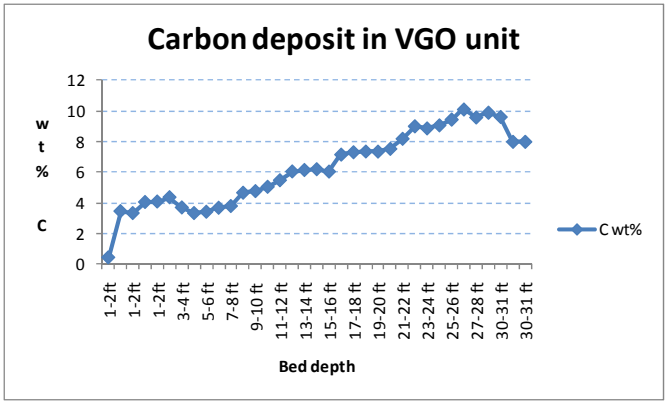

Figure 7. Carbon Deposition in Commercial VGO Unit.

The effect of excessive vaporization may cause the reaction to take place outside the TBR window. Consequently, liquid mass flux is reduced to levels that may cause maldistribution and may drop to levels too low to maintain a film of oil on every catalyst particle. This reduces oil/catalyst contacting efficiency and uniformity and essentially breaks down the fundamental conditions of the TBR process.

The effect of inhibitors, such as nitrogen compounds, H_2S, and PNA molecules, on the HDS process, has not been discussed here. The presence of inhibitors will naturally increase the severity (temperature) requirements of the HDS reaction (8). Higher severity requirements will increase the impact of vaporization effects and coking on the catalyst. Feed selection to manage inhibitor concentrations is a critical aspect of catalyst cycle management for low pressure ULSD units.

Conclusion.

From the observations of commercial low pressure distillate hydrotreating units described in this paper it is clear that the higher processing severity requirements resulting from ULSD sulfur specifications have impacted the hydrotreating process. Higher temperature requirements increase coking reactions. Higher temperature requirements also increase oil vaporization which accelerates coking. This greater potential for coking makes it necessary to determine the process capability of each unit and catalyst system design to avoid unrealistic stability projections and expectations The departure from linear deactivation near the EOR in diesel hydrotreating is highly likely due to the physical changes (higher oil vaporization, reduced oil/catalyst contacting) discussed in this paper. These effects are not attributable to the catalyst quality, but to the feed composition and the corresponding severity required to produce ULSD. Therefore, it becomes essential to evaluate and determine the process capabilities of a particular unit to process certain feeds. ULSD catalyst system and unit designs must take V/L behavior and effects in consideration because they play an important role in the catalyst deactivation from coking reactions in hydrotreating.

References.

(1) Froment, Gilbert F., Depauw, Guy A., and Vanrysselberghe, Valerie; *Ind. Eng. Chem. Res. 33* 1994, 2975
(2) T. Kabe, A. Ishihara, W. Qian, Hydrodesulfurization and Hydrodenitrogenation,
Kodansha Ltd./Wiley-VCH, Tokyo/Weinheim, 1999
(3) R. Prins, in: G. Ertl, H. Knőzinger, F. Schűth, J. Weitkamp (Eds.), second ed.,
Handbook of Heterogeneous Catalysis, vol. 6, Wiley-VCH, Weinheim, 2008, 2695.
(4) M. Egorova, R. Prins, *J. Catal*. 225 2004, 417.
(5) X. Li et al, *J.Cat.,* 250 (2007) 283
(6) Ho, T.C., *J.Catal.;* 219 (2003) 442
(7) Jong de, K; *Ind.Eng.Chem.Res*. 33, 1994, 3141
(8) Koltai, T., Macaud, M. Guevara, A., Schulz, E. Lemaire, M., Bacaud, R., Vrinat, M. ; *Appl. Catal. A*: General 231 (2002) 253

Combined CoMo/NiMo Catalyst System Advantages in ULSD Production: Part I – Pilot Plant Studies

Lawrence (Larry) S. Kraus & Patrick J. Gripka

Criterion Catalysts & Technologies, 16825 Northchase Drive, Suite 1000, Houston, TX 77060

Abstract

Catalyst systems can be designed for commercial Ultra Low Sulfur Diesel (ULSD) hydroprocessing units that maximize catalyst activity while controlling H_2 consumption to remain within unit H_2 constraints. Catalyst systems utilizing $CoMo/Al_2O_3$ (CoMo) and $NiMo/Al_2O_3$ (NiMo) catalysts in various proportions and in various configurations (stacked beds and "sandwich" beds) can yield synergistic benefits in ULSD production. These benefits can be utilized to process more ULSD feed, process more difficult ULSD feeds, or extend cycle life.

Pilot plant data are shown comparing the ULSD hydrodesulfurization (HDS) activities and H_2 consumptions for individual CoMo and NiMo catalysts to various CoMo/NiMo catalyst systems. Both a Type II CoMo (CoMo A) catalyst and a conventional CoMo (CoMo B) catalyst were used in this study. The NiMo tested was a Type II catalyst. The ULSD activities of the individual CoMo and NiMo catalysts were compared to NiMo/CoMo/CoMo (1/1/1 - Volume Basis) and CoMo/NiMo/CoMo (1/1/1 - Volume Basis) catalyst systems. The feed tested was a Middle East Straight Run Gas Oil (ME SRGO) with S = 1.71 wt%, N = 190 wppm, and a Final Boiling Point (FBP) = 808°F (431°C). The processing objective in these tests was product S = 10 wppm. The process conditions used were: P = 800 psig (55 barg), LHSV = 1 hr^{-1}, and H_2/Oil = 1550 SCFB (261 Nl/l).

Under the feed and processing conditions used, the NiMo catalyst had 60 – 130% higher ULSD HDS RVA (Relative Volume Activity – "activity") than the CoMo A and CoMo B catalysts, respectively. The H_2 consumption with the NiMo catalyst was 25 – 32% higher than with the CoMo A and CoMo B catalysts. Combining NiMo catalyst with the CoMo catalysts increased ULSD HDS RVA by 28 – 35% with CoMo A and 43 – 53% with CoMo B over the individual CoMo catalysts. The activity increases from NiMo incorporation into the catalyst system were accompanied by a 6 – 9% H_2 consumption increase in the case of CoMo A and a 9 – 12% increase in H_2 consumption in the case of CoMo B. Catalyst system configuration had a significant impact on performance. The CoMo/NiMo/CoMo catalyst system had 5% higher ULSD HDS activity than the NiMo/CoMo/CoMo catalyst system in the case of the CoMo A. With CoMo B, the CoMo/NiMo/CoMo system was 7% more active than the NiMo/CoMo/CoMo catalyst system. The CoMo/NiMo/CoMo activity was 12% higher than the linear average of the CoMo and NiMo activities using CoMo A and was 7% higher than the linear average of the CoMo and NiMo catalysts when using CoMo B. This shows that with properly designed catalyst systems (proper catalyst selection and catalyst configuration) there is a synergistic effect from combining CoMo and NiMo catalysts. The CoMo A/NiMo catalyst systems tested achieved 44 – 56% of the individual NiMo catalyst activity advantage over CoMo A while incurring only 24 – 36% of the additional H_2 consumption observed with NiMo.

Introduction

To fully utilize refinery Ultra Low Sulfur Diesel (ULSD) hydrotreating assets, catalyst systems that maximize catalyst ULSD hydrodesulfurization (HDS) activity and unit performance while remaining within unit H_2 supply constraints are required. Catalyst systems utilizing $CoMo/Al_2O_3$ (CoMo) and $NiMo/Al_2O_3$ (NiMo) catalysts in various proportions and in various configurations, such as stacked beds and "sandwich" beds, can be designed to maximize ULSD HDS activity while managing H_2 consumption. This additional activity can be utilized to increase unit throughput, process more difficult feeds (higher refractory S content, higher N content), or extend cycle life.

This paper presents a pilot plant study that was performed with various CoMo, NiMo, and combined CoMo/NiMo catalyst systems in ULSD HDS operation using commercial feed and process conditions. The objective of this study was to establish the ULSD HDS performance benefits of combined CoMo/NiMo catalyst systems.

Catalyst System Testing

A pilot plant study was performed comparing the Ultra Low Sulfur Diesel (ULSD) hydrodesulfurization (HDS) activities, hydrodenitrogenation (HDN) activities, aromatics saturation (ASAT) activities, and H_2 consumptions of various CoMo, NiMo, and combined CoMo/NiMo catalyst systems. In this study, a Type II CoMo (CoMo A) and a conventional CoMo (CoMo B) were used. The single NiMo tested was a Type II catalyst. The ULSD activity of the individual CoMo and NiMo catalysts were compared to NiMo/CoMo/CoMo (1/1/1 - Volume Basis) and CoMo/NiMo/CoMo (1/1/1 - Volume Basis) catalyst systems. The objective of this study was to evaluate the performance benefits of combined catalyst systems. The catalyst loads consisted of three equally sized catalyst beds utilizing CoMo A/NiMo and CoMo B/NiMo combinations. 100% CoMo A, 100% CoMo B, and 100% NiMo catalyst systems were also tested to provide reference levels of performance. The catalyst combinations tested are shown in Table 1.

Table 1. Catalyst Systems Tested

Catalyst System		
Top 1/3	**Middle 1/3**	**Bottom 1/3**
CoMo A	CoMo A	CoMo A
NiMo	CoMo A	CoMo A
CoMo A	NiMo	CoMo A
NiMo	NiMo	NiMo
CoMo B	CoMo B	CoMo B
NiMo	CoMo B	CoMo B
CoMo B	NiMo	CoMo B
NiMo	NiMo	NiMo

The test feed properties and process conditions used are shown in Tables 2 and 3, respectively. The feed tested is a typical Middle East Straight Run Gas Oil (ME SRGO). All tests were performed isothermally in a downflow reactor. The process objective was product S = 10 wppm.

Table 2. Pilot Plant Test Feed Properties

Property	Units	Value
API Gravity	(°)	32.1
Density	g/cc	0.8648
Total S	wt%	1.71

Total N	wppm	190
UV Aromatics		
Mono-	wt%	5.55
Di-	wt%	4.70
Tri-	wt%	2.42
Tetra-	wt%	0.68
Total	*wt%*	*13.35*
D-2887 Distillation		
IBP	°F / °C	343 / 173
10 wt%	°F / °C	484 / 251
30 wt%	°F / °C	556 / 291
50 wt%	°F / °C	621 / 327
70 wt%	°F / °C	676 / 358
90 wt%	°F / °C	734 / 390
FBP	°F / °C	808 / 431

Table 3. Pilot Plant Test Operating Conditions

Process Conditions	Units	Value
Temperature	°F / °C	634 – 680 / 334 - 360
Pressure	psig / barg	800 / 55
H_2/Oil	SCFB / Nl/l	1550 / 261
LHSV	hr^{-1}	1.0
Product S	wppm	< 10

Table 4 contains the temperature requirements of the various catalyst systems tested to achieve product S = 10 wppm, the corresponding H_2 consumptions, and product N data. Table 4 also contains RVA and Relative H_2 Consumption (RHC) data.

Table 4. Pilot Plant Test Results: ULSD HDS Temperature Requirements, H_2 Consumption, & Product N

Catalyst System Top 1/3	Middle 1/3	Btm 1/3	T Required (S=10 wppm) (°F / °C)	ULSD HDS RVA
CoMo A	CoMo A	CoMo A	665 / 352	100
NiMo	CoMo A	CoMo A	651 / 344	128
CoMo A	NiMo	CoMo A	648 / 342	135
NiMo	NiMo	NiMo	634 / 334	163
CoMo B	CoMo B	CoMo B	680 / 360	70
NiMo	CoMo B	CoMo B	665 / 352	100
CoMo B	NiMo	CoMo B	662 / 350	107
NiMo	NiMo	NiMo	634 / 334	163
CoMo A	CoMo A	CoMo A	415 / 70	100	0.5
NiMo	CoMo A	CoMo A	440 / 74	106	0.1
CoMo A	NiMo	CoMo A	450 / 76	109	0.1
NiMo	NiMo	NiMo	520 / 88	125	0.1
CoMo B	CoMo B	CoMo B	390 / 66	95	1.7
NiMo	CoMo B	CoMo B	430 / 73	104	0.7
CoMo B	NiMo	CoMo B	440 / 74	106	0.3
NiMo	NiMo	NiMo	520 / 88	125	0.1

Table 4 (Continued). Pilot Plant Test Results: ULSD HDS Temperature Requirements, H_2 Consumption, & Product N

Catalyst System Top 1/3	Middle 1/3	Btm 1/3	H_2 Consumption (SCFB / Nl/l)	RHC	Product N (wppm)

For purposes of comparison, CoMo A was used as the overall reference catalyst. CoMo A was assigned the ULSD HDS RVA (Relative Volume Activity) of 100 and the relative H_2 consumption (RHC) of 100. The 100% CoMo B catalyst system had the lowest ULSD HDS activity (RVA = 70) and the lowest relative H_2 consumption (95). CoMo A, the NiMo/CoMo B/CoMo B, and CoMo B/NiMo/CoMo B catalyst systems had similar ULSD HDS RVA values of 100, 100, and 107, respectively. These catalyst systems also had similar respective relative H_2 consumptions of 100, 104, and 106. The respective ULSD HDS RVA values of the NiMo/CoMo A/CoMo A and CoMo A/NiMo/CoMo A catalyst systems were 128 and 135. The corresponding relative H_2 consumptions were 106 and 109. The substantially better performance of the CoMo A catalyst system series illustrates that catalyst selection is a critical factor in combined CoMo/NiMo catalyst system design. The 100% NiMo system was the most active catalyst system with an ULSD HDS RVA of 163 and had the highest relative H_2 consumption at 125. When comparing the performance of the CoMo A, NiMo/CoMo A/CoMo A, CoMo A/NiMo/CoMo A, and NiMo catalyst systems, it is seen that the combined CoMo A/NiMo catalyst systems achieve 44 – 56% of the NiMo activity advantage over CoMo A while incurring only 24 – 36% of the additional H_2 consumption observed with the NiMo over CoMo A. The disproportionately high activity increase observed with the CoMo A/NiMo catalyst systems for the additional H_2 consumption incurred represents a significant advantage for H_2 constrained commercial ULSD hydrotreating units.

Figure 1 shows the ULSD HDS RVA values for the various catalyst systems tested. For the NiMo/CoMo/CoMo and CoMo/NiMo/CoMo catalyst systems the expected RVA values from linear averages of the individual CoMo (A & B) and NiMo catalysts are shown. From this figure it is seen that the CoMo A/NiMo/CoMo A, NiMo/CoMo A/CoMo A, and CoMo B /NiMo/CoMo B catalyst systems have 6 – 12% higher activity than would be calculated from the linear average of the individual CoMo and NiMo catalyst activities.

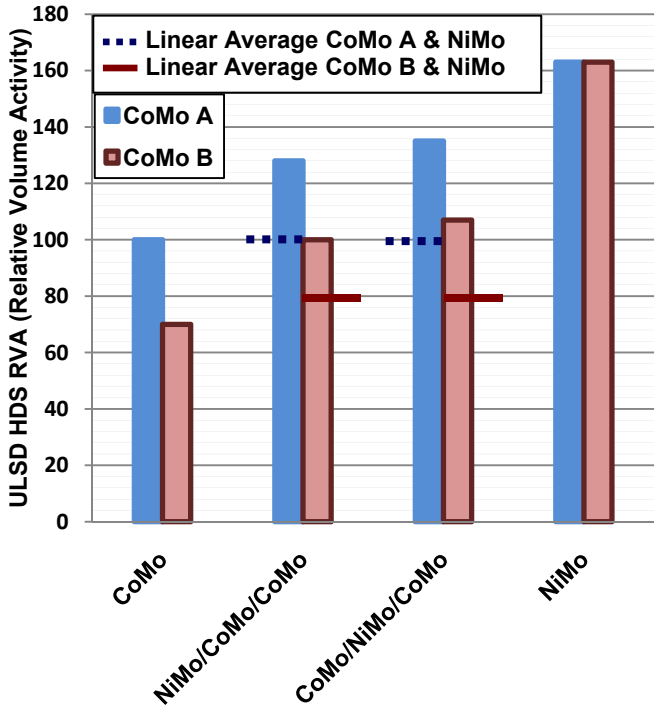

Figure 1. Catalyst System ULSD HDS RVA Values

Figure 2 shows a plot of relative H_2 consumption as a function of ULSD HDS RVA. With both the CoMo A/NiMo and the CoMo B/NiMo catalyst system series, H_2 consumption increases with catalyst activity. This is consistent with the preferred path for ULSD HDS being the indirect (hydrogenation + hydrogenolysis) mechanistic route[1-6]. However, Figure 2 also shows that higher ULSD HDS activity is not simply related to higher H_2 consumption.

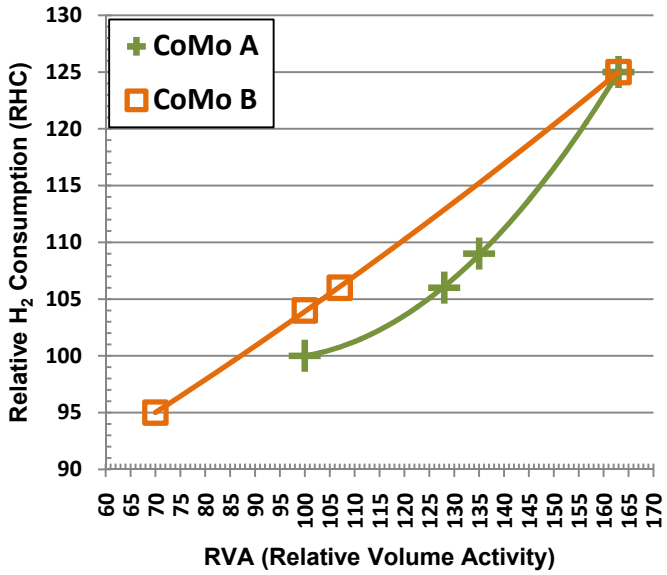

Figure 2. Catalyst System Relative H_2 Consumption (RHC) / ULSD HDS RVA Relationship

From Table 4 it is seen that catalyst system ULSD HDS RVA and product N roughly correlate. In general, the highest ULSD HDS activity catalyst systems have the lowest product N levels. This is illustrated in Figure 3.

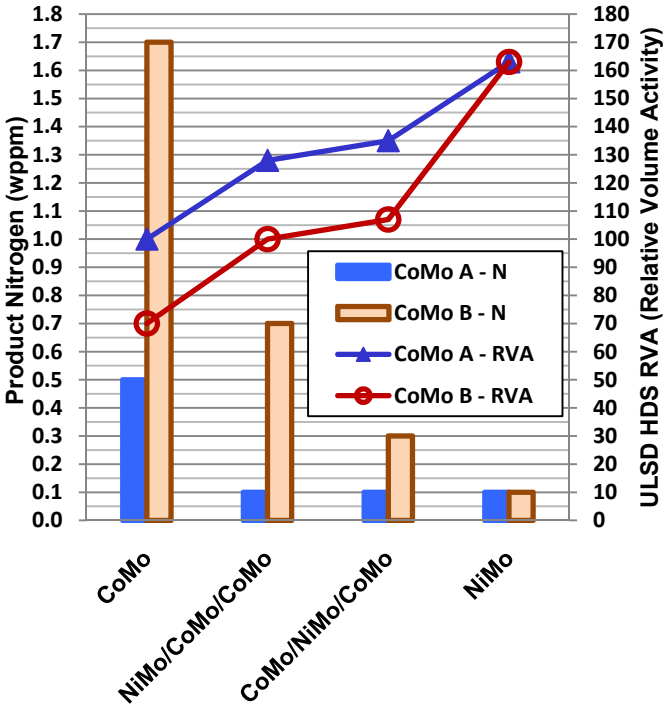

Figure 3. Product N / ULSD HDS RVA Relationship

Organic nitrogen is well-known as a strong inhibitor for ULSD HDS reactions[7,8], so improved ULSD HDS activity with improved HDN is expected. Using the NiMo/CoMo A/CoMo A, CoMo A/NiMo/CoMo A, and NiMo catalyst systems resulted in product N = 0.1 wppm. Since these product N levels are equal, they do not provide relative HDN rate information or any information on the location in the catalyst bed where this product N level is reached. The faster this low N level is reached, the greater the amount of uninhibited catalyst surface available for HDS reactions, and the higher the catalyst system ULSD HDS activity[9]. From this it can be inferred that the HDN activities of the three catalyst systems that achieved product N = 0.1 wppm are: NiMo > CoMo A/NiMo/CoMo A > NiMo/CoMo A/CoMo A. This along with the data for the CoMo B catalyst series indicates that the position of the NiMo catalyst in CoMo/NiMo combined catalyst systems significantly impacts the HDN activity of the catalyst system. With both CoMo/NiMo catalyst series locating the NiMo catalyst in the middle third of the catalyst system resulted in better utilization of the NiMo HDN activity and a greater increase in catalyst ULSD HDS activity.

The aromatics saturation (ASAT) data obtained in this study and the accompanying ULSD HDS RVA data are contained in Table 5 and Figure 4. Both total ASAT and PNA (polynuclear aromatics: 2+ ring aromatics) ASAT data are presented. These data show that higher ULSD HDS RVA is accompanied by higher total and PNA ASAT. This is expected given the greater efficiency of the indirect (hydrogenation + hydrogenolysis) mechanistic route for ULSD HDS and is consistent with the higher H_2 consumption observed with increasing ULSD HDS activity.

Table 5. Pilot Plant Test Results: ULSD HDS Temperature Requirements, H_2 Consumption, & ASAT

Catalyst System Top 1/3	Middle 1/3	Btm 1/3	T Required (S=10 wppm) (°F / °C)	ULSD HDS RVA
CoMo A	CoMo A	CoMo A	665 / 352	100
NiMo	CoMo A	CoMo A	651 / 344	128
CoMo A	NiMo	CoMo A	648 / 342	135
NiMo	NiMo	NiMo	634 / 334	163
CoMo B	CoMo B	CoMo B	680 / 360	70
NiMo	CoMo B	CoMo B	665 / 352	100
CoMo B	NiMo	CoMo B	662 / 350	107
NiMo	NiMo	NiMo	634 / 334	163

Table 5 (Continued). Pilot Plant Test Results: ULSD HDS Temperature Requirements, H_2 Consumption, & ASAT

Catalyst System Top 1/3	Middle 1/3	Btm 1/3	H_2 Consumption (SCFB / Nl/l)	RHC	ASAT (wt%) (PNA / Total)
CoMo A	CoMo A	CoMo A	415 / 70	100	79.0 / 33.0
NiMo	CoMo A	CoMo A	440 / 74	106	85.1 / 36.6
CoMo A	NiMo	CoMo A	450 / 76	109	85.9 / 39.9
NiMo	NiMo	NiMo	520 / 88	125	90.9 / 54.0
CoMo B	CoMo B	CoMo B	390 / 66	95	73.5 / 29.8
NiMo	CoMo B	CoMo B	430 / 73	104	82.3 / 36.8
CoMo B	NiMo	CoMo B	440 / 74	106	82.3 / 39.1
NiMo	NiMo	NiMo	520 / 88	125	90.9 / 54.0

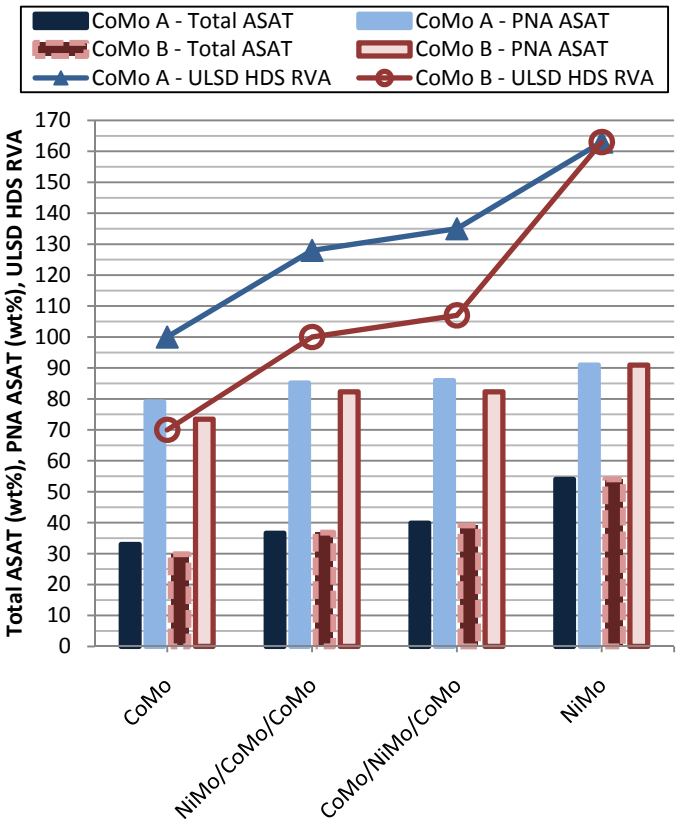

Figure 4. ASAT / ULSD HDS RVA Relationship

Conclusions

- CoMo/NiMo catalyst systems show synergistic behavior. Combined catalyst systems can have higher activity than that expected based on individual catalyst activities. CoMo/NiMo catalyst systems can show disproportionately high ULSD HDS activity increases over CoMo catalysts for the associated H_2 consumption increases. Not all CoMo/NiMo catalyst systems show synergistic behavior.
- In CoMo/NiMo catalyst systems both individual catalyst selection and catalyst system configuration significantly affect catalyst system synergy and performance.
- The increased ULSD HDS performance of CoMo/NiMo systems as compared with CoMo catalysts is due to increased HDN and aromatic saturation activities.
- CoMo/NiMo catalysts systems offer the opportunity to substantially increase commercial unit ULSD HDS activity while managing/controlling H_2 consumption and staying within unit H_2 supply limitations.

References

(1) Froment, G.F., Depauw, G.A., and Vanrysselberghe, V., *Ind. Eng. Chem. Res.* **1994,** 33, p-2975.

(2) Kabe, T., Ishihara, A., and Qian, W., *Hydrodesulfurization and Hydrodenitrogenation*, Kodansha Ltd./Wiley-VCH, Tokyo/Weinheim, 1999

(3) Prins, R., in: G. Ertl, H. Knözinger, F. Schüth, and J. Weitkamp (Eds.), *Handbook of Heterogeneous Catalysis, 2nd Edition*, Volume 6, Wiley-VCH, Weinheim, 2008, p-2695.
(4) Egorova, M. and Prins, R., *J. Catal*. **2004,** 225, p-417.
(5) Li, X., Wang, A., Egorova, M., and Prins, R., *J. Catal.* **2007,** 250, p-283.
(6) Wang, H. and Prins, R., *J. Catal.* **2009,** 264, p-31.
(7) Ho, T.C., *Catalysis Today* **2004,** 98, p-3.
(8) Koltai, T., Macaud, M. Guevara, A., Schulz, E. Lemaire, M.,Bacaud, R., and Vrinat, M., *Applied Catalysis A: General* **2002,** 231, p-253.
(9) Gripka, P. and Kraus, L. "Increase ULSD Production with Customized ULSD Catalyst System Design", Paper 44a, 2010 AIChE Spring Meeting

Combined CoMo/NiMo Catalyst System Advantages in ULSD Production: Part II – Commercial Experience

Lawrence (Larry) S. Kraus & Patrick J. Gripka

Criterion Catalysts & Technologies, 16825 Northchase Drive, Suite 1000, Houston, TX 77060

Abstract

A commercial example illustrating the use of a CoMo/NiMo catalyst system in Ultra Low Sulfur Diesel (ULSD) production is presented and discussed. A refiner in North America implemented a CoMo/NiMo/CoMo "sandwich" system in a low/moderate pressure ULSD unit. This unit has four parallel reactors with two catalyst beds per reactor and interbed quench. The typical operating conditions of this unit are LHSV = 0.7 hr^{-1}, Inlet P = 620 psig (43 barg), and H_2/Oil = ~1300 SCFB (~220 Nl/l). This ULSD unit processes a blend of Coker Naphtha (CN), Straight Run Diesel (SRD), Straight Run Kerosene (SRK), FCC Light Cycle Oil (LCO), and "Mixed Stocks". The composition of the "Mixed Stocks" feed stream consists of Coker Gas Oil (CGO), Purchased LCO, Light Vacuum Gas Oil (LVGO), and slop streams. This unit had previously used a CoMo catalyst system to minimize H_2 consumption. The motivation for changing to the CoMo/NiMo/CoMo catalyst system was to process greater quantities of more difficult feeds while maintaining catalyst cycle length and H_2 consumption at the levels observed with the previous CoMo catalyst load. The CoMo/NiMo/CoMo catalyst system allowed higher endpoint (D-2887 90 wt%: +12°F (~+7°C), D-2887 98 wt%: +15°F (~+8°C)) and higher nitrogen content (~190 wppm N as compared to ~115 wppm N) feed to be processed into ULSD without shortening catalyst cycle length or significantly increasing H_2 consumption.

Introduction

Combined CoMo/NiMo catalyst systems offer the opportunity to maximize catalyst Ultra Low Sulfur Diesel (ULSD) hydrodesulfurization (HDS) activity while managing/controlling H_2 consumption[1,2]. Managing H_2 consumption is a critical concern with H_2 constrained ULSD units. A North American refiner replaced a CoMo catalyst system with a CoMo/NiMo/CoMo "sandwich" catalyst system in a low/moderate pressure ULSD unit. The unit configuration is four parallel reactors with two beds and interbed quench. This unit processes a blend of straight run and cracked stocks. The unit is H_2 constrained and had previously used CoMo catalysts to minimize H_2 consumption. The motivation for changing to the CoMo/NiMo/CoMo catalyst system was to process greater quantities of more difficult feeds while maintaining catalyst cycle length and H_2 consumption at the levels observed with the previous CoMo catalyst loads.

This paper compares the commercial ULSD unit performance with the CoMo/NiMo/CoMo catalyst system being used in the current catalyst cycle to the unit performance with the CoMo catalyst system used in the previous catalyst cycle. The feed properties and unit performance characteristics for the first ~500 days of operation of the current catalyst cycle (Cycle 2) that utilizes the CoMo/NiMo/CoMo catalyst system are compared with the performance of the ULSD unit in the first ~500 days of operation in the previous catalyst cycle (Cycle 1) that utilized a CoMo catalyst system.

Commercial Catalyst System Comparison

The ULSD unit being evaluated processes a blend of Coker Naphtha (CN), Straight Run Diesel (SRD), Straight Run Kerosene (SRK), FCC Light Cycle Oil (LCO) and "Mixed Stocks". The composition of the "Mixed Stocks" feed stream consists of Coker Gas Oil (CGO), Purchased LCO, Light Vacuum Gas Oil (LVGO), and slop streams. The composition of the "Mixed Stocks" stream is not well-characterized and varies substantially. (This refiner is taking action to more completely characterize the "Mixed Stocks" feed stream in the future.)

The feed properties and performance characteristics for the first ~500 days of operation of the current catalyst cycle (Cycle 2) that utilizes the CoMo/NiMo/CoMo "sandwich" catalyst system is compared with the performance of the ULSD unit in the previous catalyst cycle (Cycle 1) that utilized a CoMo catalyst system for the same time period. This ULSD unit typically achieves a ~24 month catalyst cycle length.

The typical operating conditions used at the ULSD unit are shown in Table 1.

Table 1. Commercial ULSD Unit Operating Conditions

Process Conditions	Units	Value
Inlet Pressure	psig / barg	620 / 43
Average ppH_2	psia / bara	500 / 35
Overall LHSV	hr^{-1}	0.7
Treat Gas Rate	SCFB / Nl/l	1275-1350 / 215-228
Treat Gas Purity	Vol%	85 - 90

The average feed blend compositions for the current cycle (Cycle 2) using a CoMo/NiMo/CoMo catalyst load and the previous catalyst cycle that used CoMo catalyst (Cycle 1) are shown in Table 2.

Table 2. Average Feed Composition: Current & Previous Catalyst Cycles

Cycle 1: CoMo Average Feed Composition	
	MBD
"Mixed Stocks"	24.8
SRD	29.2
SRK	8.4
LCO	5.6
CN	4.2
Total	72.2

Cycle 2: CoMo/NiMo/CoMo Average Feed Composition	
	MBD
"Mixed Stocks"	25.6
SRD	28.0
SRK	13.6
LCO	3.6
CN	3.2
Total	74.0

The average feed blend compositions shown in Table 2 resulted in the average feed blend properties shown in Table 3.

Table 3. Average Feed Properties: Current & Previous Catalyst Cycles

Cycle 1: CoMo Average Feed Properties	
API Gravity (°)	35.5

Cycle 2: CoMo/NiMo/CoMo Average Feed Properties	
API Gravity (°)	33.8

Specific Gravity	0.8473
Total S (wt%)	0.50
Total N (wppm)	117
D-2887 Distillation	°F / °C
IBP	209 / 98
10 wt%	362 / 183
50 wt%	510 / 266
90 wt%	639 / 337
98 wt%	689 / 365

Specific Gravity	0.8560
Total S (wt%)	0.48
Total N (wppm)	192
D-2887 Distillation	°F / °C
IBP	214 / 101
10 wt%	372 / 189
50 wt%	519 / 271
90 wt%	651 / 344
98 wt%	704 / 373

The average total sulfur contents of the feeds processed in the two catalyst cycles are very similar. However, there are several significant differences in the feeds. The feed blend being processed in the current catalyst cycle (Cycle 2 - CoMo/NiMo/CoMo) has average T-90 (D-2887 90 wt% Point) and T-98 (D-2887 98 wt% Point) distillation values that are 12°F (7°C) and 15°F (8°C) higher, respectively, than those for the average feed processed in Cycle 1. As the boiling range endpoint increases, the amount of difficult to convert sulfur species in the feed increases[2]. The Cycle 2 feed has an organic N content ~65% higher than that of the Cycle 1 feed. Organic nitrogen species are strong catalyst inhibitors[3,4]. The higher organic N content of the feed along with its higher boiling range result in a feed that is intrinsically more difficult to process into ULSD[2]. The "Mixed Stocks" T-98 for the current and previous catalyst cycles is shown in Figure 15. It has been observed with this unit that the most reliable indicator of unit temperature requirements to meet product sulfur specifications is the "Mixed Stocks" T-98. The "Mixed Stocks" T-98 values for the current and previous catalyst cycles are shown in Figure 1. The "Mixed Stocks" T-98 has been 10°F - 40°F (6°C - 22°C) higher in the current cycle as compared with the previous cycle.

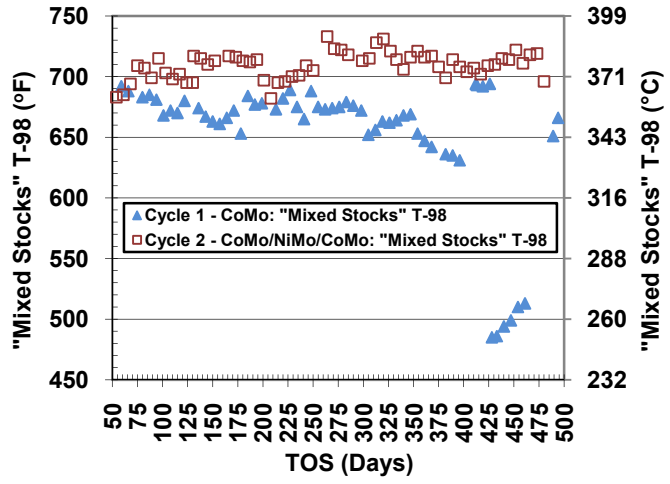

Figure 1. "Mixed Stocks" T-98: CoMo/NiMo/CoMo & CoMo Catalyst Cycles

The feed being processed in the current ULSD unit cycle (Cycle 2) is on average substantially more difficult to process than the feed processed in the previous cycle. The normalized weight average bed temperature (WABT) requirements for this unit in the current and previous catalyst cycles are shown in Figure 2. From this figure it is seen that utilizing a CoMo/NiMo/CoMo catalyst system has allowed the refiner to process a feed with higher endpoint and higher N content without an increase in operating WABT requirements. The CoMo/NiMo/CoMo catalyst system will achieve the same cycle length as the CoMo catalyst system used in the previous cycle. In the current cycle, operating temperature requirements were lower in the TOS 200-250 day period when the "Mixed Stocks" T-98 was reduced. The significant normalized WABT gap between the current cycle with the CoMo/NiMo/CoMo catalyst system and the previous catalyst cycle in the TOS 425 – 475 day range is due to the extremely low "Mixed Stocks" T-98 during this period of the previous catalyst cycle as shown in Figure 1.

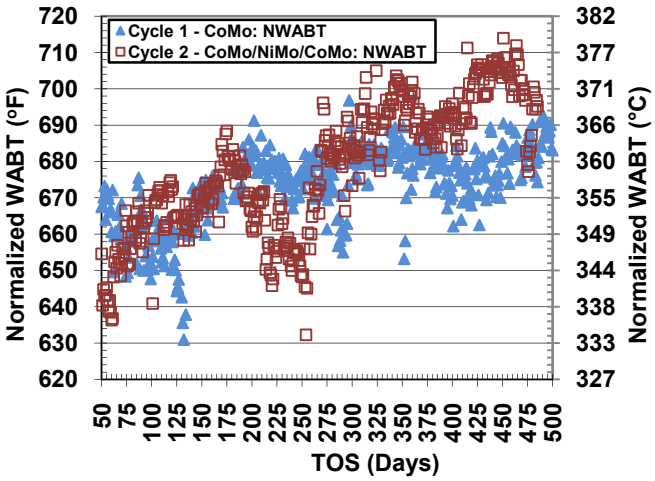

Figure 2. Normalized WABT Comparison: CoMo/NiMo/CoMo & CoMo Catalyst Cycles

A comparison of the H_2 consumption observed in the CoMo/NiMo/CoMo and CoMo catalyst cycles is shown in Figure 3. In the initial stages of the CoMo/NiMo/CoMo catalyst cycle (TOS up to ~100 days), the H_2 consumption is substantially higher than what was observed with the CoMo catalyst system. The reasons for the higher H_2 consumption with the CoMo/NiMo/CoMo catalyst system at the beginning of this catalyst cycle are understood by examining feed properties. In the first ~75 - 100 days of operation, the total S content of the feed processed in Cycle 2 (CoMo/NiMo/CoMo catalyst) was about 0.30 wt% higher than the total S level of the feed that was processed in the same time period in Cycle 1 (CoMo catalyst). This is shown in Figure 4. This higher feed S accounts for ~40 SCFB (~7 Nl/l) of the additional H_2 consumption observed in the first ~75 - 100 days of the CoMo/NiMo/CoMo cycle. The remainder of the additional H_2 consumption is likely due to aromatics saturation (ASAT). The total feed density is higher during this period of the current cycle as shown by API gravity data in Figure 5. (For reference, Table A in Appendix A shows the specific gravity values that correspond to the API gravity range of 30° – 40°.) In the first ~75 - 100 days of the current cycle the API gravity was much lower (the specific gravity was much higher) than usual. Since the boiling range of the total feed in the CoMo/NiMo/CoMo catalyst cycle during this time period is typical, as shown in by the total feed T-98 (D-2887 98 wt% Point) in Figure 6, this higher density is most likely due to the feed being more aromatic. The higher aromaticity of the feed during the first ~75 - 100 days of the current catalyst cycle and the favorable hydrogenation conditions [low temperature, high ppH_2 (low hydrocarbon vaporization)] present at SOR resulted in higher H_2 consumption during this period. As the current cycle progressed, feed total S contents were reduced to typical levels and feed API gravities increased (specific gravity decreased) to typical levels. This

resulted in the H_2 consumption with the CoMo/NiMo/CoMo system returning to the levels observed in the previous cycle with the CoMo catalyst system.

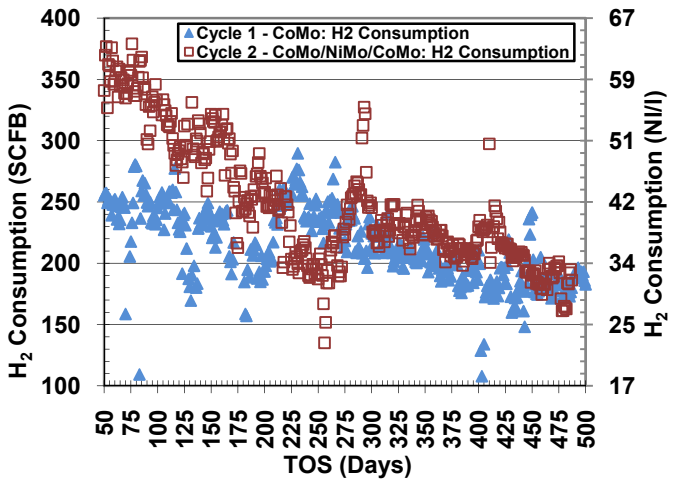

Figure 3. H_2 Consumption: CoMo/NiMo/CoMo & CoMo Catalyst Cycles

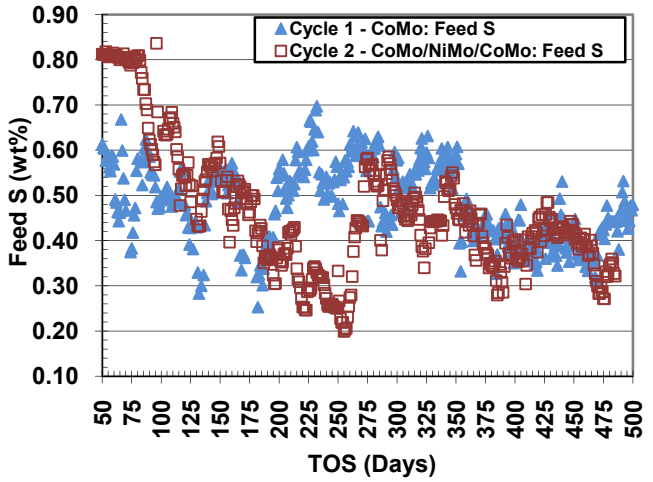

Figure 4. Feed Total Sulfur Content: CoMo/NiMo/CoMo & CoMo Catalyst Cycles

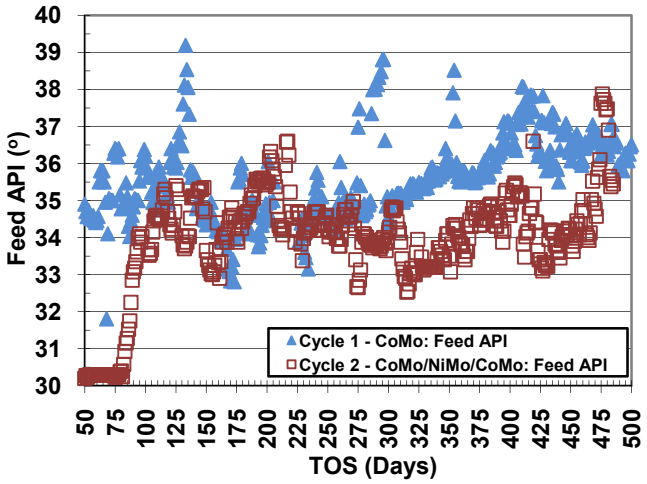

Figure 5. Feed API Gravity: CoMo/NiMo/CoMo & CoMo Catalyst Cycles

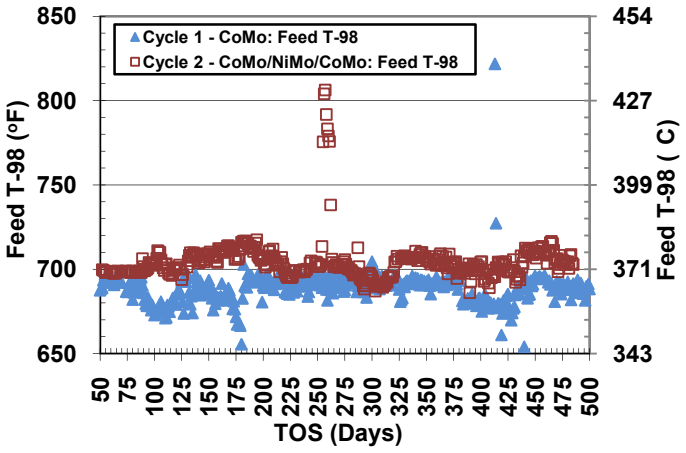

Figure 6. Total Feed T-98: CoMo/NiMo/CoMo & CoMo Catalyst Cycles

Conclusions

Utilization of a CoMo/NiMo/CoMo "sandwich" catalyst system in a low/moderate pressure commercial ULSD unit has allowed a refinery to process more difficult feeds (higher endpoint, higher nitrogen content) at higher throughput while maintaining catalyst cycle length. These benefits have been achieved while maintaining H_2 consumption at the same levels observed with the CoMo catalyst system used in the previous unit cycle.

References

(1) Kraus, L. and Gripka, P., "Combined CoMo/NiMo Catalyst System Advantages in ULSD Production: Part I - Pilot Plant Studies", *Prepr. Pap.-Am. Chem. Soc., Div. Pet. Chem.* **2010**, 55 (2), xxxx

(2) Gripka, P. and Kraus, L., "Increase ULSD Production with Customized ULSD Catalyst System Design", Paper 44a, 2010 AIChE Spring Meeting

(3) Ho, T.C., *Catalysis Today* **2004**, 98, p-3.

(4) Koltai, T., Macaud, M. Guevara, A., Schulz, E. Lemaire,

M., Bacaud, R., and Vrinat, M., *Applied. Catalysis. A: General* **2002,** 231, p-253.

Appendix A

Table A. Corresponding API Gravity & Specific Gravity Values: API Gravity Range 30° - 40°

API Gravity (°)	Specific Gravity
30.0	0.8762
30.5	0.8735
31.0	0.8708
31.5	0.8681
32.0	0.8654
32.5	0.8628
33.0	0.8602
33.5	0.8576
34.0	0.8550
34.5	0.8524
35.0	0.8498
35.5	0.8473
36.0	0.8448
36.5	0.8423
37.0	0.8398
37.5	0.8373
38.0	0.8348
38.5	0.8324
39.0	0.8299
39.5	0.8275
40.0	0.8251

Arab Light Vacuum Residue Processing via High Space Velocity Visbreaking and Steam Catalytic Cracking

Mazin M. Fathi and Pedro Pereira-Almao

Schulich School of Engineering, University of Calgary,
Calgary, Alberta, T2N 1N4, Canada

Abstract

In this work Arabian Light Vacuum Residue (AL VR) upgrading reactivity is investigated in a continuous up flow tubular reactor. Kinetic modeling is performed on two different processes, namely, thermal cracking and steam catalytic cracking using an ultra dispersed bi-metals catalyst. Thermal and steam catalytic cracking were studied at different space velocities and temperatures. Steam catalytic cracking was investigated by producing emulsions of AL VR, water, surfactant and catalytic metals according to a given formulation. Thermal cracking aided with steam was conducted in order to isolate the upgrading effect of the steam, if present, in order to quantify the upgrading effect of the ultradispersed catalyst. Upgrading was quantified by measuring the conversion as the measure of the percentage reduction of 540°C+ hydrocarbon present originally in the feed and by determining products selectivity. AL VR upgraded products characteristics measure were kinematic viscosity, P-value, SARA, MCR and SimDist. Kinetic parameters were generated utilizing the accumulated data from both processes using a cascade lump model.

Introduction

Heavy refinery residues have a commercial value to a great extent lower than their BTU value. However, as a result of increasing crude oil prices, demands, and inventory of residual heavy oils, as a byproduct of processing conventional and unconventional crude oils, residual oil upgrading has become more economically attractive to fulfill the increasing oil demand. AL VR is considered one of the hard residues to process. This residue is composed of a mixture of large and complex hydrocarbon molecules along with one or more heteroatoms. AL VR is adversely affected by the presence of asphaltenes. These fractions contain most of the sulfur, nitrogen and metals. Furthermore, asphaltenes increase oil viscosity and produce plugging and transportation problems. In addition, asphaltenes are difficult to convert to lighter fractions and their indigenous high metals content poison the catalysts that are essential to convert them. Asphaltenes precipitate due to changes in the oil physical conditions such as temperature and/or pressure or chemical composition. AL VR visbreaking occurs via a combination of endothermic reactions taking place via a free radical mechanism. AL VR visbreaking has long been used in many refineries around the world but not much data has been disclosed. Limited data are available on the reactivity of AL VR under visbreaking or steam cracking conditions. Ultra dispersed bi-functional catalytic steam cracking via emulsion of AL VR was investigated in this work for the first time in academia. Since limited data are available, thermal and steam cracking reactivity tests and kinetic data evaluation were conducted in this work to establish a base line for the reactivity tests via steam catalytic cracking. It is found that a number of characterization data reported by literature are different from one another to some extent due to analysis method, stock oil cut point, oil source, and its history. As a result, for the sake of consistency all the characterization results considered in this work were made in the same lab for both the feed and the treated oils.

Experimental Procedure

Reactivity & Characterization Tests

The reactivity tests were carried out in a pilot plant with up flow configuration setup. The experimental plan is shown in Figure 1.

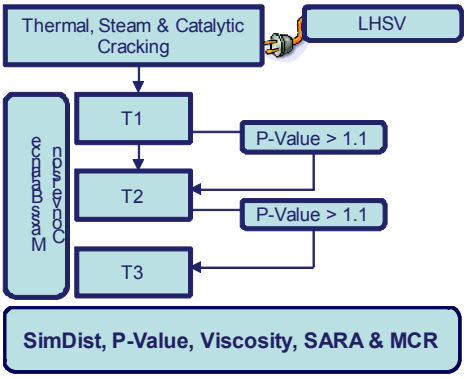

Figure 1. Reactivity Tests Plan

The reactivity tests consisted of thermal and steam catalytic cracking. Thermal cracking reactivity tests were conducted with and without steam addition at different Liquid hourly space velocities (1.5–5hr^{-1}) and temperatures (390-430°C). The space velocities were fixed aiming to test high space velocities and temperatures until the stability limit of P-value[1] of 1.2 is reached, a measure of the asphaltenes tendency to precipitate. Steam catalytic cracking using unsupported bi-functional nickel potassium ultradispersed catalyst was tested on AL VR at temperatures (430-445°C) and LHSV (5-10.5hr^{-1}). Steam catalytic cracking via ultra dispersed catalyst was implemented according to the Aquaconversion® as proposed by UOP and others[2]. This is a thermal process in the presence of steam and ultra dispersed dual function catalyst, which generates hydrogen through the catalytic dissociation of the steam and promotes hydrogen addition to the produced free radicals. This process increases the conversion of heavy residues to lighter products and maintains or improves the stability and quality of products of thermally cracked process, which employs heat exclusively. Due to high viscosity of AL VR the catalyst was prepared in a mixture of AL VR-naphtha in a predetermined ratio prior to emulsion preparation. The blended naphtha was flashed out, after forming the oil suspended catalyst, the oil SimDist was obtained as shown in Figure 2.

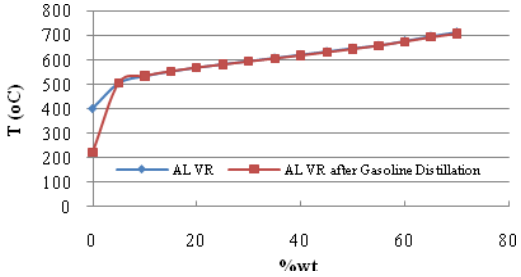

Figure 2. SimDist of original AL VR & AL VR after distilling out naphtha.

The original and converted AL VR oil were characterized by different well established indicative measurements. Stability index measurement is an important decisive technique used to determine

the maximum achievable conversion limit. Residual oils stability index was determined by P-values. SARA, as a qualitative fast measurement, was determent by first isolating asphaltenes from the oil sample by microdeasphalting using n-heptane and then analyze the maltenic phase via Thin Layer Chromatography method combined by Flame Ionization Detection method (TLC-FID)[3] via Iatroscan. Micro carbon (MCR)[4] measurement was used to determine coke formation affinity of the oils using muffle furnace.

Results

From SimDist analysis, it is observed that the 540°C+ hydrocarbon content in AL VR is 88wt%. Table 1 compares the results of upgrading reactivity and characterization tests on AL VR oils at $5hr^{-1}$ done via thermal, steam and steam catalytic cracking. It is observed that AL VR is rich in aromatics and resins and low in paraffins. The percent weight conversion in this table is based on 540°C+ hydrocarbons conversion. From Table 1 it is observed that steam-aided thermal cracking didn't have any effect on conversion or stability of the reactivity test products. It is also observed that the asphaltene and MCR production was ceased and P-value was increased while more resin was converted when the ultra dispersed catalyst was used with AL VR as compared to thermal and steam cracking at 430°C. This is an explicit indication of the stability and upgrading gain achieved using bi-functional ultradispersed catalyst with AL VR. This add on stability level has allowed more room for upgrading as it is seen from Table 1 with a product having a P-value of 1.35.

Table 1:Reactivity & Characterization Tests of AL VR

	AL VR	TC	TC	SC	SCC
Temperature (°C)		413	430	430	430
LHSV(hr^{-1})		2.5	5	5	5
% conversion		27.1	28.4	27.2	28.9
P-Value	2.9	1.2	1.2	1.2	1.35
MCR wt%	21.5	29.83	31.1	29.4	30.4
Saturates wt%	6.2	9.3	8.1	8.2	8.7
Aromatics wt%	61.6	65.3	65.9	66	69.9
Resins wt%	22.1	10.4	12.5	12.8	8.7
Asphaltenes wt%	10.1	15.0	13.5	12.9	12.7
60°C Viscosity, cP	36091	8220	8233	8855	9131

Figure 3 shows the experimental data of AL VR upgrading via thermal cracking at $5hr^{-1}$. It is observed from this figure that the kinematic viscosity decreases sharply with temperature. It is also observed that aromatic, MCR, saturates and asphaltene increases gradually at the expenses of resins as the conversion level is increased. However, saturates seemed to be declining as the severity level is increased close to stability limit.

Figure 4 shows the progression of AL VR conversion data with space time for both thermal and catalytic cracking. From this curve it is noticed that thermal cracking conversion, at the stability limit, has increased steadily as indicated by the dotted curve. Sudden jump in conversion profile has been observed at $6.5hr^{-1}$ after incorporating the ultradispersed catalyst as indicated by the continuous curve. It is also observed that above 430°C and at space velocities higher than $5h^{-1}$ higher conversion can be achieved via Aquaconversion.

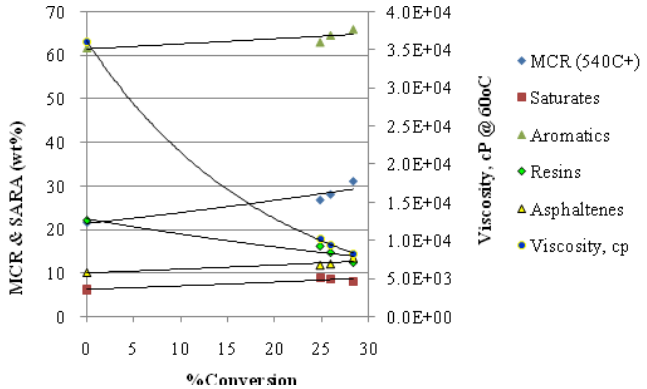

Figure 3. AL VR thermal cracking product MCR & SARA vs. %wt conversion at $5hr^{-1}$.

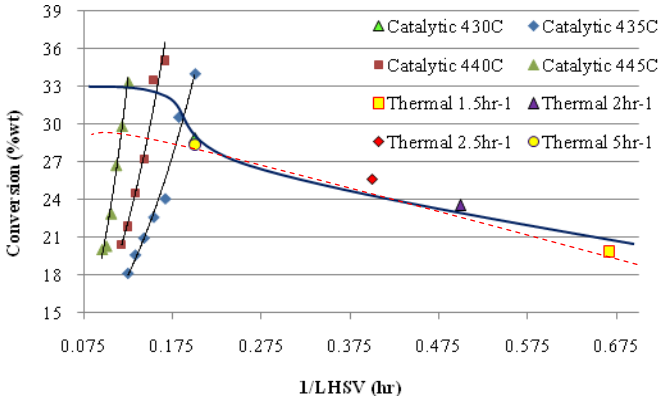

Figure 4. Effect of Space Time on wt % Conversion

Figures 5 and 6 show the stability and conversion trend of thermal cracking and Aquaconversion of AL VR, respectively. From both figures one important observation has been noticed; operating at higher temperatures and space velocities favors higher conversion and stability indices, which is a desirable feature for refiners who seek high production rate. This behavior can be observed from Table 1 where AL VR thermal cracking %conversion at 413°C and $2.5hr^{-1}$ was found to be 27.1wt% at a P-value of 1.2 while the conversion at 430°C and $5hr^{-1}$ was found to be 28.4wt% at a P-value of 1.2.

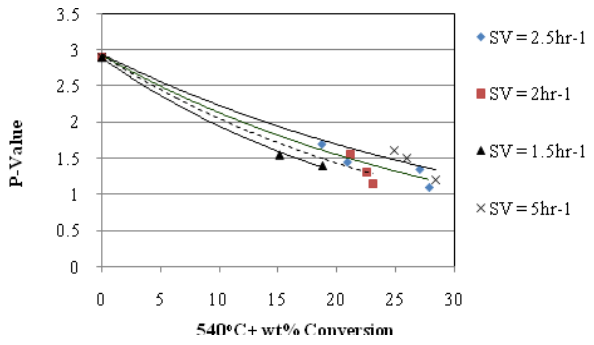

Figure 5. Thermal cracking stability indices and (540°C+ HC) Conversions as a function of different LHSV.

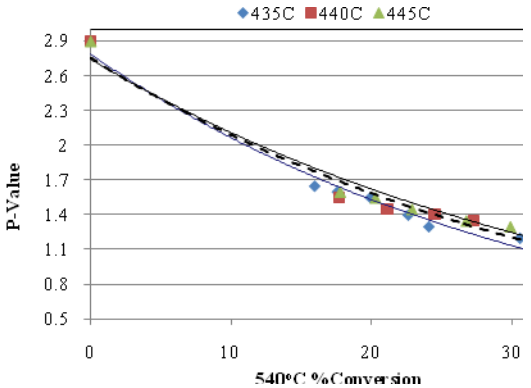

Figure 6. Steam catalytic cracking stability indices and (540°C+ HC) conversions as a function of different temperatures.

Arabian Light vacuum residue thermal cracking and steam catalytic cracking reactivity kinetics were estimated assuming first order with respect to the percent conversion of 540°C+ hydrocarbons. It is found that AL VR upgrading reactivity via thermal and steam catalytic cracking follow first order kinetics with activation energy of 168 and 167 KJ/mol as shown in Figures 7 and 8, respectively.

Kinetic Modeling of AL VR Upgrading

One of the objectives of conducting the Aquaconversion experiments at different conditions is to develop a kinetic model that can be used to estimate the upgrading parameters that closely match the experimental values to a great extent. A first order kinetic model is assumed.

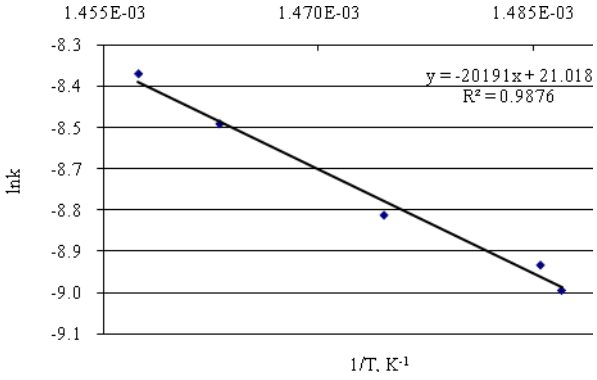

Figure 7. AL VR thermal cracking reactivity follow 1st order kinetics.

In order to simplify the kinetic model a lumped kinetics technique is used based on simulated distillation cut points as follows:

Residue(540°C+)

VGO(455-540°C)

Distillates(204-455°C)

Naphtha(IBP-204°C)

Gases

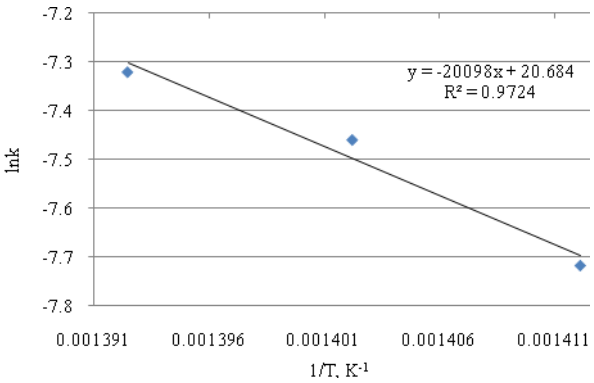

Figure 8. AL VR steam catalytic cracking reactivity 1st order kinetics

The kinetic model is used to estimate the thermal cracking process as the base line for the Aquaconversion's kinetic model estimation. Figure 9 shows the proposed model.

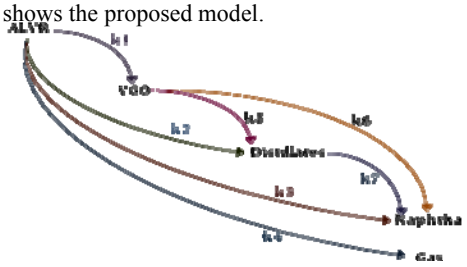

Figure 9. Proposed Lumped Kinetic Model

Table 2 shows the kinetic parameters generated utilizing the accumulated data from steam catalytic cracking process using a cascade lump model.

Table 2. Estimated Reaction Constants

k1 = 0.828	k2 = 0.354
k3 = 0.281	k4 = 0.612
k5 = 7.014	k6 = 0.061
k7= 0.485	

The corresponding mathematical model is as follows:

$$r_{Residue} = -(k1+k2+k3+k4)*C_{Residue}$$
$$r_{VGO} = k1*C_{Residue} - (k5+k6)*C_{VGO}$$
$$r_{Distillates} = k2*C_{Residue} + k5*C_{VGO} - k7*C_{Distillates}$$
$$r_{Naphtha} = k3*C_{Residue} + k6*C_{VGO} + k7*C_{Distillates}$$
$$r_{Gas} = k4*C_{Residue}$$

Table 3 shows comparison between the experimental and kinetic model estimated composition of LHSV 8.0hr^{-1} at 440°C product.

Table 3. Experimental & Estimated

	Component	Experimental wt	Calculated wt
LHSV 8.0hr^{-1}	$C_{Residue}$	0.637	0.631
	C_{VGO}	0.122	0.124
	$C_{Distillates}$	0.163	0.159
	$C_{Naphtha}$	0.029	0.032
	C_{Gas}	0.050	0.055

A complete comparison between the experimental and calculated composition at 440ºC is shown in Figure 10. From this figure it is observed that both results are in close agreement.

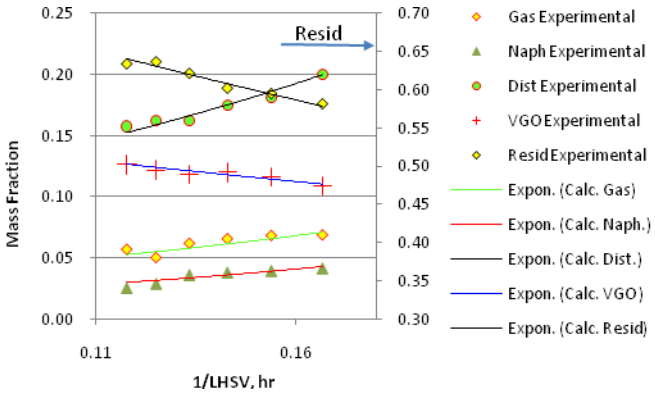

Figure 10. Comparing Experimental and Model Composition Data

Conclusion

Experimental reactivity tests based on thermal, steam and steam catalytic cracking at different severities and condition were performed and a kinetic model that explains the reaction system was proposed AL VR oils (Original & Reacted) were characterized via P-Value, SimDist, SARA, MCR and kinematic viscosity. It is observed that high space velocities favor the use of high reaction temperatures increasing cracking reactions more than condensation reactions, keeping reasonable product stability and higher residue conversion into liquids. It is also proven that the catalytic steam cracking improves the reactivity and stability of the products by converting more resins while neutralizing or subsiding further asphaltene flocculation reactions.

Acknowledgement

This work was supported by Saudi Aramco who provided oil samples and academic financial support. It was also supported by Alberta Ingenuity Fund, now Alberta Innovates, via an Scholar award provided to Dr. Pereira Almao. Help from several members of the Catalysts for Bitumen Upgrading and Hydrogen Production (CBUHP) group from University of Calgary on analytical and technical matters is also acknowledged.

Nomenclature

AL = Arabian Light Crude Oil
VR = Vacuum Residue
TC = Thermal Cracking
SC = Steam Cracking
SCC = Steam Catalytic Cracking
SARA = Saturates, Aromatics, Resins, Asphaltenes
P-Value = Peptizing Value
LHSV = Liquid Hourly Space Velocity
MCR = Micro Carbon Residue
SimDist = Simulated Distillation
cc = Cubic Centimeter

References

[1] Heithaus, J.J., (1962). *Journal of the Institute of Petroleum,* Vol.6, Number 458, pp. 45-53.

[2] Pereira, Pedro et al., "Aquaconversion Technology Offers Added Value to E. Venezuela Synthetic Crude Oil Production", *Oil Gas J.* 2001, *99*, 79-85.

[3] Lante et al. "Characterization of Athabasca Vacuum Residue and Its Visbroken Products. Stability and Fast Hydrocarbon Group-Type Distributions", *Energy & Fuels* 2007, *21,* 1631-1639.

[4] Hassan et al., "Development of an alternative setup for the estimation of microcarbon residue for heavy oil and fractions: Effects derived from air presence", Fuel 2008, 87, 3631–3639.

HOW DOES VGO HDS ACTIVITY DEPEND ON FEED BOILING POINT?

Tommy L. Jørgensen[*], *Angelica Hidalgo-Vivas, Kim G. Knudsen, Rasmus G. Egeberg, Per Zeuthen, Michael T. Schmidt*

Haldor Topsøe A/S, Nymøllevej 55, 2800 Kgs. Lyngby, Denmark.
[*]Phone: +45 45272061. E-mail: tolj@topsoe.dk

Introduction

Over the past years legislators have forced the oil industry to produce cleaner and more environmentally friendly fuel oils and transportation fuels [1,2,3]. Moreover further emphasis has been placed on the catalytic upgrading of heavy petroleum fractions and residues such as oils in the vacuum gas oil (VGO) range [4]. It is difficult to hydrotreat oils in this range down to low sulfur levels, as oils of that type normally contain significant amounts of the sulfur compounds, which are the most difficult to desulfurize [5]. In addition, heavy oil fractions also contain significant amounts of organic nitrogen which inhibit hydrodesulfurization [5]. The most refractive sulfur compounds are higher molecular weight dibenzothiophenes with side chains positioned in such a way that they sterically hinder the access to the sulfur atom [1,3,6].

This article focuses on the impact of boiling point range and inhibiting effect of organic nitrogen species on the HDS reactivity of oils in the diesel and VGO range. This may contribute to a better understanding of the underlying HDS kinetics and may help in the design of future hydrotreaters for the refining industry. Furthermore such kinetic studies may be used when revamps and optimization of existing units are needed to handle heavier and more difficult feeds.

Experimental and analysis

A coker gas oil in the VGO range was fractionated into three new feeds: IBP-350ºC, 350-400ºC and 400-EBP. These three feeds were analyzed for specific gravity, sulfur, total and basic nitrogen as well as hydrogen, aromatics and cold flow properties. Furthermore the distillation curves were determined. The content of As, Fe, Ni and V was also measured.

The feeds were hydrotreated at three different temperatures and 45-60 barg at LHSV = 1.0 h^{-1} and H_2/oil = 400 Nl/l. The four different test conditions used during the test are specified in Table 1.

Table 1. Test Conditions applied during Activity Test on Fractionated VGO.

Condition	T [ºC]	P [barg]	LHSV [h^{-1}]	H_2/oil [Nl/l]
I	Base	45	1.00	400
II	Base + 20	45	1.00	400
III	Base + 40	45	1.00	400
IV	Base + 20	60	1.00	400

The unit chosen for the test was a bench scale reactor setup with five reactors in a single furnace. There was downflow, and three separate heating zones in the furnace allowed isothermal operation during the activity test. Each reactor has a total reactor volume of 177 ml, and the design is single stage. Pure once-through hydrogen was used as treat gas, and the liquid product from each reactor was separated from the exit gases in a high-pressure separator (HPS). The liquid product from the HPS was sent to a low-pressure stabilizer (LPS) for removal of remaining gases and non-condensed light hydrocarbons. Nitrogen was used as stripping agent.

Two commercial Haldor Topsøe catalysts were used for the test. A CoMo catalyst (TK-562 BRIM^{TM}) was loaded into three of the reactors and used to hydrotreat each of the three feeds, whilst a NiMo catalyst (TK-561 BRIM^{TM}) was loaded into the remaining two reactors to treat the two heaviest feeds. The dilution degree was 40 vol% obtained by carborundum.

The total liquid product (TLP) was collected from each reactor at each condition after steady state had been obtained. All the TLPs were analyzed for specific gravity, sulfur, total and basic nitrogen as well as hydrogen and aromatics. The distillation curves were also determined. Furthermore the sulfur and nitrogen distributions of the three feeds and selected product samples were determined by GC-AED analysis with a Hewlett-Packard 6890 equipped with a G2350A AED detector.

Feeds properties

The original coker VGO had an IBP of approximately 200ºC and an EBP of 550ºC (simulated distillation). This oil was fractionated into IBP-350ºC, 350-400ºC and 400-EBP, and the mass of the three new feeds relative to the mass of the original feed was 27%, 31% and 42%, respectively. Thus the IBP-350ºC feed was actually a diesel, the 350-400ºC feed a relatively light VGO, whilst the 400-EBP feed was a heavier VGO. The content of sulfur, total nitrogen and basic nitrogen of the three new feeds was determined next, and the results are given in Table 2.

Table 2. Content of Sulfur, Total and Basic Nitrogen of the three Test Feeds.

Feed	S [wt%]	Total N [wt ppm]	Basic N [wt ppm]
IBP-350ºC	2.10	707	306
350-400ºC	2.38	1598	471
400-EBP	2.21	3097	882

This enabled us to focus on the distribution of sulfur and nitrogen compounds as a function of feed boiling point. Figure 1 shows the relative distribution of sulfur, total and basic nitrogen as well as mass between the three new feeds. It can be seen that the sulfur was distributed rather evenly as compared with the mass of the new feeds. As opposed to this, both total and basic nitrogen were mainly concentrated in the 400-EBP feed, as 66% and 62% of the total amounts of these compounds were present in this feed, respectively.

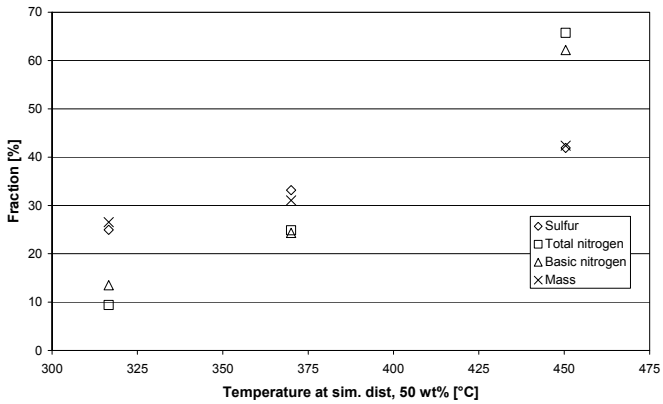

Figure 1. Relative distribution of sulfur, total and basic nitrogen as well as mass in the three feeds obtained.

With respect to aromatics it was found that the mono-aromatics were evenly distributed, whereas a high relative amount of the di-aromatics was present in the lightest feed (40%). On the other hand, tri+-aromatics were highly concentrated in the heaviest feed (72%).

With respect to metals, As, Fe, Ni, V and Si are often present in VGOs. An example of this is Si, which is often present in oils originating from coker units. Such metals may deactivate hydrotreating catalysts by adsorption on the active sites. The content

of As, Fe, Ni and V was measured and the distribution determined. In the case of As, the distribution between the fractions was 10%, 13% and 77%, respectively, whilst for Fe, Ni and V, almost all of these metals were concentrated in the 400-EBP feed (≥97.5%). The activity measurements in this study were not affected by the presence of metals due to the fact that the pilot plant test was relatively short.

The sulfur and nitrogen distributions of the three feeds were determined by GC-AED. The sulfur chromatograms of the two lightest feeds are given in Figure 2 and 3. It is interesting to see that the IBP-350ºC feed contained both thiophenes, benzothiophenes and dibenzothiophenes, whilst the 350-400ºC feed contained mainly dibenzothiophenes and heavier sulfur compounds such as benzonaphthothiophenes, etc. The chromatogram of the 400-EBP feed is not given, but this feed was shown to contain heavier compounds than the 350-400ºC feed. Thus the sulfur compounds of the 400-EPB feed are mainly based on a dibenzothiophene skeleton.

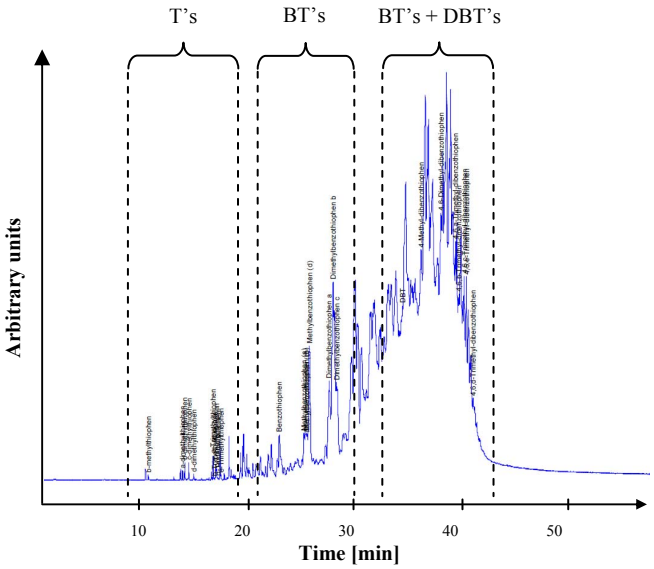

Figure 2. GC-AED sulfur chromatogram of the IBP-350ºC feed. T = thiophenes, BT = benzothiophenes, DBT = dibenzothiophenes.

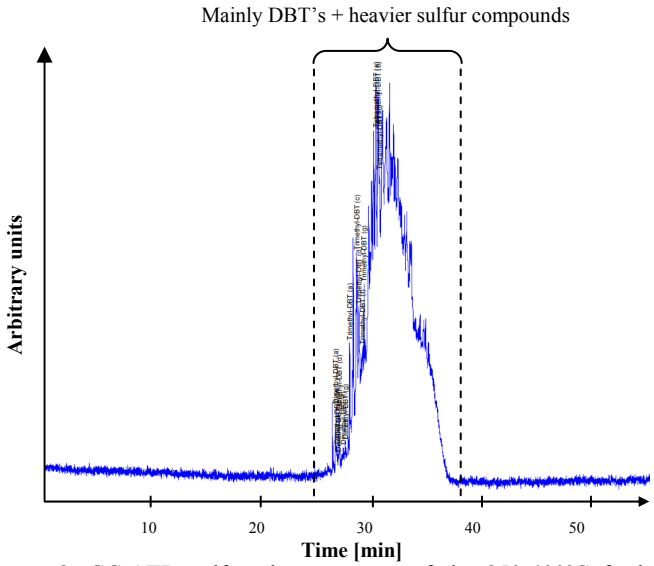

Figure 3. GC-AED sulfur chromatogram of the 350-400ºC feed. DBT = dibenzothiophenes.

Results and discussion

In the following, the main results of the activity test will be presented and discussed. Our focus is experimental observations, relative reactivities between the three feeds and the two catalyst types as well as the inhibiting effect of basic nitrogen on the HDS activity.

Experimental observations. The most important analysis results obtained for the products were sulfur, total nitrogen and basic nitrogen, which are given in Figure 4 – 6 for condition I, II and III.

Figure 4 shows the sulfur levels of the products on a logarithmic scale as a function of temperature. It is very interesting to see that the CoMo catalyst had a higher HDS activity than the NiMo catalyst at these conditions. Probably the rather low reactor pressure of 45 barg was responsible for the higher HDS activity of the CoMo catalyst. With respect to the impact of feed boiling point range on the HDS activity, the apparent reactivity trend of the three feeds is as follows:

IBP-350ºC >> 350-400ºC > 400-EBP (1)

This is supported by the fact that the sulfur levels of the feeds were almost identical (see Table 2).

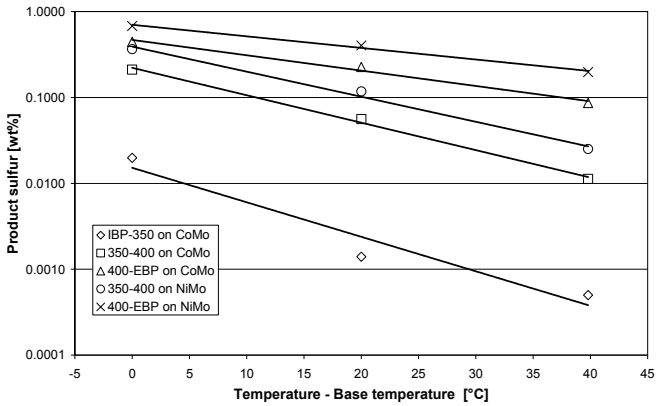

Figure 4. Product sulfur levels at condition I, II and III as a function of reactor temperature.

Figure 5 provides the total nitrogen levels of the products on a logarithmic scale as a function of temperature.

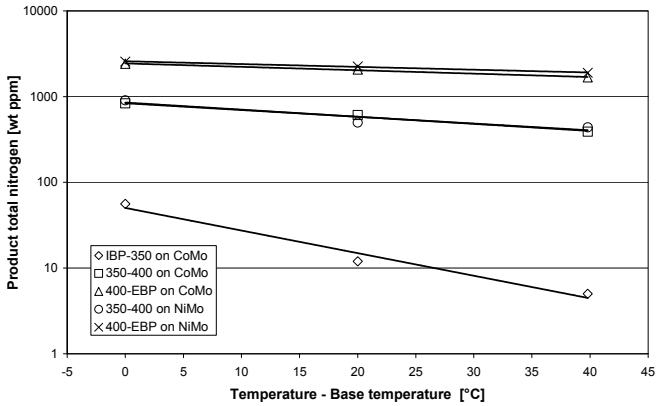

Figure 5. Total nitrogen levels of the products at condition I, II and III as a function of reactor temperature.

In this case the HDN activity was approximately the same for the CoMo and NiMo catalyst. It was also seen that the HDN reactivity trend of the three feeds followed the HDS reactivity trend, namely as

specified by inequality (1). This was the case despite the fact that the feed nitrogen level was different for the three feeds. For condition I, the HDN conversion of the three feeds treated by the CoMo catalyst was e.g. 92.1%, 47.9% and 22.1%, respectively.

Figure 6 shows a similar plot of the basic nitrogen levels of the products. As can be seen, the activity for removing basic nitrogen at these conditions was approximately the same for the CoMo and NiMo catalysts. Only one data point is shown for the lowest boiling feed, because the remaining product basic nitrogen levels were <2 wt ppm, which is the lower detection level for basic nitrogen.

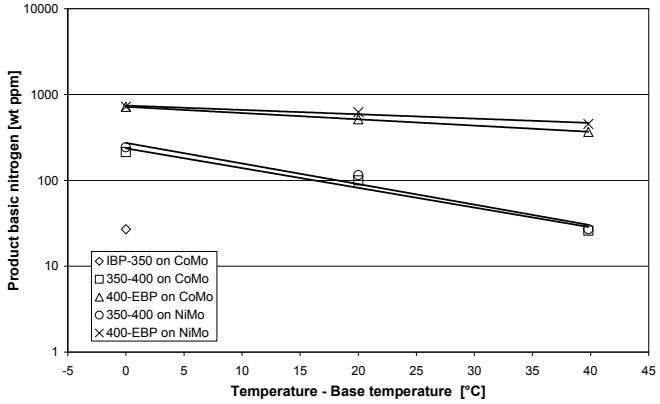

Figure 6. Basic nitrogen levels of the products at condition I, II and III as a function of reactor temperature.

Apparent relative HDS reactivities. At this point it has been shown that there is a large difference in HDS reactivity of the three feeds tested. Even though the sulfur concentrations of the three feeds were approximately the same, the product sulfur level of the IBP-350ºC feed was significantly lower than that of the 350-400ºC feed, which again was lower than that of the 400-EBP feed.

A kinetic model must be considered to quantify the relative HDS reactivities. Although first-order kinetics may be used to describe desulfurization of each sulfur-containing compound, a reaction order for the total sulfur concentration different from one is often applied to describe the desulfurization rate of the mixture of individual sulfur species [7]. It has been found that a reaction order *n* for HDS of 1.5-1.8 often fits oils in the diesel range [1,7]. For heavier feeds such as VGOs, the best fit of the reaction order *n* is usually found in the range 1.8-2.3 [1,4,8]. For a comparison of the HDS reactivities of the three feeds, the same reaction order should be applied.

By considering a simple reaction rate expression of HDS without inhibition:

$$R_S = k_{HDS} \cdot C_S^n / C_{S,in}^{n-1} \cdot \left(P_{H_2} / P_{ref}\right)^{\alpha} \qquad (2)$$

with a typical reaction order of a VGO, such as $n = 2.0$, it is possible to evaluate the apparent relative HDS reactivities of the three feeds. The temperature dependence of the rate constant above is considered to follow the Arrhenius law:

$$k_{HDS} = k_{HDS}^0 \cdot \exp\left(\frac{-E_{A,HDS}}{RT}\right) \qquad (3)$$

A fit to the experimental data gives $E_{A,\,HDS} = 42.1$ kcal/mol and $\alpha = 0.55$. With this simple model, the relative HDS reactivities of the feeds were calculated using the heaviest feed as reference for both catalyst types. The results are given in Table 3. The relative HDS activity of the two catalyst types is also provided.

Table 3. Apparent Relative HDS Reactivities of the three Test Feeds and two Catalysts when using a Simple nth Order Model without Inhibition Terms.

Feed	Relative HDS activity
$(IBP\text{-}350)_{CoMo}/(400\text{-}EBP)_{CoMo}$	33
$(350\text{-}400)_{CoMo}/(400\text{-}EBP)_{CoMo}$	5.1
$(350\text{-}400)_{NiMo}/(400\text{-}EBP)_{NiMo}$	4.7
$(350\text{-}400)_{CoMo}/(350\text{-}400)_{NiMo}$	2.2
$(400\text{-}EBP)_{CoMo}/(400\text{-}EBP)_{NiMo}$	2.0

As can be seen, the CoMo catalyst is approximately two times more active than the NiMo catalyst at these conditions. However, the apparent reactivity of the diesel was much higher than that of the heaviest VGO, and the 350-400ºC feed was approximately five times more reactive than the 400-EBP feed for both catalyst types. The reason for these large differences is discussed qualitatively in the following subsection.

Reasons for activity differences. It is generally known that diesel and VGOs contain a wide variety of organic sulfur and nitrogen species, and that the reactivity of the different species varies significantly [3]. Diesel feeds e.g. contain both thiophenes and benzothiophenes, which are easy to desulfurize. Part of the total sulfur will also consist of dibenzothiophenes with and without alkyl groups. The dibenzothiophenes without alkyl groups and those with only one alkyl group positioned away from the sulfur atom are considered to be relatively difficult to desulfurize [3]. However, the most refractive sulfur compounds are dibenzothiophenes with side chains positioned close to the sulfur atom [3]. Especially 4,6-dimethyldibenzothiophene is very difficult to desulfurize [1,3]. As seen in Figure 2 and 3, the diesel feed contained significantly more thiophenes and benzothiophenes as compared with the two VGOs, and correspondingly, the two VGOs contained more difficult sulfur species. This difference in sulfur distribution between the diesel feed and the two VGOs was certainly one of the main reasons why the diesel feed was more reactive than the two heavier ones. However, a relative reactivity of the diesel and of the heaviest VGO of >30 still seems to be surprisingly high as the diesel feed in fact contains significant amounts of alkylated dibenzothiophenes. On the other hand the majority of the sulfur species of the two heaviest feeds are probably not very different with respect to HDS reactivity, as they are mainly based on a dibenzothiophene skeleton. A similar reactivity of the 350-400ºC feed and the 400-EBP feed would thus be expected.

The different sulfur distribution of the feeds is not enough to explain the significant differences in feed reactivity. Also the content of organic nitrogen and especially basic nitrogen may play an important role [3]. Table 2 and Figure 6 show that the content of basic nitrogen species in the reactors was very different depending on which feed was used. Hence HDS of the three feeds may have been inhibited by basic nitrogen to very different degrees. This may have contributed significantly to the high reactivity differences seen in Table 3. Thus if this is taken into account, the relative HDS reactivities solely caused by the different sulfur distributions of the feeds may be separated from the inhibiting effect of basic nitrogen. This approach will give more realistic relative reactivities of the feeds.

It is generally accepted that two reaction pathways exist for HDS of dibenzothiophene and alkyl-substituted dibenzothiophenes. One route involves hydrogenation of one of the aromatic rings prior to removal of the sulfur atom (hydrogenation route). The other route involves direct extraction of the sulfur atom without ring

hydrogenation (direct route) [3,6]. The direct route of HDS is inhibited by hydrogen sulfide along with non-basic and basic nitrogen, whereas the hydrogenation route is particularly inhibited by basic nitrogen species [2,3,6]. The hydrogenation route is especially important for NiMo catalysts at high conversion levels, where the most refractive sulfur species determine the overall reactivity [3]. However, this presumes that basic nitrogen has been removed in order not to inhibit the active sites of the hydrogenation route.

The sulfur species of a given feed, which are the easiest to desulfurize (such as thiophene and benzothiophene), are removed in the first part of the reactor by direct desulfurization, whereas the most difficult sulfur compounds (such as 4,6-dimethyldibenzothiophene) are mainly converted in the last part of the bed via the direct route and/or the hydrogenation route. Again the contribution from the hydrogenation route is determined by the amount of basic nitrogen left in the reactor. Thus the reaction rate expression for sulfur removal should in principle contain at least two terms: one for the direct route and one for the hydrogenation route. However, for the sake of simplicity, the sulfur removal in this study will be described by a single term, which takes the inhibiting effect of basic nitrogen compounds into account:

$$R_S = \frac{k_{HDS} \cdot C_S^n / C_{S,in}^{n-1} \cdot \left(P_{H_2} / P_{ref}\right)^{\alpha}}{1 + K_{basic\,N} \cdot C_{basic\,N}} \qquad (4)$$

This is a combination of an n^{th} order rate equation and a Langmuir-Hinshelwood model, which takes inhibition by basic nitrogen into consideration. The temperature dependence of the rate constant is again considered to follow equation (3). As mentioned earlier, the concentration of basic nitrogen in the feeds and products was measured, and by assuming first order kinetics for the basic nitrogen compounds, the conversion of basic nitrogen down through each reactor was calculated:

$$R_{basic\,N} = k_{HDN,basic\,N} \cdot C_{basic\,N} \qquad (5)$$

Integrating equation (5) enabled us to calculate the concentration of basic nitrogen compounds at each axial position of the reactors. This was used to integrate equation (4). It is well known that new basic nitrogen-containing molecules are formed during HDN of non-basic nitrogen-containing molecules, but it is assumed that the inhibiting effect of these is the same as that of those originally found in the feed. Moreover the adsorption term of basic nitrogen, $K_{basic\ N}$, in equation (4) was assumed to be temperature independent and of the same value for all three feeds. In order to obtain a reasonable estimate of this parameter, data from [3,6] were used. In [3,6], the effect of adding specific types of nitrogen compounds to a nitrogen free diesel was studied. Pure basic nitrogen compounds were added to a diesel sample, and the HDS reactivity of this oil was directly compared with the HDS reactivity of samples containing no nitrogen compounds and the original diesel. By applying equation (4) and (5) to this dataset with a typical reaction order for a diesel of n = 1.65, the adsorption term of basic nitrogen was determined to be $K_{basic\ N} \approx$ 800 l/mol. This value of $K_{basic\ N}$ was used to determine the relative reactivities of the three feeds of this study.

Relative reactivities with basic N inhibition. By applying the approach described above, the inhibition by basic nitrogen compounds was taken into account when calculating the relative HDS reactivities of the feeds. This gives a better estimate of the relative reactivities, which can be attributed to differences in the sulfur distributions of the three feeds. By applying equation (4), (5), $K_{basic\ N} \approx$ 800 l/mol and n = 2.0, the relative HDS reactivities of the three feeds and two catalyst types were calculated. The best fit to the experimental data gave $E_{A,\ HDS}$ = 31.4 kcal/mol and $\alpha \approx 0$. The relative feed reactivities are given in Table 4.

Table 4. Relative HDS Reactivities of the three Test Feeds and two Catalysts when using an nth Order Langmuir-Hinshelwood Model with Inhibition by Basic Nitrogen.

Feed	Relative HDS activity
$(IBP\text{-}350)_{CoMo}/(400\text{-}EBP)_{CoMo}$	3.3
$(350\text{-}400)_{CoMo}/(400\text{-}EBP)_{CoMo}$	1.3
$(350\text{-}400)_{NiMo}/(400\text{-}EBP)_{NiMo}$	1.2
$(350\text{-}400)_{CoMo}/(350\text{-}400)_{NiMo}$	2.0
$(400\text{-}EBP)_{CoMo}/(400\text{-}EBP)_{NiMo}$	1.9

This model seems to provide a reasonable fit, as the activation energy of 31.4 kcal/mol is in line with the activation energies found in other studies of the HDS reactivity of oils in the VGO range. In [1], activation energies of e.g. 29 and 33 kcal/mol were found, and in [4], activation energies of approximately 33 kcal/mol were determined for oils in the VGO boiling point range. As can be seen, the relative activity of the CoMo and NiMo catalyst was still around 2 at these conditions. However, the relative reactivities of the feeds are now more realistic, as the impact of basic nitrogen on the HDS activity has been included. The diesel feed was approximately 3.3 times more reactive than the heaviest feed, and the 350-400ºC feed was approximately 20–30% more reactive than the 400-EBP feed for both the CoMo and NiMo catalyst.

Conclusions

In this study three feeds were obtained by fractionation of a coker VGO: a diesel feed, a light VGO and a heavy VGO. Both a commercial CoMo and a NiMo catalyst from Topsøe were used in the test, and the below conclusions were drawn.

Basic nitrogen compounds are major inhibitors of HDS, and in the present study diesel data were used to estimate an adsorption constant. It was shown that a simple n^{th} order rate model without inhibition terms could not be used to quantify the relative feed HDS reactivities, as this model resulted in surprisingly high relative reactivities when taking the sulfur distributions of the feeds into account. Thus the inhibiting effect of basic nitrogen was included when calculating the relative HDS reactivities of the feeds. By applying the adsorption constant for basic nitrogen and a typical reaction order of a VGO, realistic relative HDS reactivities of the three feeds and two catalyst types were calculated. The diesel feed was approximately 3.3 times more reactive than the heaviest VGO, and the light VGO was around 20–30% more reactive than the heaviest VGO for both the CoMo and NiMo catalyst.

References

[1] Ancheyta, J.; Angeles, M. J.; Macías, M. J.; Marroquín, G.; Morales, R. *Energy and Fuels*, **2002**, 16, 189-193.

[2] Zeuthen, P.; Knudsen, K. G.; Whitehurst, D. D. *Catalysis Today*, **2001**, 65, 307-314.

[3] Cooper, B. H.; Knudsen, K.G., Prepr. Pap. – *Am. Chem. Soc., Div. Petr. Chem.*, **2001**, 46 (4), 338-340.

[4] Tsamatsoulis, D; Papayannakos, N. *Chem. Eng. Sci.*, **1998**, 53 (19), 3449-3458.

[5] Ma, X.; Sakanishi, K.; Mochida, I. *Ind. Eng. Chem. Res.*, **1996**, 35, 2487-2494.

[6] Knudsen, K. G; Whitehurst, D. D; Zeuthen, P. *AIChE Spring Meeting*, Atlanta, GA, **2000**.

[7] Girgis, M.J.; Gates, B.C. *Ind. Eng. Chem. Res.*, **1991**, 30, 2021-2058.

[8] Hidalgo-Vivas, A.; Knudsen, K.G.; Zeuthen, P. AIChE Spring Meeting, **2003**.

EFFECTIVENESS OF METAL ORGANIC FRAMEWORKS FOR REMOVAL OF REFRACTORY ORGANOSULFUR COMPOUND PRESENT IN LIQUID FUELS

G. Blanco-Brieva[a], J. M. Campos-Martin[a], S.M. Al-Zahrani[b], J. L. G. Fierro[a]*

[a] Sustainable Energy and Chemistry group. Instituto de Catálisis y Petroleoquímica, CSIC, c/Marie Curie, 2 Cantoblanco, 28049 Madrid, Spain (http://www.icp.csic.es/eac/)
[b]Chemical Engineering Department, College of Engineering, King Saud University, Riyadh, Kingdom of Saudi Arabia
* Corresponding author: gblanco@icp.csic.es, FAX: +34 915854760

Introduction

The sulfur content in fuels is an environmental concern because upon combustion sulfur is converted to SOx, which not only contributes to acid rain, but also poisons catalytic converters for the treatment of exhaust emissions, which are very expensive due to are based on noble metals [1]. More stringent environmental regulations reduce the sulfur concentration limits in liquid fuels [2] (diesel and gasoline), and it will certainly be lowered in the near future. The hydrodesulfurization (HDS) [3] (industry standard process) eliminates efficiently nonaromatic sulfur compounds and thiophenes, but is less effective by more sterically hindered as dibenzothiophene (DBT), fuel contaminants and have limitations in terms of product quality and cost, which are undesirable to refiners [4]. Processes different from HDS have been proposed to produce ultra-low sulphur diesel (ULSD); oxidative microbial transformations [5], physical extraction with a liquid6 selective adsorption on suitable materials [7]-[9] and catalytic oxidation [10] remain prominent.

Adsorption of S-compounds presents some advantages, such as mild operation conditions and no need of H_2 or O_2. Studies have been undertaken to develop adsorbents for the desulfurization of transportation fuels using zeolites [7] mesoporous materials [8] and activated carbons [9],[11]. From the studies using activated carbons it was concluded that BET specific area, total pore volume, and micropore volume are correlated with sulfur adsorption capacity. Micropore volume plays a crucial role in sulfur compound adsorption [12].

Other class of porous materials that can be used to adsorb selectively organo-sulfur compounds includes the Metal-Organic Framework (MOF) family [13]. MOF compounds consist of metal clusters linked by polyfunctional organic linkers yielding porous three-dimensional networks with large pore volumes and high inner surface areas. Their very large pores and high inner surfaces areas offer a wide range of promising applications in gas storage, separation, sensing and catalysis [13],[14].

In this study we have used several commercial MOFs systems and evaluated their performance for the adsorption of dibenzothiophene (DBT) under different experimental conditions.

Experimental procedure

Commercial Basolite F300 ($C_9H_3FeO_6$), Basolite A100 ($Al(OH)(C_8H_4O_4)$) y Basolite C300 ($Cu_3(C_9H_3O_6)_2$) metal-organic frameworks were purchased from Sigma-Aldrich. Prior to adsorption experiments, each sample was degassed under vacuum in order to remove water and other contaminants. A Y-type zeolite (Conteka) was used as reference.

The textural properties of the commercial MOFs were determined from the nitrogen adsorption-desorption isotherms recorded at 77 K with a Micromeritics TriStar 3000 apparatus. X-ray photoelectron spectra (XPS) were acquired with a VG Escalab 200R spectrometer. X-ray diffraction patterns were recorded using a PANalytical X'Pert Pro diffractometer with Cu Kα radiation (λ=1.5405 Å).

The Adsorption performance of MOFs was tested in a liquid-phase glass batch reactor under atmospheric pressure and stirring. Solid was suspensed in solution of the sulfur compound in 2,2,4-trimethylpentane (TMP); (simulates a liquid fuel). This mixture was kept under vigorous stirring for 72 h, to reach the thermodynamic equilibrium. Solid was then filtered for its characterization, and liquid was analyzed by GC-FID to evaluate the sulfur compound concentration.

Results and discussion

The adsorption properties of the three MOFs systems were compared with that of a widely investigated Y-type zeolite15 in DBT over a wide concentration range (10-1700 ppmw of sulfur) at temperature constant and close to ambient (304 K).

The amounts of sulfur retained at equilibrium, expressed as g of sulfur per kg of sorbent, indicates that DBT adsorption is much higher on MOFs samples than on the benchmarked Y-type zeolite. C300 and A100 displayed substantially higher adsorption capacity than the parent F300 MOF system. It is emphasized that the extent of DBT adsorption on the MOF systems investigated in the present work are in the order of 6-8 times higher than that previously reported using conventional zeolite or activated carbons sorbents.

Textural properties for the three MOFs systems, indicates that C300 records the largest BET area value (1277 m^2/g) and then decreases for F300 (854 m^2/g) and even more for A100 (673 m^2/g). A similar trend is observed for both pore size and pore volumes though differences are much less marked.

The very small difference in porosity between C300 and F300 substrates cannot explain the almost double adsorption capacity recorded for DBT in the former one Figure 1. The higher adsorption capacity of DBT observed on C300, which in turn displays the highest BET specific area, suggests that the extent of adsorption at equilibrium is governed among others by the BET area of the substrate. Notwithstanding, the decrease in both BET area and pore volume observed for A100 sample might well account for its drop in

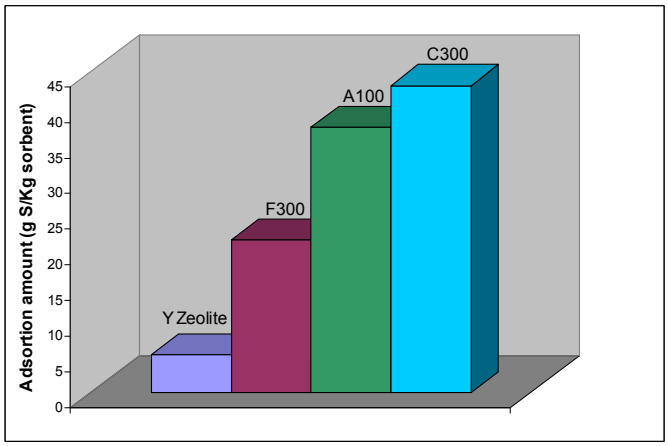

Figure 1 Adsorption capacity of different sorbents employed

DBT adsorption was determined within the temperature range 283-333 K under atmospheric pressure for the two MOF systems: A100 and C300 samples. The isotherms were constructed by employing DBT concentrations within the range 10-1700 ppmw of S. In the low and medium concentration region the extent of adsorption

increases with increasing sulphur concentration in the liquid phase and then tended to level off at higher concentrations. This fact can be taken as indicative that saturation has been reached at each temperature.

The DBT isotherms indicate clearly a strong influence of adsorption temperature on the extent of adsorption on Basolite C300 sample. This effect is clearer for DBT concentrations in the liquid phase somewhat above 200 ppmw of S. On the contrary, differences in the adsorption isotherms of DBT on Basolite A100 sample are less marked and also they tend to flatten off at DBT concentrations above 900 ppmw of S.

Surpassingly, the extent of adsorption at equilibrium does not decrease with adsorption temperature. This is opposite to what is observed in the adsorption of many gaseous molecules on solid surfaces. Two different mechanism of adsorption can be considered. At low temperature, adsorption is governed by weak van der Waals forces, however, at higher temperature; chemisorption is produced showing an increase in the sorption capacity of the sample. The process of physisorption can be reversed by heating but in chemisorption, the forces of attraction between the sorbate and the adsorbent are very strong [11].

The maximum adsorption capacity is similar for both sorbents, but a careful study shows that the maximum adsorption is produced at 304 K for C300.

X-ray photoelectron spectroscopy (XPS) is useful for studying the chemical state of the atoms present in the surface layer region of solid materials. Significant results were obtained studying the energy regions of S 2p core-level. Two sulfur species were detected. One appeared at a binding energy of 163.9 eV, typical of S-C bonds in organic compounds [16], and another at 169.2 eV originated from S(VI) in sulphone-like species [17]. The observation of highly oxidized S(VI) species can be taken as conclusive on the strong interaction of S-atom of adsorbate with the MOF surface via true chemisorption process. However, knowing the high stability of S-atom in the aromatic rings of DBT, the appearance of these oxidized S(VI) species is unexpected because neither oxidant was present in the liquid phase nor changes had occurred in the chemical state of Cu^{2+} (C300), Al^{3+} (A100) and Fe^{3+} (F300) ions along the adsorption process. A tentative explanation to this behavior is based on the ability of the supports to chemisorb oxygen [11]. If so, as the oxidation of S-atom in organosulfur compounds into S(VI)-containing moieties is an activated process the concentration of oxidized species should increase with adsorption temperature. The proportion of S(VI) species is higher when increasing adsorption temperature. Quantitative S/Cu surface atomic ratios of used MOF C300 sample show that the irreversibly retained sulfur quantity on the surface depends on the adsorption temperature. Thus, while the S/Cu atomic ratios are similar for samples used in adsorption experiments at 293 and 304 K, such a ratio is considerably lower when adsorption is conducted at 333 K. This trend is in agreement with the maximum adsorption capacity of C300. Complete regeneration of MOFs requires harsh conditions, i.e. longer regeneration time, for heavier S-containing adsorbates.

Crystallinity of the C300 MOF system in both fresh and used samples was studied (X-ray diffraction) with the aim to reveal possible deterioration of crystalline structure upon use in adsorption experiments. Cristallinity percentage was determined by considering the ratio of the sum of the intensity of ten mayor peaks. C300 fresh, was considered as standard for the calculations. The crystallinity degree of C300 samples after use in DBT is still high.

Conclusions

The removal of S-containing aromatic molecules (DBT) via adsorption on commercial MOF systems of the type Basolite C300, A100 and F300 follows the order C300 > A100 > F300 and the amounts of the organosulfur compound retained at equilibrium are 6-9 times higher than that recorded for a standard Y-type zeolite reference adsorbent. For DBT adsorption the temperature influences both the shape of the retention isotherm and the amounts of the adsorbate retained at equilibrium. XPS of MOF systems used demonstrated that two different S-containing compounds remain strongly held on the MOFs surface. One of these S-species, characterized by the binding energy of 163.9 eV, belongs to typical S-C bonds in organic compounds, and another placed at approximately 169.2 eV arises from S(VI) in sulphone-like species. The appearance of this highly oxidized S(VI) species can be taken as conclusive on the strong interaction of S-atom of adsorbate with the MOF surface via true chemisorption process. It is suggested that oxidation of adsorbed organosulfur compound can occur through chemisorbed oxygen. Finally, due to the extremely high adsorption capability of Basolite type materials, they appear as good candidates to be employed in the final removal of refractory organosulfur compounds from transportation fuels.

Acknowledgement.

We thank to our research sponsor The King Saud University, Riyadh (Saudi Arabia).

References

[1] (a), Serio, D.M.; Teaser, R.; Pengmei, L.; Santacesaria, E. *Energy Fuels*. **2008**, 22 (1), 207-217. (b), Bartolomew, C. I-L.; Agraval, P. R.; Katzer, J. R.; *Adv. Catal.,* **1982**, 31, 135.

[2] Transportation Air Quality: Selected Facts and Figures; Publication No. FHWA-HEP-05-045; U.S. Department of Transportation: Washington D.C., **2006**.

[3] Babich, V. I.; Moulijn, J. A. *Fuel*. **2003**, 82, 607-631.

[4] Song, C. S. *Catal. Today*. **2003**, 86, 211- 263.

[5] Monticello, D. J.. *CHEMTECH* **1998**, 28 (7), 38-45.

[6] Nie, Y.; Li, C.; Sun, A.; Meng, H.; Wang, Z. *Energy Fuels*. **2006**, 20, 2083-2087.

[7] Hernández-Maldonado, A. J.; Yang, R. T. *Catal. Rev.-Sci. Eng.* **2004**, 46, 111-150.

[8] Ko, C. H.; Park, J. G.; Park, J. C.; Song, H. J.; Han, S. S.; Kim, J. S. *Appl. Surf. Sci.* **2007**, 253, 5864-5867.

[9] Zhou, A.; Ma, X.; Song, C. S. *J. Phys. Chem. B.* **2006**, 110, 4699-4707.

[10] Campos-Martin, J. M.; Capel-Sanchez, M. C.; Fierro, J. L. G. *Green Chem.* **2004**, 6, 557-562.

[11] Deliyanni, E.; Seredych, M; Bandosz, T. J. I *Langmuir.***2009**, 25 (16), 9302-9312.

[12] Cychosz, K. A.; Wong-Foy, A. G.; Matzger, A. J. *J. Am. Chem. Soc.* **2008**, 130, 6938–6939.

[13] Mueller, U.; Schubert, M.; Teich, F.; Puetter, H.; Schierle-Arndt, K.; Pastre. J., *J. Mater. Chem*. **2006**, 16, 626-636.

[14] Férey, G. *Chem. Soc. Rev.* 2008, 37, 191–214.

[15] Savage, D. W.; Kaul, B. K.; Dupre, G. D. O'Bara, J. T.; Wales, W. E.; Ho, T. C. US Pat. 5,454,933, 1995.

[16] Mateos, J. M. J.; Fierro, J. L. G. *Surface Interface Anal*. **1996**, 24(4), 223-236.

[17] Wagner, C. D., Riggs, W. M., Davis, L. E., Moulder, J. F, (G. E. Muilenberg, editor) Handbook of X-ray Photoelectron Spectroscopy, 1st ed., Perkin-Elmer Corporation (Physical Electronics), **1979**.

Optimization of Dry Catalyst Impregnation in a Double Cone Blender: An Experimental and Computational Approach

*Francis S. Romanski, Atul Dubey, Arthur W. Chester, M. Silvina Tomassone**

Catalyst Manufacturing Science and Engineering Consortium
Rutgers Chemical and Biochemical Engineering
98 Brett Rd. Piscataway NJ, 08854 (732)-445-4949
silvina@sol.rutgers.edu

Introduction

In the manufacture of hydrotreating catalysts, impregnation of the active metals is a crucial step in determining the ultimate activity and selectivity of the catalyst. In this step, metal salts or complexes are dissolved in an aqueous solution and contacted with a porous oxide catalyst support alumina (Al_2O_3) or silica (SiO_2)[1-3]. In a typical dry impregnation, the focus of this work, metal solutions are sprayed using various types of nozzles over a rotating powder mixing vessel so that the amount of solution sprayed is 95-101% the pore volume of the support. During a process time of typically 30-60 minutes the metal is adsorbed from the solution onto the high surface areas support. Subsequently, the catalyst support is subject to drying and further pretreatment to transform the metal from its precursor state into its active form. During impregnation the particles are affected by liquid bridging and other forces which cause cohesion potentially disrupting flow in the granular mixing process. While double cone blending has been studied in the past for both catalyst and pharmaceutical blending[4], dry impregnation is subject to a change in the mixing and liquid distribution as a result of the increased cohesion, which in turn can adversely affect the homogeneous dispersion of the metal precursor in the solid. This can lead to several manufacturing issues such as poor quality control, longer processing times, and non uniform distributions of metal. As a result, several open questions remain: : i) how mixing and flow are affected when particles have a certain degree of moisture or are saturated with liquid, ii) whether the liquid is homogeneously distributed into the powder bed and iii) the extent and distribution of dead zones for a given impregnator configuration.

Currently, there are no guidelines for mixing as the cohesion, solution content, and density of the powder bed increases in the double-cone blender over time, nor are there any heuristics for spray rate. Unfortunately, experimental techniques for analyzing powder mixing are difficult to analyze and interpret. However, modern computational techniques such as Discrete Element Analysis (DEM) can fill in the gaps existing in experimental techniques[5-7]. DEM is a popular numerical technique used for simulation of granular materials such as soil, powders, catalyst pellets etc. Starting from an initial configuration, the positions of all particles and/or geometry elements in the system are calculated and it is determined which surfaces are in contact. A contact force model is used to impart numerically calculated forces on to contacting surfaces based on a small amount of overlap. The application of these forces results in the change in particle positions. The new positions are then used to calculate new forces and the cycle is repeated. DEM has found numerous applications in various fields such as pharmaceuticals, cosmetics, environmental sciences etc. However, in the area of catalysis, the applications have been limited. The main objective of this work is to evaluate the effect of liquid flow on a rotating bed of catalyst support for both mixing and content uniformity using experimental observations and novel DEM simulations.

Methods

Experimental. Double cone blending experiments were conducted using a Patterson-Kelly 10-quart rotating double cone blender (24 cm in diameter). An impregnator was retrofitted into the system using Swage-lock ¼" fittings combined with one Microwhirl™ ¼" NPT nozzles from BETE Fog Nozzle, USA; the spray zone was approximately 8 cm. 1.3 mm γ-Alumina spheres were purchased from Nor-pro St. Gobain with a 30% pore volume. Copper (II) Nitrate Trihydrate was purchased through Fisher Scientific (USA) and used to create the 1 M impregnation solutions.

Experiments were ten minutes in duration; each minute seven samples were removed from the catalyst bed using a disposable powder thief for a total weight of approximately two grams bed; samples were 3.5 cm apart. Samples were dried and weighed for water content. Subsequently, samples were soaked in 10 mL of 0.1 M HCl for 12 hours to remove the metal, the resulting solutions were then tested for copper concentration using an Ocean Optics (USA) UV-Spectrophotometer. Mixing experiments were performed by dying predetermined masses of particles using Rit-brand nylon clothing dye (Phoenix Brands, LLC., USA) and oven drying samples at 300ºC. Impregnation flow rates were 1.5, 2.5, and 5 L/hr with volume fill levels of 30% and 45% by volume equating to 1.75 and 3 kg of alumina, respectively. Mixing was characterized by the relative standard deviation (eq. 1):

$$RSD = \frac{s}{\bar{c}} \qquad (1)$$

$$s = \sqrt{\frac{n\sum C^2 - (\sum C)^2}{n(n-1)}}$$

where *n* is the number of samples, *C* is the concentration of metal or water, and *Cbar* is the average concentration of the powder bed.

Computational. Commercially available EDEM™ software was used (DEM Solutions Inc. (New Hampshire, USA)). DEM is a technique for simulating the behavior of granular materials with each particle treated as a discrete unit as opposed to continuum models where the material is treated as bulk. In this method, the motion of each particle is tracked based on the calculated positions and velocities which are a result of the forces experienced by it. Forces on particles are of two types – contact forces and body forces (eq. 2). The contact forces are due to interparticle or particle-boundary collisions. The boundary can be any physical object in the system, such as the walls, and baffles. The forces are resolved into normal and tangential components that are independent of each other.

$$F_{Total} = \sum F_{Contact} + \sum F_{Body} \qquad (2)$$

In eq. (2) F_{Total} is the resultant force on a given particle due to all its interactions with other particles and/or boundary elements as well as due to the effect of external force fields such as the gravitational field, cohesive or electrostatic interactions. The term $\sum F_{Contact}$ accounts for all the normal and tangential contact forces and $\sum F_{Body}$ denotes the sum of all body forces. This resultant force is computed for each particle at a high frequency (a time-step being typically of the order of 10μsec.) and the new particle position is computed by numerically solving the equations of motion. Using Newton's law the position of a particle *i* that has *j* number of contacts with its surroundings is related to the resultant force by eq. (3).

$$m_i\ddot{x}_i = \sum_j \left[F_{ij}^n + F_{ij}^t\right] + \sum_k F_{body} \qquad (3)$$

$$I_i\ddot{\theta}_i = \sum_j \left[R_i \times F_{ij}^t\right] + \sum_i \tau_{body}$$

In eq. (3), m_i is the mass of the particle of radius R_i, x_i is its position, $\ddot{x}_i$ its acceleration, and I_i is its moment of intertia. F_{ij}^n and F_{ij}^t are the normal and tangential components of the contact force on particle i due to its jth contact respectively. The term $\sum_k F_{body}$ accounts for all body forces acting on the particle using a summation index k. In this study, gravity is considered to be the only source of the body force on the particles (k = 1, $\sum_k F_{body} = m_i g$). The rotational components of motion are the angular displacement θ, angular acceleration $\ddot{\theta}$, and sum $\sum_l \tau_{body}$ of all torques due to body forces using summation index l.

In addition to the above contact dynamics, additional features have been developed in the model in order to allow water absorption, accumulation and transfer among the particles. The water spray was modeled as made up of discrete droplets which would get absorbed in the catalyst medium particles upon contact. This leads to increase of mass as well as cohesive properties of the host particles. Defining the mass flow rate of water as:

$$Q_{spr} = m_{sprquest} / \sec \tag{4}$$

The particles can absorb water up to 30% of their weight. If they receive more water than this, they become supersaturated and can transfer their excess water to other contacting unsaturated particles. The amount of water transferred between two particles when one of them is supersaturated, is given by:

$$Q_{Tr} = \frac{\kappa}{2N}\left[\frac{m_{Tr}}{\Delta t}\right] \tag{5}$$

where κ is a proportionality constant which dictates the rate of water transfer, m_{Tr} is the mass of excess water on the supersaturated particle, Δt is the time of contact and N is the number of particles in contact. Figure 1 shows the EDEM™ setup for a catalyst dry impregnation.

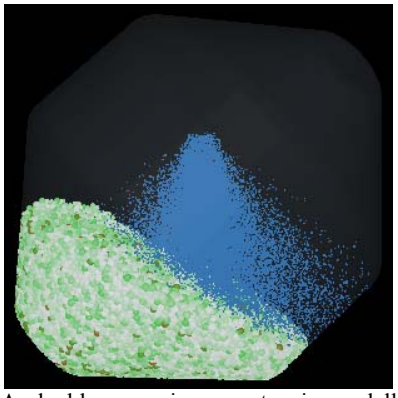

Figure 1: A double cone impregnator is modelled using a conical spray nozzle and spherical catalyst particles. The impregnator rotates clockwise at a speed of 25rpm. Particles are colored according to their water content.

Results

Experimentally, water content and copper concentration were evaluated. It was found, as predicted, that the water content in a high flow-rate environment of 5 L/hr lead to a poorly mixed system for both water and metal content. The water content over time and position using a lower flow-rate of liquid yielded much less variation as a function of time, the same is true for the metal content. Figure 2 shows the water content as a function of axial position (3.5 cm apart), clearly the center has significantly more water content in comparison to the sides, indicating that the mixing is not adequate enough to allow for the dry particles to reach the spray zone.

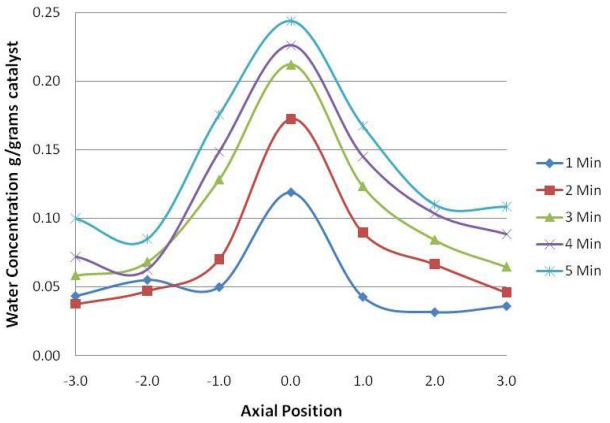

Figure 2: Water concentration in grams of water per gram of catalyst (max 0.3 for 30% pore volume) as a function of time and axial position (3.5 cm between samples) at 5 L/hr liquid flow rate.

However, when using significantly slower flow rates, the water and metal content are correspondingly more homogeneous in the powder bed. Figure 3 shows the water concentration across the experimental powder bed in identical parameters as Fig. 2, where it is strikingly clear that the liquid is now much more evenly dispersed in the bed.

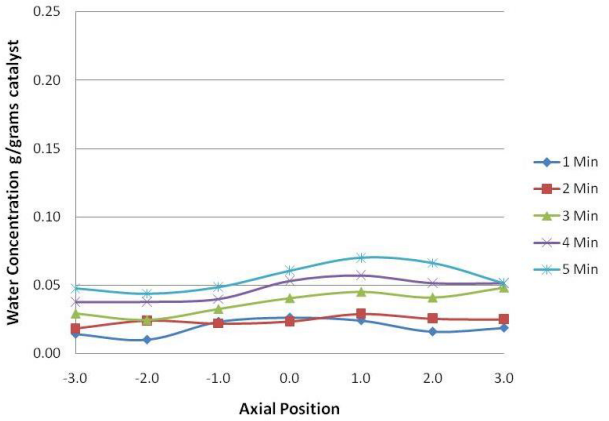

Figure 3: Water concentration in grams of water per gram of catalyst (max 0.3 for 30% pore volume) as a function of time and axial position (3.5 cm between samples) at 1.5 L/hr liquid flow rate.

An additional method of characterizing the poor mixing in the high flow rate systems is observing the relative standard deviation, which compares the individual zones with the averaged amount; a more homogeneously mixed system will have a low relative standard deviation which oscillates around an equilibrium point typically approximately 0.2. Figure 4 shows the averaged water and metal content relative standard deviation for 1.5, 2.5, and 5 L/hr spray-rates.

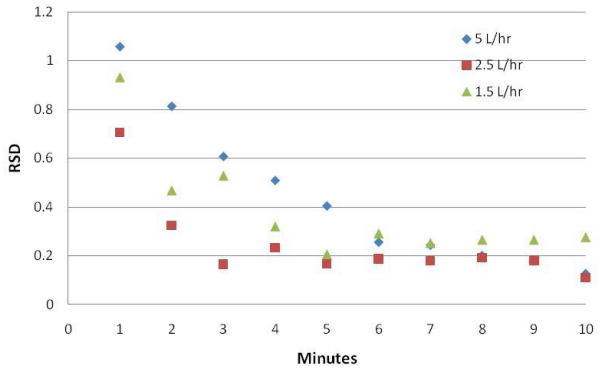

Figure 4: Water concentration in grams of water per gram of catalyst (max 0.3 for 30% pore volume) as a function of time and axial position (3.5 cm between samples) at 5 L/hr liquid flow rate.

Based on the experimental analysis of both the relative standard deviation as well as the content of the bed, it is clear that the water and metal content uniformity in a dry impregnation is highly dependent on the flow-rate of the material and the mixing of the system. These results were also found by examining the results of several DEM simulations according to the aforementioned methodology. Figure 5 and Figure 6 show the residence time of the particles in the spray zone of the impregnator for 5 L/hr and 1.5 L/hr, respectively.

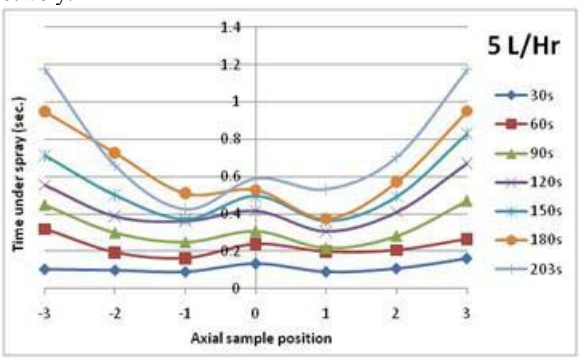

Figure 5: Residence time of particles taken from samples at seven locations located on the top of the bed along the axis of rotation for a spray rate of 5 L/hr, residence time corresponds to amount of time particles remained in the spray zone.

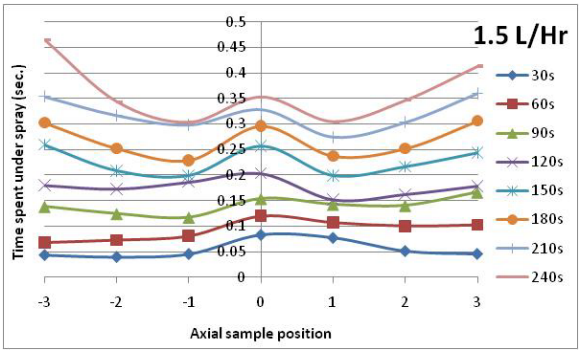

Figure 6: Residence time of particles taken from samples at seven locations located on the top of the bed along the axis of rotation for a spray rate of 5 L/hr, residence time corresponds to amount of time particles remained in the spray zone.

In accordance with experimental results, the DEM simulations appear to mimic the theory that higher flow rates result in less homogeneity in the powder bed with respect to water and/or metal content. Again, the 5 L/hr simulations had a clear increase at the center, while the results are less dramatic at the 1.5 L/hr level. However, there exists a clear increase in saturation at the edges, particularly as time increases for rotation. It is hypothesized that the increased density of the particles results in a tendency to collect on the outside of mixing vessel.

Mixing can be visually and quantitatively observed using DEM modelling fairly simply. As an example, a powder bed can be divided with colored and non-colored particles at two different interfaces: parallel and perpendicular to the axis of rotation. Figure 7 shows a comparison of mixing after one minute of simulation in the double cone blender in two positions: parallel to the axis of rotation (left) and perpendicular (right).

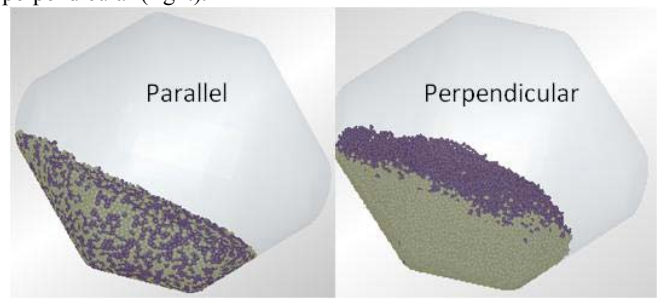

Figure 7: The impregnator is loaded such that half the particles are grey and half are perpendicular and is loaded such that the line dividing the two groups is parallel (left) and perpendicular (right) to the axis of rotation.

Following one minute of rotation, the particles that were loaded front to back or parallel to the axis of rotation are clearly well mixed, while the particles loaded side to side or perpendicular to the axis of rotation remain segregated. This further describes the poor axial mixing common in double-cone blenders. Unfortunately, during impregnation the center third of the bed is sprayed with liquid, it is no surprise that if the spray rate is too fast the liquid will build up in the center until the particles are supersaturated. As a result, it would be advantageous for an impregnation process to utilize a slow flow-rate of impregnation liquid, larger radius spray nozzle, or even multiple spray nozzles. Future studies will be aimed at optimizing these variables for particular systems.

Conclusions

The computational and experimental results show that the poor axial mixing of the double cone blender can have a significant impact on the content uniformity of the dry impregnation process. With sufficiently high flow-rates, particles on the outsides of the spray-zone are impregnated with significantly less water and metal precursor. As a result, dry impregnations using double-cone blenders should be impregnated with a relatively low flow-rate to ensure particles have enough migration time to spend equal time in the spray zone. Experimentally and computationally, it was shown that axial mixing is poor when compared to mixing parallel to the axis of rotation, leading to the local increase in water and metal content in the center of the rotation. This work has also shown the value and predictability of using commercially-based software, specifically the EDEM™ discrete element method software. Simulations have clearly matched the results from the experiments. Since it is quite difficult to quantitatively analyze granular systems, a powerful new tool for the optimization of impregnation has been developed and demonstrated.

References

(1) Lekhal, A.; Glasser, B. J.; Khinast, J. G. *Chemical Engineering Science* **2004**, *59*, 1063-1077.
(2) Lekhal, A.; Glasser, B. J.; Khinast, J. G. *Chemical Engineering Science* **2001**, *56*, 4473-4487.
(3) Liu, X.; Khinast, J. G.; Glasser, B. J. *Chemical Engineering Science* **2008**, *63*, 4517-4530.
(4) Chester, A. W.; Kowalski, J. A.; Coles, M. E.; Muegge, E. L.; Muzzio, F. J.; Brone, D. *Powder Technology* **1999**, *102*, 85-94.
(5) Chaudhuri, B.; Muzzio, F. J.; Tomassone, M. S. *Powder Technology* **2010**, *198*, 6-15.
(6) Faqih, A.; Chaudhuri, B.; Alexander, A. W.; Davies, C.; Muzzio, F. J.; Silvina Tomassone, M. *International Journal of Pharmaceutics* **2006**, *324*, 116-127.
(7) Mehrotra, A.; Muzzio, F. J. *Powder Technology* **2009**, *196*, 1-7.

Effect of ZrSBA-15 support on hydrotreating catalytic functionalities of Mo, CoMo, and NiMo catalysts

G Murali Dhar[a], Kapil Soni[a], Shelu Garg[a], Muthu.Kumaran G[a], Thallada Bhaskar[a]*

[a]Catalytic Conversion Processes Division, Indian Institute of Petroleum, Dehradun, 248 005, India
*Corresponding author: dhargm@gmail.com (G Murali Dhar)

INTRODUCTION

The development of more active HDS catalysts is one of the main goal of the modern refining industry. Such a demanding task requires catalysts that are several times more active than the present catalysts used to achieve 500 ppm sulfur [1]. It is not only the high activity but they should also have different activity profiles with respect to different functionalities. In order to modify the activity to achieve these objectives several approaches have been pursued among which variation of support is an important one [2-4].

γ-Al_2O_3 is a widely used support in commercial HDS catalysts applications. Many other supports have been tried with considerable success. Among them Clays, Carbon, Oxides, Mixed oxides, Zeolites, and mesoporous materials like MCM-41, HMS and SBA-15 have been studied. SBA-15 supported CoMo and NiMo catalysts are reported to exhibit higher activities for conversion of thiophene than γ-Al_2O_3. Vradman et al. [5] reported higher activities for HDS and hydrogenation using NiW-S/SBA-15 catalysts. Song and Reddy demonstrated that MCM-41 supported CoMo catalyst is substantially more active than γ--Al_2O_3 supported catalysts. Klimova et al. [6] have shown that Al-SBA-16 supported NiMo catalysts are highly active for HDS of 4,6-DMDBT and Zepeda et al. [7] reported on Ti-HMS of various Si/Ti ratio for HDS of DBT suggested that Ti containing HMS supported catalysts displayed higher activities than the γ-Al_2O_3 supported catalysts. Earlier our group reported that effect of heteroatom Al in HMS [8] and SBA-15 [9] on various hydrotreating functionalities, Al in mesoporous support increases the HDS of thiophene and hydrogenation of cyclohexene. In continuation of our work on the effect of heteroatoms in mesoporous materials on hydrotreating functionalities, in this communication a systematic study was carried out on effect of ZrSBA-15 on hydrodesulfurization of thiophene on Mo,CoMo and NiMo catalysts. A comparison has been made with SBA-15 and γ-Al_2O_3 supported catalysts [10].

EXPERIMENTAL

Zirconium containing SBA-15 supports with different Si/Zr ratios were prepared by self-generated acidic environment (without using HCl) using TEOS and Zirconiumoxychloride as silicon and Zirconium source respectively [11]. Supported Mo catalysts (2-12wt%Mo) were prepared by the incipient wetness impregnation method by taking appropriate concentration of ammonium hepta molybdate tetahydrate using ZrSBA-15 as support. The Co and Ni promoted catalysts were prepared by impregnating the corresponding salt on oven dried 8%Mo/ZrSBA-15 catalysts. The impregnated catalysts were dried in air at 110^{o}C overnight and all the catalysts were calcined at 550^o C for 6h.

RESULT AND DISCUSSION

All the supports and catalysts were characterized with XRD, FT-IR and N_2 adsorption-desorption analysis. N_2 adsorption–desorption analysis of Zr containing SBA-15 support and catalysts shows a typical type IV isotherm with H1-type hysteresis loop indicating that the structure is intact after Mo loading. The low angle XRD patterns of SBA-15 and ZrSBA-15 show well resolved low angle diffraction peaks that can be indexed to (100), (110), and (200). The diffraction peaks for both SBA-15 and ZrSBA-15 are related to long range 2D hexagonal ordering in the p6mm space group symmetry. FT-IR spectra of Zr-SBA-15 support shows the characteristic 966 cm^{-1} band for Si-O-Zr stretching indicating the incorporation of Zr into SBA-15 framework. Broad angle XRD analysis indicates that the dispersion remains more or less constant up to 8wt% Mo and beyond this loading larger MoO_3 crystallites are observed. TPR studies reveal the promotional activity of CoMo and NiMo supported catalysts can be attributed to the increase in the reducibility of molybdenum. This study shows that the incorporation of Zr into the SBA-15 material is beneficial for catalyst morphology, providing better dispersion for oxide and sulfide metal species, which in turn favor the formation of higher number of anion vacancies. Finally, a comparison of Co(Ni)8%Mo/ZrSBA-15 catalysts supported over SBA-15 and γ-Al_2O_3 supported ones, indicates the superior activity of the former catalyst for both HDS and hydrogenation reactions. The promotional effect is observed maximum at 3 wt% for both Co and Ni. The observed promotional activity can be attributed to the increase in the reducibility of molybdenum oxide. The catalytic activities were evaluated at 400^{0}C for HDS of Thiophene and HYD of cyclohexene on various Mo, CoMo and NiMo catalysts on various supports in a fixed-bed catalytic micro-reactor operating at atmospheric pressure on presulfided catalysts. The detailed experimental procedure is given elsewhere [11]. It can be noted that the HDS and HYD activities increases with the Zr content in the support. A similar trend can be seen in the case of oxygen chemisorption also for 8%MoZrSBA-15 with different Si/Zr ratio (fig 1). In the case of ZrSBA-15 (20), the catalytic activities for HDS and HYD, increases with molybdenum loading up to 8wt%Mo and then starts decreasing. The O_2 uptake is also plotted in the same figure and varies in a manner similar to that of the activities because it is well known that HYD and HDS reactions take place on anion vacancies and as oxygen is also known to chemisorb on anion vacancies, the similarity in behavior is expected (fig. 2)

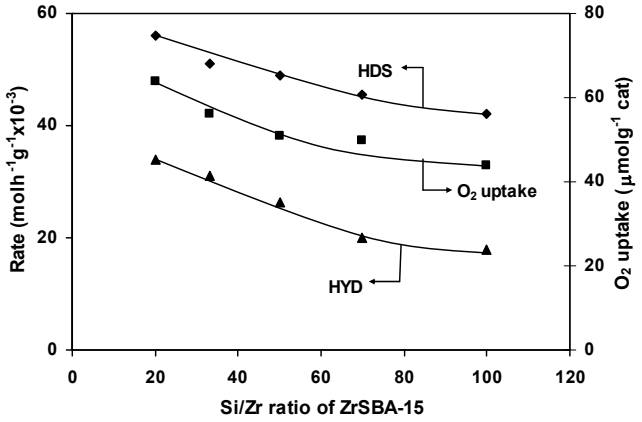

Figure 1.

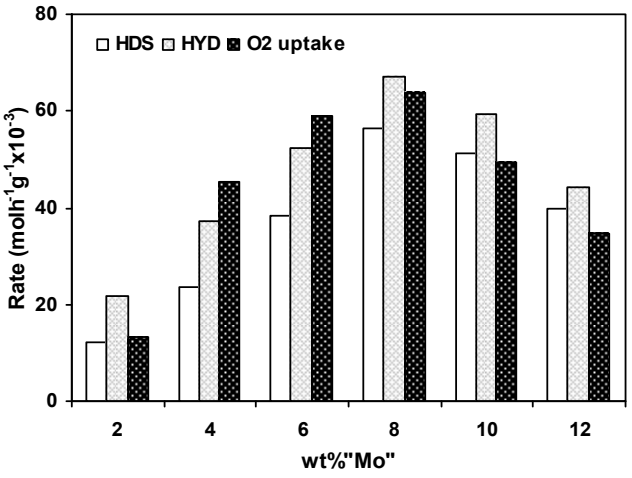

Figure 2

References

1. C. Song, Catal. Today 86 (2003) 211.
2. Y. Okamoto, M. Breysse, G.M. Dhar, C. Song, Effect of support in hydrotreating catalysis for ultra clean fuels, Catal. Today 86 (2003) (1–4) (special issue)
3. G. Murali Dhar, B.N. Srinivas, M.S. Rana, M. Kumar, S.K. Maity, Catal. Today 86 (2003) 45.
4. M. Breysse, P. Afanasiev, C. Geantet, M. Vrinat, Catal. Today 86 (2003) 5.
5. L. Vradman, M.V. Landau, M. Herskowitz, V. Ezersky, M. Talianka, S.Nikitenko, Y. Koltypin, A. Gedanken, J. Catal. 213 (2003) 163
6. T. Klimova, M. Calderon, J. Ramirez, Appl. Catal. A: Gen. 240 (2003) 29.
7. T.A. Zepeda, J.L.G. Fierro, B. Pawelec, R. Nava, T. Klimova, G.A. Fuentes, T. Halachev, Chem. Mater. 17 (2005) 4062.
8. T. Chiranjeevi, G. Muthu Kumaran, J.K. Gupta, G. Murali Dhar, Catal. Commun. 6 (2005) 101.
9. G. Muthu Kumaran, Shelu Garg, Kapil Soni, Manoj Kumar, L.D. Sharma, G. Murali Dhar, K.S. Rama Rao, Appl. Catal. A: Gen. 305 (2006) 123.
10. G. Muthu Kumaran, Shelu Garg, Kapil Soni, K.S. Rawat, L.D. Sharma, K.S. Rama Rao, G. Murali Dhar, Ind. Eng. Chem. Res. 46 (2007) 4747
11. S.-Y. Chen, L.-Y. Jang, S. Cheng, Chem. Mater. 16 (2004) 4174.